Synthesis and analysis of electron doped superconductors

A M.Sc project at NBI

Cédric Holme Qvistgaard

KU-ID: zwn759

Councelors

Machteld E. Kamminga

Kim Lefmann

Niels Bohr Institute
University of Copenhagen

20th of May 2022

Abstract

This thesis covers our work done in synthesizing and characterizing variations of the electron doped superconductor $Nd_{2-x}Ce_xCuO_4$ (NCCO). Various powder samples were produced using the solid state synthesis technique and afterwards characterized using x-ray scattering and Rietveld refinement.

Growth of a large single phase crystal using the Traveling-Solvent-Floating-Zone method was attempted in collaboration with Lund University, although the crystal was never completed due to technical difficulties.

A high purity superconducting sample of NCCO was successfully synthesized and characterized using X-rays, Rietveld refinement and a magnetometer, validating our synthesis process. Multiple attempts were then made at creating new superconductors by changing the doping material from Ce to other candidates such as Sn, Zr, Sr and Ba, albeit none of the theorized compounds successfully formed.

The effects on doping in the cuprate copper-oxide layers was also investigated. It was shown that when doping the Cu layer of $La_{2-x}Sr_xCuO_4$ (LSCO) with both Zn and Ni, the resulting superconducting magnetic response behaves as an average of LSCO samples doped with each element separately, suggesting that the effects of slight elemental doping in the copper-oxide layer is linear and independent of other dopants.

Finally the viability of replacing Ce doping with Ga doping in the NCCO copper-oxide layers were conducted, showcasing no evidence that such a replacement is possible for Ga levels above 3%.

Contents

1 Introduction **1**

2 Theory of superconductivity **3**
2.1 Attributes and London Equations 3
2.2 Type 1 and Type 2 superconductivity 4
2.3 BCS theory 6
2.3.1 Cooper pairs 6
2.3.2 BCS ground state 6
2.3.3 Finding observables 7
2.4 Ginzburg-Landau Theory 10
2.4.1 Classical Landau theory 10
2.4.2 The order parameter 11
2.4.3 The Ginzburg-Landau equations 11
2.4.4 Application of GL equations 12

3 NCCO **15**
3.1 Structure 15
3.2 Properties 16
3.3 Annealing 18
3.4 Charge carriers 21

4 Solid state synthesis **23**
4.1 Calculation of compound masses 23
4.2 Powder synthesis using solid state method 24
4.3 Crystal synthesis using TSFZ method 26
4.3.1 Rod preparation 26
4.3.2 Crystal growth using mirror furnace 30

5 Characterization methods **32**
5.1 X-ray scattering 32
5.1.1 Theoretical background 32
5.1.2 Instrument 34
5.1.3 Experimental procedure and analysis 35
5.2 Rietveld refinement 37
5.2.1 Initial procedures 38
5.2.2 Le Bail refinement 38
5.2.3 Structural refinement 39

5.3 Neutron Scattering 40
5.4 Superconducting Quantum Interference Device 42
5.4.1 Theoretical background 42
5.4.2 Instrument 42
5.4.3 Experimental procedures 44

6 NCCO synthesis and superconductivity measurements 47
6.1 Superconductivity test 48
6.2 Effects of reductive annealing on spin gap 49
6.3 Impurity analysis 53

7 Exploratory synthesis of new superconductors 57
7.1 New electron doped superconductors 57
7.1.1 $Nd_{2-x}Sn_xCuO_4$ and $Nd_{2-x}Zr_xCuO_4$ 58
7.2 Hole doping electron doped superconductors 59

8 Effects of doping in the cuprate layer 62
8.1 Cuprate layer spin dependency in LSCO 62
8.1.1 Sample quality 63
8.1.2 Magnetic response measurements 63
8.1.3 Analysis 67
8.2 Carrier doping in the NCCO cuprate layer 70
8.2.1 Sample quality 70

9 Summary and final remarks 74

Bibliography 76

A XRD patterns 81

B Magnetization measurements 95

Acknowledgements

To start of this thesis i would like to thank the many people that helped assisting and supporting me in its creation. First of all I would like to express my sincerest gratitude to my supervisor Machteld Elizabeth Kamminga for always being of assistance. Whether it be synthesis, measurements, interpretation or general life advice, her input has been invaluable, and her ability to cheerfully assist everyone around her is truly inspiring.

Secondly I would like to thank my co-supervisor Kim Lefmann. His infectious optimism and enthusiasm is eternally motivating, and his suggestions and feedback has been utmost valuable.

I would also like to thank to Elizabeth Blackbird and her department for their kind hospitality and assistance in our attempted crystal growth, as well as Astrid Tranum Rømer for her assistance in finding new experiments and in furthering my knowledge of superconductivity in general. Their help has been utmost appreciated.

Finally I would like to give a truly special thanks to my friends and family for their unwavering support. It has meant the world to me and without them finishing this thesis would not have been possible.

Nomenclature

Physical Constants

Symbol	Description	Values
ϕ_0	Magnetic flux quantum	$2.067833848 \times 10^{-15}$ Wb
e	Electron charge	$1.6021766208 \times 10^{-19}$ C
μ_0	Magnetic permeability of free space	$4\pi \times 10^{-7}$ TmA^{-1}
h	Planck constant	$6.626070040 \times 10^{-34}$ Js
$\hbar$	Reduced planck constant	$1.054571800 \times 10^{-34}$ Js

Physical Symbols

λ_L	London penetration depth
Φ	Magnetic flux
H	Magnetic field strength
ξ	Coherence length
B	Magnetic flux density
j	Electrical current density
χ	Magnetic susceptibility
H_c	Critical magnetic field strength for superconductivity
T_c	Critical temperature for superconductivity

Abbreviations

ADP	Atomic Displacement Parameter
AFM	Anti Ferro-magnetic
BCS	Bardeen–Cooper–Schrieffer
CIF	Crystallographic Information File

FC	Field cooling
GL	Ginzburg-Landau
LSCO	$La_{2-x}Sr_xCuO_4$
NCCO	$Nd_{2-x}Ce_xCuO_4$
NCO	Nd_2CuO_4
PCCO	$Pr_{2-x}Ce_xCuO_4$
PLCCO	$Pr_{1.3}La_{0.7-x}Ce_xCuO_4$
SC	Superconducting or Superconductor
SQUID	Superconducting Quantum Interference Device
TSFZ	Traveling Solvent Floating Zone
XRD	X-Ray Diffraction
ZFC	Zero-field cooling

Chapter 1

Introduction

April 8th, 1911 marks a critical point in the history of solid state physics, where the entire field was fundamentally changed. It was on this date that the Dutch scientist Kamerlingh-Onnes and his students, while immersing a mercury wire in liquid helium, discovered a material in which electric currents could run without any resistance at all [1]. A phenomenon henceforth known as superconductivity. The superconductors almost magical attribute was overflowing with potential, and with many scientists imagining a lossless electricity grid across the world, or perfect batteries revolutionizing the technology available, the investigation of these exotic materials quickly became one of the biggest fields in materials science. There was one problem however, superconductivity could only be achieved at temperatures below 25K, and even when a full-fledged theory for the phenomena was found, superconductivity anywhere near room temperature under ambient conditions still seemed impossible.

With this the interest in the field dwindled, and the exotic phenomena was viewed as an interesting niche without much use, that is, until a second breakthrough was made in 1986 by Bednorz and Müller [2]. While experimenting with a chemical technique called doping, in which a small amount of one element in a compound is replaced with another element to enhance certain attributes, they discovered the first high temperature superconductor. With a critical temperature of 30K, their La-Cu-O compound doped by replacing 15% of La atoms with Ba, was superconducting at significantly higher temperatures than anything seen before, and in a completely new type of material, the cuprates.The conventional theory did not seem to apply to cuprates, and the new class of superconductors had massively increased critical temperatures, quickly exceeding 80K. It was found however that only cuprates doped with materials that contained less electrons than the ones replaced, also called hole doping, would be superconducting, and for a while it was believed that these positively charged holes were essential to high temperature superconductivity, as no attempts at doping with materials containing extra electrons had any success.

That was until 1989 where Takagi et al. [3] found that the electron doped compound, $Nd_{2-x}Ce_xCuO_4$, abbreviated as NCCO, was in fact superconducting, but only after a second reductive annealing, removing some oxygen from the sample. This find caused the electron doped superconductors to be known as n-type superconductors, with the n being due to doping with negative charges (electrons) and the

hole doped cuprates labeled as p-types due to the positive charge doping. Having two types of cuprates significantly changed the theoretical landscape of superconductivity, as new theories should function both with holes and electrons, but it also opened new avenues for experimental investigation. As time went on, it quickly became apparent that p and n-type conductors were not equals, the critical temperature never increased significantly beyond the 24K of the first compound found, and the additional work needed to make the samples superconducting, not to mention the many mysteries surrounding the reductive annealing process, caused the community at large to abandon interest in the n-type superconductors.

We however, believe that abandoning the field would be a critical error, as the field of n-type superconductors still have several crucial questions unanswered, and as a complete understanding of the superconducting phenomena still with all likelihood still requires understanding of both p and n-type superconductors. Thus the main goal of this thesis is to further explore the otherwise underexplored n-type cuprates. This will be done by attempted synthesis of new and potentially interesting variations of the basic NCCO compound, exploration of the underlying mechanisms with which reductive annealing makes the compounds superconducting, as well as investigation of other essential differences between p and n-type superconductors. The thesis assumes the reader to have knowledge of the field equivalent to a B.Sc. degree in solid state physics or equivalent.

Chapter 2

Theory of superconductivity

In this section we will talk about the general theories that pertain to superconductivity, and discuss some of the different phenomena that arises as a consequence. The sections pertaining to London and Ginzburg-Landau theory are written closely following the Condensed Matter Physics lecture notes from Brian Andersen[4] and the sections concerning BCS theory are written following the book *Introduction to Superconductivity* by Michael Tinkham[5].

2.1 Attributes and London Equations

A material in the superconducting phase has two characterizing features. The first is that there is no electric resistance inside it making it a perfect conductor, hence the name. The other is the fact that they expel magnetic fields from within them, a phenomena called the Meissner effect [6]. This causes superconductors to become perfect diamagnets. The way the magnetic field is expelled is through the creation of what is called surface currents. These currents flow along the surface of the superconductor producing fields that exactly cancel out all incoming magnetic fields. To measure superconductivity we as such either measure the electric resistance or magnetic susceptibility of a material.

In 1937 the brothers London developed a theory to describe some of the first physical results that these two features would lead to, which we will review here [7]. We start off considering the equation for a current in a superconductor. It must function similarly to a regular current, except that some effect has made the electrons superconducting, so we take into account that perhaps their fundamental attributes could have changed by labeling superconducting particles with a *, we will later uncover that these particles are Cooper pairs consisting of two joint electrons. As such we propose

$$\mathbf{j_s} = -e^* n_s \mathbf{v_s} \tag{2.1}$$

This is analogous to the current in a normal conductor, just that here n_s is the density of the superconducting electrons, e^* is their charge and v_s their velocity. Given that there is no resistance, an electric field would cause them to accelerate freely $m^* \frac{d\mathbf{v_s}}{dt} = -e^*\mathbf{E}$. This allows us to write the London equations

$$\frac{d\mathbf{j_s}}{dt} = \frac{n_s e^{*2}}{m^*}\mathbf{E} \quad \text{and} \quad \mathbf{j_s} = -\frac{n_s e^{*2}}{m^*}\mathbf{A}$$

(2.2)

Where the second equation stems from Maxwell's law $\nabla \times \mathbf{E} = -\frac{\partial \mathbf{B}}{\partial t}$. From these equations some interesting attributes can be found, for instance if we consider another one of Maxwell's laws $\nabla \times \mathbf{B} = \mu_0 \mathbf{j}$ taking the curl of both sides, and using that we can freely pick the potential gauge such that $\boldsymbol{\nabla} \cdot \mathbf{A} = 0 \longrightarrow \boldsymbol{\nabla} \times \boldsymbol{\nabla} \times \mathbf{B} = \nabla^2 \mathbf{B}$, the second equation nets us

$$\nabla^2 \mathbf{B} = \frac{1}{\lambda_L^2} \mathbf{B} \quad \text{with} \quad \lambda_L^2 = \frac{m^*}{\mu_0 n_s e^{*2}} \tag{2.3}$$

Here we have defined the parameter λ_L. If we solve this equation in one dimension we receive that

$$\mathbf{B} = \mathbf{B_0} e^{-x/\lambda_L} \tag{2.4}$$

Showing us that external magnetic fields are exponentially deteriorating inside the superconductor, penetrating only around a length λ_L into the material. It is for this reason we call λ_L the penetration depth. This also explains part of the Meissner effect as a result of the perfect conductivity inside the superconductor.

2.2 Type 1 and Type 2 superconductivity

As the field of superconductivity grew it became apparent that not all superconductors behaved quite the same. This has led to the categorization of superconductors into type 1 and 2. The way to distinguish between these two types of superconductors is through their behavior in large magnetic fields. As explained the superconductors perfect diamagnetism arises from the creating of surface currents, however the superconductor can of course not create infinitely large currents along the surface, thus there is a critical level of external magnetic field, H_c, upon which the superconducting phase deteriorates. However the superconductors response to such a field is drastically different and a comparison of the two can be seen in Figure 2.1.

A type 1 superconductor is either fully superconducting or it is not superconducting at all. Once it reaches the critical field it behaves much as if the critical temperature had been reached and the superconductivity abruptly stops. As such there is only one critical magnetic field H_c. We note that type 1 superconductors often are simple in structure, typically created by cooling a conventional metal down to a critical temperature at which point it becomes superconducting. It is also only type 1 superconductors that we are able to describe fully using BCS theory, a theory which we will cover later.

Type 2 superconductors on the other hand deteriorates slowly once we reach a critical field. Here only part of the material stops being superconducting, and small vortexes of non-superconductivity opens up in the bulk allowing a small quantized amount of magnetic field to pass through, in a process called flux pinning. These vortices slowly increase in size as the exterior field increases, until finally all superconductivity is gone. Thus for type 2 superconductivity one talks about two critical fields, H_{c1} where the superconductivity begins to deteriorate and the

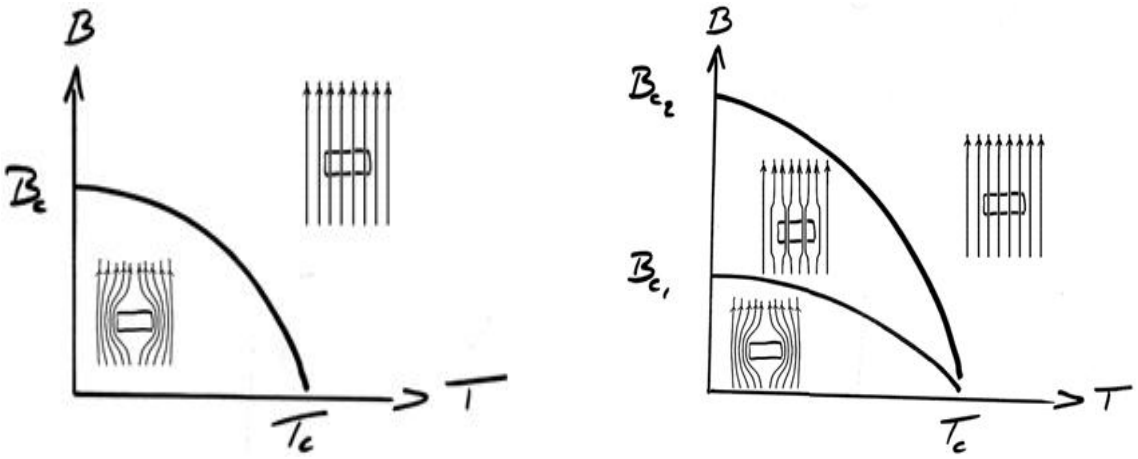

Type 1 Type 2

Figure 2.1: Difference in superconductor response to external magnetic field. Type 1 SC repels all magnetic field up to the critical field strength B_c, after which superconductivity abruptly vanishes. Type 2 SC enters a mixed state allowing progressively more field to pass through between B_{c1} and B_{c2}, at which point superconductivity stops. Originally from [8]

material enters what is called the mixed state, or vortex state, and H_{c2} where all traces of superconductivity are gone. Type 2 superconductors are usually the more modern superconductors like cuprates, the main subject of this thesis, consisting of many different elements in more advanced structures. Additionally these types of superconductors tend to have higher critical temperatures than type 1.

2.3 BCS theory

A common theme for superconductivity seems to be the difficulty of developing a theory properly explaining the phenomenon. While conventional superconductivity as said was first discovered in 1911 it would take up till 1957 before the first proper microscopic explanation was found. This theory was the BCS theory named after the founders Bardeen, Cooper and Schrieffer [9]. While it only applies to type 1 superconductors it is still a hallmark of its time, and as such we outline the most important aspects here.

2.3.1 Cooper pairs

The theory takes onset in Coopers discovery of what is called Cooper pairs. He envisioned two electrons in a Fermi sea with equal but opposite momentum such that the total momentum of the system was 0, and wondered what would happen to them if an attractive potential was present. Solving the Schrödinger equation using a rough approximation that the interaction potential was uniformly -V at all energy levels below a threshold $\hbar\omega_c$, he found the energy of the pair to be

$$E \approx 2E_f - 2\hbar\omega_c e^{-2/N(0)V} \tag{2.5}$$

Where N(0) is the density of states at the Fermi level. From this we see that the two electrons have a bound ground state with energy below E_f as long as there exists a pairing potential V. This bound state is what we call Cooper pairs and they are driving force behind the superconductivity. While not completely accurate one can imagine the pair now having the attributes of bosons instead of Fons, allowing multiple pairs to occupy the same energy levels condencing into a Bose-Einstein condensate. In this state all pairs behave identically, thereby avoiding internal interaction leading to the zero resistance.

2.3.2 BCS ground state

For a complete theory a quantum mechanical wavefunction for the entire system was needed, explaining why more and more Cooper pairs form until eventually the system is separate enough from a Fermi sea to be at equilibrium. This highly complex state is what is known as the BCS wavefunction. We will not cover the exact quantum mechanics that lead to the finding of such a wavefunction, but only a few key steps.

The first step was writing out the general wavefunction which would be

$$|\psi_N\rangle = \sum_k g(k_i, ..., k_t) C^*_{k_i\uparrow} C^*_{k_i\downarrow} \cdots C^*_{k_l\uparrow} C^*_{k_l\uparrow} |\phi_0\rangle \tag{2.6}$$

With $C^*_{k_i\uparrow}$ being the creation operator for an electron with momentum $k_{initial}$ with spin up going all the way to k_{last}, $|\phi_0\rangle$ being the vacuum state of no particles and g being a weight function.

Having to find weight functions for all k values in the band would be impossible, so the next essential step was to argue that a mean field approximation would work

assuming that state **k** depends only on the average occupancy of the other states. Thus the work was only statistical, meaning N was no longer exact but only had a well defined average, fortunately N is a very large quantity so this error is negligible. This led to the proposal of the new wave function

$$|\psi_G\rangle = \prod_{k_i..k_l} (u_k + v_k c^*_{k\uparrow} c^*_{-k\downarrow}) |\phi_0\rangle \tag{2.7}$$

introducing the probability of pair $(k_\uparrow, -k_\downarrow)$ being occupied as $|v_k|^2$ and unoccupied as $|u_k|^2 = 1 - |v_k|^2$. Thus they had an intuitive structural form of the BCS wavefunction, a product of every possible momentum state with a weighted chance of creating a pair. Yet to be done however was to evaluate these probabilities and assign it physical value.

2.3.3 Finding observables

To find values for v_k and u_k, BCS first solved the pairing Hamiltonian.

$$\mathcal{H} = \sum_{k\sigma} \epsilon_k n_{k\sigma} + \sum_{kl} V_{kl} c^*_{k\uparrow} c^*_{-k\downarrow} c_{-l\downarrow} c_{l\uparrow} \tag{2.8}$$

This is a simplified Hamiltonian, with the first term being the static particle energy and the second term being the potential matrix V_{kl} between the paired electrons. This is presumed to contain all the important dynamics of superconductivity, but we note that it does not contain for instance the unpaired electrons which might be relevant for other physical phenomena in the material.

This solution is fairly long, so again we stick to the main ideas. First a term $-\mu N_{op}$ was added to the Hamiltonian allowing for variation of the mean number of particles. This however was equivalent to moving the zero point energy up to the Fermi energy µ, meaning that instead of ϵ_k we could define the relative single particle energy $\xi_k = \epsilon_k - \mu$

The goal was now to minimize the expectation value such that.

$$\delta \langle \psi_G | \mathcal{H}' | \psi_G \rangle = 0 \tag{2.9}$$

The Hamiltonian can be rewritten as

$$\langle \psi_G | \mathcal{H}' | \psi_G \rangle = 2 \sum_k \xi_k v_k^2 + \sum_{kl} V_{kl} u_k v_k u_l v_l \tag{2.10}$$

The first term is obtained using $\bar{N} = \sum_k 2|v_k|^2$ and the second by realizing that V_{kl} transforms (l,-l) pairs to (k,-k) pair and vice versa thus requiring a probability amplitude of $v_l u_k$ in the initial state and $v_k^* u_l^*$ in the final state, while limiting ourselves to real probabilities.

To minimize the expectation value we propose $v_k = \cos(\theta_k), u_k = \sin(\theta_k)$ as a natural solution type to v and u given the constraint $u_k^2 + v_k^2 = 1$. Using various trigonometry we get.

$$0 = \frac{\partial}{\partial \theta_k} \langle \psi_G | \mathcal{H}' | \psi_G \rangle = -2\xi_k \sin(2\theta_k) + \sum_{kl} V_{kl} \cos(2\theta_k) \sin(2\theta_l) \tag{2.11}$$

This allows us to write

$$\tan(2\theta_k) = \frac{\sum_l V_{kl} sin(2\theta_k)}{2\xi_k} = -\frac{\Delta_k}{\xi_k} \tag{2.12}$$

Where we have simply defined $\Delta = -\frac{1}{2}\sum_l V_{kl} sin(2\theta_k)$ for ease of notation. We will also preemptively define $E_k = \sqrt{\Delta_k^2 + \xi_k^2}$. This definition allows us to split tan up to retrieve

$$\sin(2\theta_k) = 2u_k v_k = \frac{\Delta_k}{E_k} \tag{2.13}$$

$$\cos(2\theta_k) = v_k^2 - u_k^2 = -\frac{\xi_k}{E_k} \tag{2.14}$$

We recall that $sin(2\theta_k)$ was also present in the definition of Δ_k, allowing us to use equation 2.13 to generate a self consistent equation for Δ_k

$$\Delta_k = -\frac{1}{2}\sum_l \frac{\Delta_l}{E_l} V_{kl} \tag{2.15}$$

This equation has the trivial solution of $\Delta_K = 0$ while $\xi_k \neq 0$, From eq.2.14 we see that this corresponds to v=1 until we hit the Fermi energy, which is the classical setup that we expect where all energy levels are filled until E_f. If we recall however the original assumption justifying the existence of Cooper pairs, and thus superconductivity, there should be another solution if V_{kl} is negative. Using coopers original assumption $V_{kl} = -V$ when $\xi < \hbar\omega_c$ and zero otherwise, we see that $\Delta_K = \Delta$ for $\xi < \hbar\omega_c$ and 0 otherwise. With Δ being a constant it can simply be divided out in eq2.15 leaving us with the easily solvable equation

$$1 = \frac{V}{2}\sum_k \frac{1}{E_k} = N(0)V \int_0^{\hbar\omega_c} \frac{1}{\sqrt{\Delta^2 + \xi^2}} d\xi = N(0)V \sinh^{-1}\frac{\hbar\omega_c}{\Delta} \tag{2.16}$$

Solving for Δ we get

$$\Delta = \frac{\hbar\omega_c}{\sinh(1/N(0)V)} \approx 2\hbar\omega_c e^{-2/N(0)V} \tag{2.17}$$

Having found Δ we immediately notice the similarity to the energy difference that Cooper originally found. All that is left is plugging it into the original hamiltonian and see whether the nonzero solution indeed does have lower energy. Skipping straight to the result it turns out that

$$U_s - U_n = -\frac{1}{2}N(0)\Delta^2 \tag{2.18}$$

From this we see that the energy of the superconducting state indeed is lower and matches a naive extrapolation of Coopers results expecting that the energy gained is approximately equal to the energy gain of a Cooper pair, times half the density of states which is the amount of Cooper pairs available.

Setting N(0)=2 for a single pair we see that Δ^2 is exactly the minimum condensation energy for a single Cooper pair, and is constant for a given attractive field.

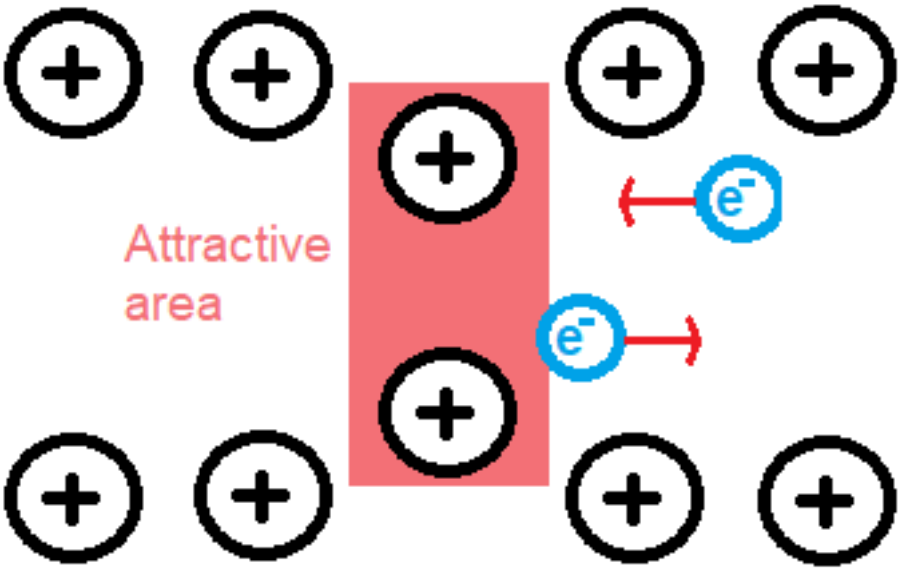

Figure 2.2: Schematic illustration of the phonon-driven attractive force between electrons. One electron attracts nearby atom cores, creating an area of higher charge in its wake. This area attracts another nearby electron, indirectly creating an attractive force between the two electrons.

This is certainly experimentally observable, and Δ is known as the superconductor energy gap.

All of the above theory takes onset in one assumption however, that there exists an interactive potential allowing electrons to form Cooper pairs. The question was what mechanism could give rise to such an interactive potential, after all electrons repel each other, so how one electron could cause an attractive force to be applied to another was a mystery. A solid proposition was that this attractive force between two electrons is caused indirectly by mediation of the positively charged atom cores. When an electron passes the core a slight attraction happens and the cores are pulled closer to the electron. This in turn causes an increase in positive charge following the electrons trail, resulting in a slight attractive force applied to the second electron moving towards it. Thus the two electrons have a positive attraction to each other separated by time, avoiding the more instant repulsion caused by the Coulomb interaction. A schematic of this can be seen in Figure2.2. That the attractive potential is mediated by phonons, also gives physical meaning to the value ω_c which is now clearly identified as the phonon frequency of the material.

Once the theory had predicted an observable the only thing left was to test it out. As we saw before Δ is directly proportional to the phonon frequency ω_c. The frequency for the atoms depends on the mass, and as such it was theorized that heavy isotopes of the same material should have a lower phonon frequency and thus a smaller energy gap. While the gap also depends on other factors such as V, for many well behaving classical systems it was found that this "Isotope effect" aligned almost perfectly with the theory, acting as one of the most solid proofs for the BCS theory's validity.

Unfortunately BCS theory only works for a certain subset of superconductors. If we recall the basis of the entire theory was that a small excitation of the Fermi sea could spawn Cooper pairs, however intrinsic in this assumption is that the material is a metal with a clear Fermi level when not in the superconducting state. In modern high temperature superconductors of type-2 this is not the case, the normal state of these materials are not conventional metals, instead being insulators or semiconductors with complex Fermi surfaces. This is the major reason for the failure of the BCS theory to explain type-2 superconductivity. Luckily there are other tools available to describe some of these phenomena, albeit not at a microscopical level like the BCS theory does, and as such the search for a complete theory of superconductivity is still very much a work in progress.

2.4 Ginzburg-Landau Theory

Classical Landau theory is a phenomenological theory that makes calculations based almost purely on symmetry and energy considerations of the system, used primarily to describe the physics of phase transitions. It is a powerful tool as it can explain many phenomena without any prior microscopical knowledge of a system, which is exactly what we lack in the case of type 2 superconductors.

Fortunately the superconductive state is actually a phase of matter and we can think about it in many of the same ways we think about states of matter like liquids and solids. In much the same way that liquids crystallize and heavily changes attributes once we reach freezing temperatures, the transition between ordinary and superconducting materials is also sharp and happen spontaneously at a critical temperature T_c. Thus the framework of the classical Landau theory should in theory also be able to explain the phenomenon of superconductivity.

One problem arose however for the early attempts at trying to apply classical Landau theory to superconductors. In order to use Landau theory an order parameter that breaks at phase transition is needed. An order parameter is a measure of the order of an attribute in an material, for instance the magnetic order parameter is the degree to which spins align, also known as the magnetization. For a long time no suitable order parameter could be found for the case of superconducting systems, preventing the usage of Landau theory. That was until Ginzburg realized that the parameter was an imaginary phase, which could not be directly measured, giving name to the modified Ginzburg - Landau(GL) theory.

2.4.1 Classical Landau theory

In classical Landau theory the key assumption is that the system's free energy is a function of an order parameter, and as such can be taylor expanded near phase transitions. The classical example of this is the ferromagnet where it is assumed that the free energy follows the relation

$$F(M) = F_0 + \sum_n a_n M^n \tag{2.19}$$

Where a_n is a constant and the magnetization, M, acts as the order parameter of the system. Through symmetry considerations we see that all n=odd terms has to be zero, as the free energy of a magnet would otherwise change if someone were to turn it upside down, which would be unphysical. Thus one can approximate the energy to

$$F(M) \approx F_0 + aM^2 + bM^4 \tag{2.20}$$

To find the coefficients Landau theory considers the properties of the system. Below T_c the ferromagnet must have lower energy when ordered, and after the phase transition at T_c it has lowest energy when M=0. This can be accomplished by letting the constant a change sign at T_c for instance by letting $a = a_0(T - T_c)$. Likewise we can reason that b should be positive as otherwise the energy would be lowered by having infinitely large M. Minimizing F w.r.t the order parameter M renders two solutions

$$M = 0 \quad \text{and} \quad M = \pm\sqrt{\frac{a_o(T_c - T)}{2b}} \tag{2.21}$$

One can then substitute this back into the expression for the free energy, which enables the calculations of entropy, specific heat and several other attributes of interest. However for the purpose of showcasing the basis of Landau theory we will consider the work done so far adequate and continue on.

2.4.2 The order parameter

The discovery of type 2 superconductors was established at roughly the same time that Landau proposed his theory on phase transitions. Unfortunately finding a proper order parameter for the superconductors was seemingly impossible and as such prevented application of the otherwise very general theory. That was until 1950 where Landau in cooperation with Ginzburg, inspired by the rise of quantum mechanics, proposed a complex pseudowavefunction $\psi(r)$ as the order parameter, with $|\psi(r)|^2$ being the electron density of superconducting electrons. This also explained why it was so challenging to find it, normally when a phase transition occurs a symmetry is broken, spins align, molecules form crystal lattices etc. However in the superconducting phase transition the broken symmetry was not immediately obvious, it turns out that it is the complex phase of the pseudo-wavefunction that locks when transitioning to a superconducting phase. As it is complex the phase is not directly measurable, but fortunately the difference in phase between two superconductors can be measured, allowing for experimental verification of the order parameter.

2.4.3 The Ginzburg-Landau equations

Having acquired an order parameter we can write out the free energy in an expansion of similar type to the one before.

$$f_s = f_n + a(T)|\psi(r)|^2 + \frac{1}{2}b|\psi(r)|^4 + \frac{1}{2m^*}|(\frac{\hbar}{i}\nabla + e^*A(r))\psi(r)|^2 + \frac{B^2}{2\mu_0} \tag{2.22}$$

The primary difference lies in two new terms. The third term covers the possibility of spacial variations in ψ and is essentially the kinetic energy of the supercurrents, with the part $e^*A(r)$ ensuring gauge invariance. And the 4th term which is simply the magnetic energy. The * for m and e denotes that we are talking about mass or charge of a Cooper pair.

To minimize this energy it is advantageous to use the variational method. First the problem is treated as if ψ and ψ^* are completely different variables, then we find $\delta F_s = 0 = F_s(\psi, \psi + \delta\psi^*) - F_s(\psi, \psi^*)$. Removing the terms that cancel out we get

$$\begin{aligned}\delta F_s = a(T)\psi(r)\delta\psi(r)^* + b\psi(r)^2\psi(r)^*\delta\psi(r)^* + \frac{1}{2}b\psi(r)^2\delta\psi(r)^{*2} \\ + \frac{1}{2m^*}|(\frac{\hbar}{i}\nabla + e^*A(r))\psi(r)\delta\psi(r)^*\end{aligned} \tag{2.23}$$

We limit our self to terms of first order in $\delta\psi^*$, and then divide through with $\delta\psi(r)^*$ to get a result reminiscent of differentiation. The final expression becomes

$$\frac{\delta F}{\delta\psi^*} = 0 = a(T)\psi + b|\psi|^2\psi + \frac{1}{2m^*}(\frac{\hbar}{i}\nabla + e^*A(r))^2\psi \tag{2.24}$$

Which is known as the first Ginzburg-Landau equation.

To get the second Ginzburg - Landau equation one follows the same logic but instead vary with respect to the potential A(r) to first order in δA, this is a bit more work requiring integration by parts assuming vanishing surface terms, and the identity $\nabla \times \nabla \times A = -\nabla^2 A$. When finished the second GL equation looks as such.

$$j_s = \frac{\hbar e^*}{2m^* i}(\psi(r)\nabla\psi^*(r) - \psi^*(r)\nabla\psi(r)) - \frac{e^{*2}}{m*}|\psi(r)|^2 A(r) \tag{2.25}$$

These two equations, alongside the original free energy, are the ground pillars of Ginzburg Landau theory and it is from these that a lot of the interesting physical properties of superconductors can be found.

2.4.4 Application of GL equations

If we start at the first GL equation and assume that there is no magnetic field so that B=0 we retrieve

$$a(T)\psi + b\psi^3 = \frac{\hbar}{2m^*}\nabla^2\psi \tag{2.26}$$

Now if we consider simply a one dimensional case, and for a moment pretend ψ is real we can see that a solution to this problem is

$$\psi(x) = \psi_0 \tanh\left(\frac{x}{\sqrt{2}\xi(T)}\right) \quad \text{where} \quad \xi(T) = \sqrt{\frac{\hbar^2}{2m^* a(T)}} \tag{2.27}$$

Here $\xi(T)$ becomes a characteristic length scale for the system. If we set the boundary $\psi(0) = 0$ it would take around a length of ξ before the wavefunction returns to its ordinary value of ψ_0. For this reason ξ is called the coherence length, and is a measurement as to how long it takes our wavefunction to recover from disruption.

Another interesting phenomena can be found if we assume that only the complex phase of our wavefunction varies with space, such that we can write

$$\psi(r) = |\psi|e^{i\phi(r)} \tag{2.28}$$

This has the advantage that our gradients are much more straightforward to work with, and the assumption reduces the second GL equation to

$$j_s = \frac{e^*}{m^*}|\psi|^2(\hbar\nabla\theta - e^*A(r)) \tag{2.29}$$

If we consider a doughnut shaped superconductor much larger than the coherence length there should be no current deep inside such that $j_s = 0$, giving us an expression for the potential $A(r) = \frac{\hbar}{e^*}\nabla\theta$. Inserting this into the classical expression for flux in a loop we get

$$\Phi = \oint A(r)\cdot dl = \oint \frac{\hbar}{e^*}\nabla\theta = \frac{n2\pi\hbar}{e^*} = n\Phi_0 \tag{2.30}$$

Where Φ_0 is then the flux quantization, or minimum amount of flux that can be trapped inside the doughnut. This is quite interesting, as it shows magnetic flux can only be stored in integer values inside the doughnut, any deviation from this value is negated by surface currents.

If we look back at eq.2.29 we notice that we can take the divergence of both sides, since we are in the London gauge the divergence of A(r) is zero. Assuming the current is in steady state the divergence of j_s should also be zero, and as such we can conclude that $\nabla^2\phi = 0$, meaning that phi has to be constant everywhere in the superconductor. This is the symmetry break which had been so hard to find, namely that this phase is arbitrary and fluctuating in non-superconducting materials, locking in place at the phase transition. Going back to the equation setting $\nabla\phi = 0$ we are now left with something quite similar to the London equation.

$$j_s = -|\psi|^2\frac{2e^*}{m*}A = -\frac{n_s e^{*2}}{m^*}A \tag{2.31}$$

Leading to the relation

$$|\psi|^2 = \frac{n_s}{2} \tag{2.32}$$

confirming the initial assumption, that the wavefuntion is the density of superconducting electrons.

Finally we can use the result from classical Landau theory that ties our order parameter to the constants a and b,

$$|\psi|^2 = -\frac{a(T)}{b} = \frac{n_s}{2} \tag{2.33}$$

This allows us to redefine the penetration depth found earlier in terms of a and b.

$$\lambda_L^2 = \frac{m^*}{\mu_0 n_s e^{*2}} = \frac{bm^*}{2\mu_0 a(T)e^{*2}} \tag{2.34}$$

Using this in conjunction with the coherence length we define a new parameter κ as being the relation between the two. This ratio turns out to be the sole defining factor in determining if a superconductor is type 1 or type 2.

$$\kappa = \frac{\lambda_L}{\xi} = \sqrt{\frac{2m^* b}{\hbar^2 \mu_0 e^{2*}}} \tag{2.35}$$

The reason this ratio is so important can be found when calculating the surface energy between a superconducting and regular surface. It turns out there are two different scenarios depending on the value of κ.

If $\kappa < \frac{1}{\sqrt{2}}$ the surface energy is positivemaking additional surface area unfavourable. This means that the superconductor will resist deterioration as it would create more surface and thereby lose energy. This causes the material to be a type 1 superconductor resisting change until the critical magnetic field is reached and it becomes more favourable for the entire material to change phase at once.

If instead $\kappa > \frac{1}{\sqrt{2}}$ surface energy becomes favourable to the system and we end up with type 2 superconductors. They instead deteriorate slowly in proportion with the applied field letting some of it through. This is done in the form of small vortexes letting flux quanta through similar to our prior doughnut example. These vortex structures were also found by solving the GL equations, before technological advancements let us probe the material directly. Thus we see that despite not being a microscopic theory the landau framework is still capable of predicting phenomenons on atomic scale.

As such we now see how valuable the Ginzburg Landau equations have been to the science of superconductors, despite not giving any insight as to what mechanisms lie beneath the phenomena it still allowed for the description and prediction of plenty resulting properties. We also note that the use of Landau theory goes far beyond what has been discussed here, with ideas such as Landau levels, Josephson Junctions and the quantum Hall effect being able to track their roots back to this general theory. [10] [11]

Chapter 3

NCCO

Among the electron doped superconducting cuprates the most known and researched variant is the compound $Nd_{2-x}Ce_xCuO_4$ also known as NCCO. It is a cerium-doped version of neodymium cuprate Nd_2CuO_4 (NCO) which is an anti antiferromagnetic Mott insulator. NCCO was the first electron doped superconductor synthesized [3], and it is representative of many of the essential properties of the electron doped cuprate family, although a significant difference in domain size can be found in the sister compounds like $Pr_{1.3-x}La_{0.7}Ce_xCuO_4$ (PLCCO) and $Pr_{2-x}Ce_xCuO_4$ (PCCO). In this section we will cover the main findings related to NCCO and the other n-type cuprates.

To classify a superconductor some of the most important things to identify are the phase diagram and the structure of the material. A phase diagram shows the state of the material, eg. superconducting or antiferromagnetic, as a function of doping and temperature, containing information about critical temperatures, the doping ranges at which superconductivity is present and about possible phase transitions in the material. The structure of the material helps theoretical advancements as it limits the possible symmetries allowed in the systems and as the position of the different elements is essential to the internal interactions from which superconductivity must arise.

3.1 Structure

Starting with the structure it is helpful to compare with the structure of regular hole doped cuprates to set the results in perspective, and such a comparison can be found in Figure 3.1. The hole doped cuprates have a structure which is called body-centered tetragonal K_2NiF_4 structure. In this structure layers of corner-sharing CuO_6 octahedra are stacked on top of layers of dopant material acting as a charge-reservoir, like La or Sr in the case of the superconductor $La_{2-x}Sr_xCuO_4$(LSCO). This structure is commonly known as the T structure. The electron doped case is a bit different however, while still a layered structure the copper oxide layer does not form an octahedral structure, limiting itself to a flat square structure, causing the copper-oxide layer to be completely two-dimensional and the dopant layer is forced to bind with the excess oxygen. This structure is known as the T' structure, however to what degree the altered structure affects the superconductivity is not

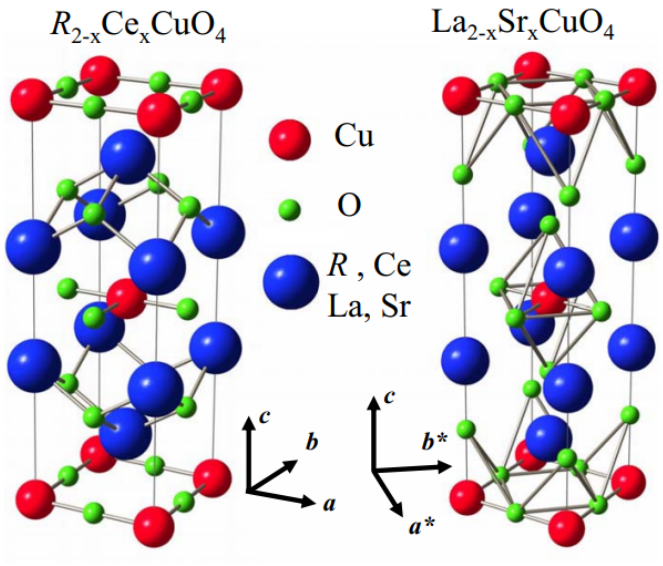

Figure 3.1: Structural differences between electron doped superconductors like NCCO (left) and hole doped superconductors like LSCO(right). Note how the n-type structure has no out-of-plane connections to oxygen in the copper-oxide layer resulting in a two-dimensional layer. Originally from Armitage et al. [13].

known. Whether a cuprate becomes T or T' structure depends on the size of the elements used in the dopant layer, this means that n-type superconductors are made almost exclusively using rare earth lanthanides as the charge reservoir due to their large atomic size, whereas regular hole doped superconductors can be made using a larger variety of smaller metals like Strontium or Yttrium.

Important when discussing the structure of a material is the lattice parameters. These parameters describe the width, depth and height of a unit cell and are labeled a,b or c. In the cuprate tetragonal structure the c-axis is perpendicular to the layers and we have $a = b \neq c$. For NCCO at x=0.15 doping the parameters are a=b=3.9441Å and c=12.0775Å. The a,b parameter does not change noticeably with doping however the c parameter is quite doping dependant and goes from c=12.16Å in undoped NCO to 12.05Å at x=0.18. [12] Knowing these constants is a great aide in fingerprinting the materials we synthesize as we can measure even small changes in lattice parameters, and use them to get an idea of how doped the crystal is, or if any impurities have distorted the lattices.

3.2 Properties

To find the key properties of NCCO we shift our attention to its phase diagram. Curiously, this is also best understood in comparison to the hole doped superconductors. As seen in Figure 3.2 NCCO has a narrow domain of superconductivity only being superconductive between 13% and 18% doping with an optimum at around 15% doping. Comparing this to the hole doped superconductors which can superconduct steadily at anything from 5 to 25% it is evident that electron doped

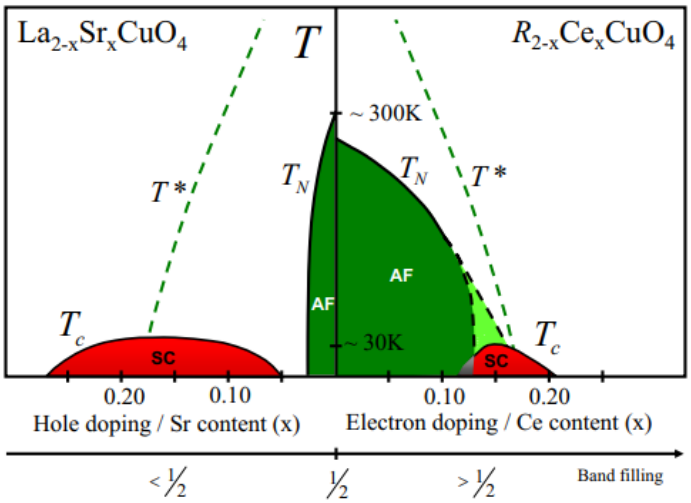

Figure 3.2: Doping dependant phase diagram of hole doped LSCO(left) and electron doped NCCO(right), illustrating the n-types smaller superconducting doping range, but larger antiferromagnetic origins. Originally from Armitage et al. [13].

superconducting domain is much less resilient. An important thing to note however is that this domain for NCCO is not absolutely clear, as the superconductivity of n-type materials are a result of a secondary process called annealing which we will discuss later. Depending on this process it might be possible to expand this domain to significantly lower doping levels [14]. This narrow doping range can be advantageous as it is significantly easier to examine the entire superconducting region for n-type superconductors experimentally. However it comes at a cost of resolution, as small errors in the synthesis can result in large changes in the resulting physics of the material.

Looking at the critical temperature which is in many ways the most important attribute, optimally doped NCCO becomes superconducting at around 25K. While this is not too much lower than the critical temperature of LCSO at around 35K,it is significantly lower than the best p-type superconductors for which T_c can reach more than 100K. This has somewhat limited interest in the electron doped superconductors as their low critical temperatures are a reoccurring problem across all variants, although other factors such as the need for annealing are also at fault for the limited interest.

What has however caught the interest of many, is the significantly larger domain of anti-ferromagnetic order found in low doped NCCO. Early experiments would often speculate if the superconducting domain overlapped with the AFM order with them being competing ground states such that a phase transition from superconducting to AFM could be found when applying strong enough fields to destroy the superconductivity. Early experiments confirmed this to be the case [15]. However upon further review it turned out that in reality such a transition did not occur and instead the elusive annealing process damaged the material causing part of it to decompose into $(\mathrm{Nd}, \mathrm{Ce})_2\mathrm{O}_3$ which would show anti-ferromagnetic response in the strong fields whilst the superconductivity died [16]. As such most scientists have

abandoned the hopes of such an AFM to SC transition, with a few still believing it possible at a single critical point in the phase diagram close to 0K.

3.3 Annealing

As mentioned before n-type superconductors are not inherently superconducting once the material is synthesized but instead they need an additional step in which the material is heated in an inert atmosphere to remove a bit of oxygen after which it suddenly becomes superconducting. While the method of annealing is covered in the synthesis chapter later on here we shall review the effects of annealing and possible explanations as to why it is so important for the superconductivity.

Serquis et al. did an experiment where they annealed NCCO for varying amounts of time at 1100°C and measured the superconducting properties of the materials [17], the results of which can be seen in Figure 3.3. Somewhat surprisingly it turned out that continuous annealing is not beneficial to superconductivity but that there instead exists a sweet spot just like doping where the superconducting qualities are greatly enhanced. This sweet spot was found to be around 4 hours, although it skips directly to 24hours and as such optima might be somewhere in between. The paper was a comprehensive study, and among other things also investigated different methods of NCCO synthesis, comparing both a nitrate decomposition and liquid-mix method. Interestingly the two methods had wildly different results when it came to how much annealing was optimal, with the liquid method favouring even shorter annealing times down to 10 minutes, showing that the synthesis process used should be kept in mind when gauging annealing conditions. Finally they also investigated the effects of copper concentration in the NCCO, comparing NCCO with a Cu concentration of 1.00 with one of 1.02 per formula unit. Curiously this minor change had a significant effect, as the 1.00 samples did not turn superconducting under 900°C heating, instead needing reductive annealing at 1000°C before showing diamagnetic signal. This was in contrast to all of the 1.02 samples which turned superconducting with only a 900°C anneal. Similar results have been reported by others such as Prado et al [12] who have been claiming to find no onset of superconductivity unless there is more than 1% excess copper in the sample. As such it seems that the copper concentration has quite a significant effect on the superconducting properties of NCCO. The exact reasons for this dependency remain a mystery, although one possible explanation is the general volatility of Cu causing part of it to evaporate in the synthesis process, resulting in Cu deficient compounds if additional Cu is not added beforehand.

Another interesting finding pertaining to annealing is the discovery that enhanced annealing techniques can improve the doping domain at which the material becomes superconducting. Regular annealing has the problem that areas close to the surface are affected significantly more by the annealing process than areas in the core. This effect often leads to an oxygen gradient along the sample, but as mentioned, increasing the heat or duration of the annealing destroys the superconductivity and as such finding methods for proper annealing has been difficult. Brinkmann et al. proposed to shield the surfaces of the crystals, covering them with polycrystaline pellets with identical composition, thereby allowing for a more

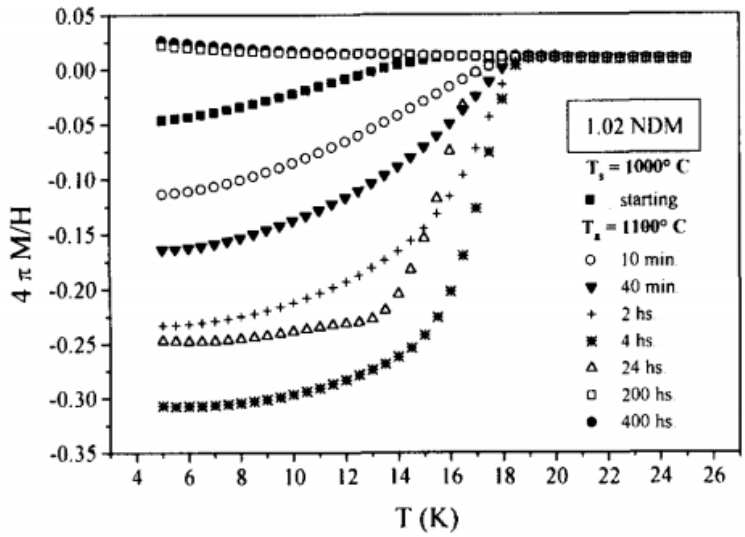

Figure 3.3: Meissner fraction against temperature for NCCO with a slight copper increase, annealed at different duration in 1100°C. Figure from Serquis et al. [17]

aggressive annealing process. In doing so the group reported superconductivity in 2x2x0.05 mm^3 crystals of PCCO with doping levels as low as 4% [14]. This raises a lot of questions about the nature of the reduction process, and it puts part of the phase diagram into question, as the phase of the materials obviously depends on many other factors than just doping level and temperature. One thing to note however is that Brinkmanns crystals were quite thin for crystal standards, and most similar experiments are conducted on thin films which are only a few atoms thick. Furthermore superconductivity at these lower doping levels have to our knowledge not yet been found for powders of the classical n-types or larger crystals, and thus one has to wonder what role the thickness of the material plays in these surprising results.

What actually happens microscopically in the annealing process that causes the onset of superconductivity is one of the greater mysteries in the field of electron doped superconductors. It is generally known that the annealing process removes a small amount of oxygen atoms, less than 2%, from the sample [18], however if these atoms are removed from the CuO plane, or from the rest of the structure, and whether or not oxygen removal is the only change caused by the annealing, is not fully known.

Given the removal of oxygen from the sample it also serves as a light electron doping, increasing the amount of carriers in the compound. It is tempting to consider whether this addition of carriers could be the cause of superconductivity, however if that was the case reductive annealing should have a similar effect to simply increasing the doping amount of the sample. As one cannot simply anneal regular NCO into superconductivity, and as the annealing remains essential to the onset of superconductivity regardless of doping concentration it seems such a theory is debunked. Fortunately many other explanations has arisen, with the three most prominent theories being as follows.

1) The T' structure has inherent defects when synthesized, resulting in many

apical oxygen atoms akin to the regular T structure. These apical oxygen atoms should increase scattering of conduction electrons and general resistivity in the sample thereby breaking the Cooper pairs and preventing superconductivity. By reducing it is believed that these impurities are removed, either by removing the oxygen all together or by forcing them back into the intended structure, and a superconducting state is reached. This theory has historically been the most accepted explanation[13] and some experiments did show that up to 60% of apical oxygen atoms were removed in the *undoped* compound Nd_2CuO_4 upon reduction[19]. However further experiments have been less in favor of this theory. In doped compounds the oxygen lost is significantly less, bringing the significance of the undoped results into question and making further studies of the reduction particularly difficult due to experimental resolution. One successful probing method however was through measurements with Raman scattering, a technique measuring molecular vibration using light, which showed that the mode associated with apical oxygen remained completely unchanged upon annealing [20], thus strongly implying that the concentration of apical oxygen atoms also remain unchanged.

2) An alternative explanation is that oxygen atoms were removed from the Cu planes creating vacancies in the charge reservoir which cause superconductivity. This theory came mainly as a result of the previously mentioned Raman measurements, as they revealed new excitations corresponding to vacancies in the cuprate layer appeared after annealing. This theory also explains why excessive annealing reduces and kills off superconductivity, as one creates too many vacancies inhibiting the conduction in the cuprate plane. The main problem of this theory however is that there is not really any good suggestions as to why creating oxygen vacancies in the Cu planes would lead to superconductivity, and as such we are lead to the third theory.

3) The third possibility takes inspiration from the previously mentioned findings by Mang et al. [16] in which reduction leads to an increase in the $(Nd, Ce)_2O_3$ impurity. While the impurity itself is not superconducting, and thus not that interesting, this theory views it as a byproduct of the process that creates superconductivity in the primary compound. It is theorized that some areas of the material acts as copper reservoirs, and under the reduction these copper atoms migrate to fill out copper vacancies elsewhere in the material, causing the leftover Ce and Nd to form the small bands of impurities that were experimentally detected. Thus at the cost of certain Cu deficient regions the majority of the compound has a drastically lowered density of Cu deficiency that would otherwise break pairs and inhibit superconductivity. This theory seem to align somewhat well with the claim that a slight amount of excess copper is required for the reduction to work. Still it is not exactly clear why such a process only occurs during reductive heating and not in common synthesis.

Ultimately none of the theories seem complete at the moment, often explaining only a handful of the experimental data and each containing large question left unanswered. As such the fundamental understanding of the annealing process is still far from complete, and further study seems needed.

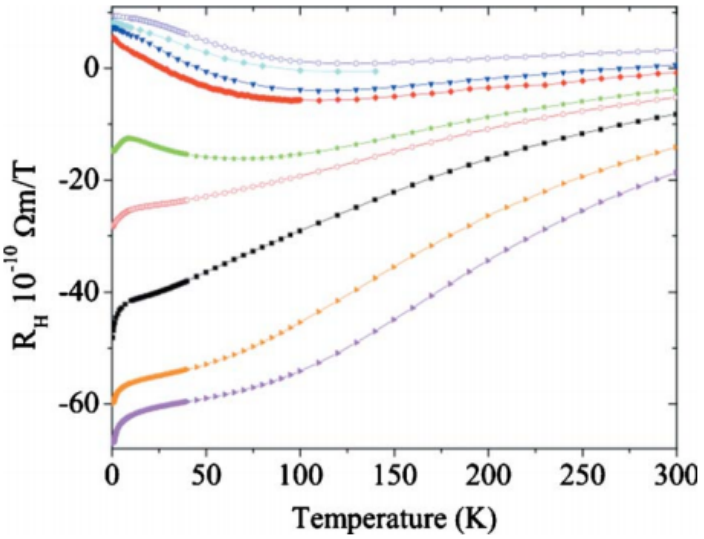

Figure 3.4: The Hall coefficient R_H for PCCO films with varying doping levels. From top to bottom x=0.19,x=0.18,...,x=0.11. Original experiment by Dagan and Greene [21] [13]

3.4 Charge carriers

When considering the electron doped superconductors one of the key distinctions comes not just from what dopant we use, but from what particle carries the charge of the system. Initial findings were that electrons were the charge carriers for the electron doped superconductors, something which made great sense given we added a surplus, and it is for this reason they are also labeled n-type for negative charge [3]. Upon further review however it seems that this behavior is less straight forward than initially assumed.

One way to measure the type of carriers is via the Hall effect, which utilizes that a current in a magnetic field induces a transverse electric field. The Hall coefficient R_H is defined as

$$R_H = \frac{V \cdot t}{I \cdot B}$$

With V being induced voltage, t being conductor thickness, I the current and B the applied magnetic field. The advantage of this effect is its dependency on the charge of the carriers, meaning a negative coefficient implies electron conductance and a positive coefficient hole conductance. This was done for a variety of different doping levels in PCCO by Dagan and Greene [21], the results of which can be seen in Figure 3.4. Here we see that the magnitude of the Hall coefficient tend to decrease with increasing temperature, but most peculiar is that at low temperatures the magnitude drops heavily with increased doping until the sign of the coefficient changes between x=0.15 and 0.16, around where the superconducting qualities of PCCO peaks. This made many wonder if multiple carrier types were at play in the superconducting state, as that would explain this behavior.

Further experiments were conducted using the Nernst effect, a thermal version

of the Hall effect where a heat gradient dT/dx on one axis and a magnetic field B along another induces an electric field E. It is measured using the Nernst coefficient.

$$N = \frac{E_z}{B_z \cdot \frac{dT}{dx}}$$

In superconductors one expects large signal in the superconducting state stemming from induced vortices, and a small signal in regular states with a single carrier band [13]. In electron doped superconductors, however, the signal is large regardless of state, which by many is taken as further evidence for the presence of two carriers in the system [13].

Finally the Fermi surface of the material has been directly measured using techniques like ARPES or Shubnikov-de-Haas oscillations[22] which showcase large changes in the Fermi surface around optimal doping, and has further evidence suggesting multiple carries at play. As such it is commonly accepted that both electrons and holes simultaneously act as charge carries in the electron doped superconductors. This has lead to many new theoretical propositions, with one of the most controversial theories coming from J.E. Hirsch. [23]. Hirsch proposes that the mechanisms behind p and n type superconductors are ultimately the same, and that superconductivity in electron doped superconductors is actually carried by the holes. He argues that adding an electron to a Cu site would cause a repulsive effect on the electrons on nearby oxygen atoms in the Cu-O layer, pushing them away to other Cu sites. In this way he sees the surplus of electrons as causing a "hole doping effect" on the oxygen atoms, which he believes contain the bands driving the superconductivity. This theory obviously goes against much of the knowledge that is believed to be established, and it currently makes several experimental predictions which seems wrong, so for now disregarding electron carried superconductivity would be hasty, however it does bring a plausible explanation for some of the phenomena observed, and it brings forth a new avenue to consider for theoretical and experimental work going forward. Ultimately it is still not clear whether or not the hole conductors are relevant to the superconductivity, or if the increase in holes is merely a coincidence, but their existence and the possibility of abandoning the notion that superconductive theories should have an inherent symmetry between holes and electrons, suggests it is a topic worth looking further into.

Chapter 4

Solid state synthesis

A key part of this thesis has been the synthesis of various different materials. Thus this chapter will cover some of the different methods used when synthesising various materials in the solid state. There are many different processes available and the one to choose depends largely on the result desired. In this chapter we cover the classic Solid State Synthesis and Traveling-Solvent Floating Zone methods as some of the basics, however many other techniques exist.

It is also worth noting that the exact timings and temperatures required can vary from material to material, and that this chapter as such is only a general outline of methodology, using the synthesis of NCCO as the primary example.

4.1 Calculation of compound masses

The first step in synthesis is making sure one has the exact amount of each material needed, as incorrect measurements will result in impurities causing flawed experimental results or in worst case prohibiting the growth of the desired structure. The amounts needed are calculated by looking at the target compound and the desired total weight of the final product. For NCCO synthesis the compound we wished to make was the structure $Nd_{1.85}Ce_{0.15}CuO_4$ and we wanted 2g. From the structure we can calculate the molar mass, adding together the atomic mass for each of the atoms in the compound, accepting the notion of 0.15 atoms as we are working on a macro scale.

Compound	**Nd**	**Ce**	**Cu**	**O**
Molar mass	144.24	140.12	63.55	16.00
Atoms per formula unit	1.85	0.15	1	4

Resulting in 15% doped NCCO having the molar mass
$144.24 \cdot 1.85 + 140.12 \cdot 0.15 + 63.55 \cdot 1 + 16.00 \cdot 4 =$ **415.37g/mol**
After which we simply divide the target weight with the molar mass to find the desired amount of mol material. For 2g NCCO we need $4.82 \cdot 10^{-3}$ mol. Now we can take this number and multiply with the atoms pr molecule to find the desired amount of mol for each compound, eg. for neodymium we want $1.85 * 4.82 \cdot 10^{-3} = 8.91 \cdot 10^{-3} mol$.

Here we could in theory simply multiply with neodymium's molar mass and find the desired mass of Nd powder. However when synthesising we rarely use pure material powder, and instead we use other compounds like oxides or carbonates for the base compound. This is done as they are more stable in ambient conditions, can be more willing to react and as we often make oxides anyway, requiring excess oxygen. In that case we have to use the molar mass of the alternative compound, eg. Nd_2O_3 instead. For Nd we see that the oxide has 2 atoms present pr molecule, and as such we need to scale the molar mass of Nd_2O_3 by a factor 1/2 as we want $8.91 \cdot 10^{-3} mol$ of Nd, not Nd_2O_3. Nd_2O_3 has a molar mass of 336,48 g/mol, slicing that in half and multiplying with the target mol Nd we get
$0.5 \cdot 336.48 g/mol \cdot 8.91 \cdot 10^{-3} mol = 1.499 g$
which is also what we used in our 2g synthesis. The full ingredient list is in Table 4.1 excluding oxygen as it is abundant from the atmosphere, and already contained in the other oxides.

Compound	**Nd_2O_3**	**CeO_2**	**CuO**
gram needed	1.4985	0.1243	0.3830

Table 4.1: Material list for synthesis of 2g $Nd_{1.85}Ce_{0.15}CuO_4$

4.2 Powder synthesis using solid state method

Having calculated the initial compounds one can now begin to make the materials. This method is a simpler method that does not require particularly complex machinery, and thus is the main way we synthesized materials in our own lab. The downside of this method is that generating larger crystals is not possible, it primarily produces powders which is comprised of tiny crystals. This is usually fine for X-ray scans, but if one wishes to do larger scale experiments probing the bulk of the material and its crystal structure, for instance some types of neutron studies, a large crystal is needed for which one must also make use of the Travel-Solvent Floating Zone (TSFZ) technique. However even techniques making larger crystals like TSFZ often begin with powders and as such solid-state synthesis is in many ways one of the most important synthesis techniques to learn.

The process of in-flux solidification can be broken down into a few steps.

1. Weighing
2. Powder Grinding
3. Initial Heating
4. Pulverization and Reheating
5. Post treatment - Annealing

Weighing: Here one measures out the calculated amount of each material needed. It is important to be exact as errors in the initial masses becomes impurities in the final compound. We aimed to be within ± 0.0005g of the calculated mass needed, as that was the accuracy of our scale. A thing to note here is that some materials, like Nd_2O_3 or CeO_2 absorb water from the atmosphere, and as such will result in faulty measurements. To mitigate this error these water soaking materials should be heated at 600°C for some hours before weighing letting the water evaporate.

Powder grinding: Once all the materials are weighed out they need to be mixed together. The purpose of this step is to maximize the contact area of the compounds, helping to facilitate the dry powder reaction. This grinding is done using a clean mortar and pestle, here it is important that no powder is spilled as it has not been properly mixed yet, making a spill cause the same impurities as improper weighing. The powder is ground until all of it has a homogeneous color and texture, after which it is poured into an Al_2O_3 crucible. After the grinding loss of powder is less detrimental as it is now well mixed and resulting only in loss of final product, and not in impurities.

Heating: The container is put into the oven which is then set to the proper heat and duration. For NCCO we used 900°C for 16 hours, heating at a rate of 2°C/minute. Cooling the sample was done by simply turning the oven off and letting the sample rest for some hours. In my experience cooling NCCO took around 5 hours. When cooling one should beware of breaking the equipment (or sample) through thermal shock, for instance by opening the oven while the sample is still around 900°C to cool it faster. The primary purpose of this step is to decompose the materials used, e.g by letting carbon in carbonates leave the sample as CO_2, readying the key elements for reaction. This is why we heat at a lower temperature (900°C) than the melting point of the metals (around 1000°C).

Pulverization and reheating: After the initial heating and cooling is finished the sample is scraped out of the container and back into the mortar for a second grinding. Here it might have condensed into a hard pellet, so it can be an idea to to cover the top of the mortar with something to prevent small fragments from flying away when crushing the pellet. When ground to powder again the sample is put back into the oven this time for a longer duration and higher heat, for NCCO we used 24 hours at 1100°C reaching just above the 1050°C melting point of NCCO. To avoid thermal shock we still heated at 2°C/min and cooled naturally. Depending on the material this step might be repeated multiple times to ensure a complete reaction. Once enough cycles has been run and the sample has cooled down the synthesis is complete.

Post treatment - Annealing: After the previous step the powder is theoretically ready for experiments, however often some additional work needs to be done on the sample to acquire the desired result. Examples of post synthesis treatment could be quenching the sample straight out of the oven, instead of natural cooling, or as is the case for NCCO annealing the sample in a oxygen deficient atmosphere. Here we describe the annealing process. To reductively anneal the sample the ground powder is placed inside a tube furnace with a constant nitrogen flow of 6L/min. Where a regular crucible cup was recommended for the prior steps, here a boat crucible is

recommended for added stability and surface area of the powder. The sample is then heated, in our case to 1100°C, with the usual 2°C/min, and kept there for the desired annealing time. We gave our NCCO 16 hours, however as mentioned prior a shorter duration might give better results. The sample is retrieved from the tube furnace and ground back into powder, after which the entire synthesis is done.

4.3 Crystal synthesis using TSFZ method

The Traveling-Solvent Floating Zone (TSFZ) method is used to make larger single-phase crystals than what can be achieved in a regular solid state synthesis. There can be many reasons as to why such a crystals is required. For instance they are useful when trying to investigate the crystal structure using scattering, as their single phase nature allow for systematic probing of each reflection plane individually. They are also often needed in neutron scattering experiments, where the crystals need a significant size and volume in order for the neutron scattering data to be insightful. Contrary to the regular solid state synthesis, the TFSZ method is a lot more involved, and significantly more difficult. It requires a lot more specialized equipment, such as a hanging tube furnace, a vacuum pump, a pellet presser and a mirror furnace, as well as constant supervision under the actual crystal growth, which can take multiple days. The TFSZ method is however a continuation of the regular solid state synthesis, and not an alternative. It requires a large amount of pure sample powder to melt into a crystal, and this powder is made using regular solid state synthesis. This section will cover the exact experimental procedures taken in growing a single phase crystal, using our attempt at growing an NCCO x=0.15 crystal as a starting example. The growth was carried out at the University of Lund in the lab by Elizabeth Blackburn, but unfortunately it was not possible to finish the crystal due to unforeseen hardware error.

4.3.1 Rod preparation

The first step of the TSFZ crystal growth is to make two rods, which will later be melted together to form the final crystal. These are called the feed rod and the seed rod, due to their respective role in the melting process, which will be explained later. In addition to the two rods a small pellet with high Cu concentration is also made, called a solvent pill. To make these rods a large amount of powder is needed, grown using the regular solid state synthesis method mentioned above. For our crystal we prepared 50g, equivalent to around $40cm^3$, of pure NCCO powder spread over 10 different samples such that impurities in one sample would not affect the rest. Only around 30g was strictly necessary for the actual crystal growth, however the preparation process can, and likely will, be subject to some failures which come at the cost of some powder sample, so having a surplus is essential. Pictures from the rod preparation can be found in Figure 4.1.

Pressing

First the powder is inserted in a long rubber tube with a constant diameter. For our rods we found a tube with 8mm diameter to be optimal, however due to equipment shortage the feed rod was made using a 6mm tube. A knot was tied on one end of the tube, and afterwards 10cm of the tube was filled with powder. Finally the top of the tube was filled with cotton or another similar material, with the purpose of allowing air to flow through while blocking any powder from escaping.

The tube is then connected to a vacuum pump, which runs until confident the air has been removed, which for us was around five minutes. To keep the vacuum the top part of the tube is sealed, for instance by bending it in an U-shape and sealing it with some tightly wound rubber bands.

Once a vacuumed tube is obtained, it is put into a hydrostatic press. To prevent deformation an metal guide form is placed around the sample, which is then submerged in water. A hydrostatic pressure of around 2 ton/cm^2 is applied to the sample, which for our press was 70MPa. The rod is kept under high pressure for around a minute before released again.

At this point the rubber tube can be carefully removed from the press and cut open, preferably retrieving a single rod without cracks. Should the rod have cracked it might still be possible to use a high quality part of it. For our crystal the first pressed rod broke in three, but fortunately we could use a 36mm long fragment to make a seed rod, as this rod does not need to be of significant size for the synthesis to work.

Sintering

Having pressed the rod, the next step is the sintering process, wherein the rod is melted, compressing and solidifying it. First a small hole is drilled through the rod such that a thin platinum wire can be inserted. At this stage the rod is likely still fragile, so it is recommended to carefully drill the hole by hand. Afterwards the rod is hanged in the platinum wire and lowered into a vertical tube furnace for sintering. It is important that the rod is centralized as much as possible such that it receives an equal heat distribution, however to mitigate for this potential error the rod is also slowly rotated under the sintering. Furthermore, to account for possible heat gradients along the tube furnace the sample is also slowly raised and lowered throughout the process, at a speed of 20mm/min. For our sample we heated the rod at 1250°C for 48 hours, with a ramping temperature of 200°C/hour. After finished heating the rod is cooled at a natural cooling rate, after which the process is done.

Solvent pill

The solvent pill is a small Cu rich pellet that is placed between the seed and feed rod, which has proven necessary when trying to make cuprate crystals, but is not a generally mandatory element for the TSFZ method. The Cu rich solvent pill serves two purposes. First of all it has been observed that during the furnace growth a significant amount of the Cu in the sample, due to its natural volatility, evaporates. This can ruin the stoichometry of the crystal, and thus having the solvent pill add

surplus Cu to the melt prevents this from being a problem. The second function of the solvent has it roots in the fact that for most cuprates, their melting point is significantly lower in a Cu heavy solution, falling with several hundred °C at around 80% CuO. In the surface area between the Cu heavy solvent pill and the primary compound rods the solution will still have a significant amount of CuO which brings down the melting point for the entire synthesis.

For the material used in the solvent pill one can, at worst, simply use regular CuO, however the best results are obtained by mixing CuO with the other elements in the main compound. For our solvent pill we made 3g using 85 mol% CuO, mixed with 15 mol% $Nd_{1.98}Ce_{0.02}O_3$, following the recipe from Tanaka et al [24]. We only heated it for 16h at 900°C, as higher temperature heating caused the Cu to melt completely and destroy the sample. Once a proper powder mixture is obtained, it is pressed into a pellet using a regular hydraulic press and a pellet form with the same diameter as the rods. Once pressed the solvent pill is finished and can be used in the crystal growth.

a) Creating vacuum in sample tube.

c) 40mm pressed rod with platinum wire.

b) Retrieving sample from hydrostatic press

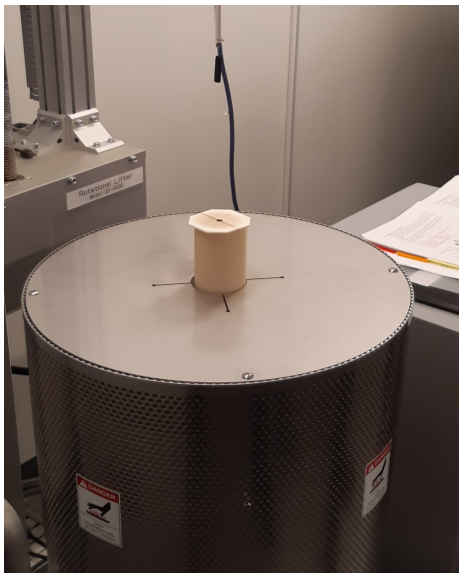

d) Sintering rod in vertical furnace

Figure 4.1: Different steps in the rod preparation process.

4.3.2 Crystal growth using mirror furnace

Once the seed rod, feed rod and solvent pellet is done the actual furnace growth can begin. While this section was supposed to continue following our NCCO crystal synthesis, the mirror furnace broke before we could finish the crystal, and will instead be finished in future work. For that reason this section only crudely explains the theory behind the image furnace usage, taking inspiration from Kira Eliasens thesis [25].

While many floating zone techniques exist the vertical floating zone technique using a mirror furnace is the most popular. The essence of this setup can be seen in Figure 4.3.2. As seen the seed rod is placed in a vertical holder inside a quartz tube, with the solvent pellet balancing on top of the rod. This is the reason they should have similar dimensions, as the solvent pellet might otherwise fall off or overflow when melted. The feed rod is hung in its platinum wire directly above the seed rod and then carefully lowered into contacting the pellet. The rods are again set spinning in opposite directions to minimize inhomogenous heating and finally mirror furnace can be turned on, beginning the melting process. The mirror furnace consists of a halogen lamp and a highly specialized mirror that reflects all of the light into a single concentrated position, creating massive heating at a single well controlled point.

To understand how the actual growth process occurs we first have to look at what is called the binary phase diagram for Nd_2O_3 and CuO, which is found in Figure 4.3. This diagram illustrates the melting point of the CuO+Nd_2O_3 mixture based on the CuO concentration, as well as the possible secondary phases it might form. When growing a crystal we are interested in achieving a single homogeneous phase with the structure of Nd_2CuO_4, albeit doped with Ce. At the focus point of the mirror furnace the high temperatures will cause the rods and solvent to melt, creating what we call the molten zone. Depending on the Cu concentration and temperature applied to the molten zone it will represent a different point in the binary phase diagram. The goal of this synthesis is then to ensure that all the conditions for the molten zone are met, to keep the phase of the zone right at the edge of the desired phase transition, represented by the purple axis in Figure 4.3. If they are not met the result is that secondary phases are created in the zone, which ultimately causes them to also be present in our final crystal. Due to inherent Cu variations from continuous evaporation and influx from the solvent, it is important to always be monitoring the molten zone during the crystal growth to ensure that it remains stable.

While the zone is stable, the focus point of the furnace is slowly moved up along the feed rod, at a speed of around 1mm/h, thereby moving the molten zone with it. The lower part of the molten zone will then slowly cool off, thereby crystallizing into a single phase just as desired. Once crystallizing the melt will prioritize following the structure of the crystal underneath it, which is why we utilize a seed rod. While the ideal seed rod would be an already single phase crystal, these are not often available. Instead we use the seed rod which still contains the correct lattice parameters and serve as a good starting point for the crystal to form on, thereby acting as a seed for the growth, hence the name. As the molten zone is moved up larger and larger

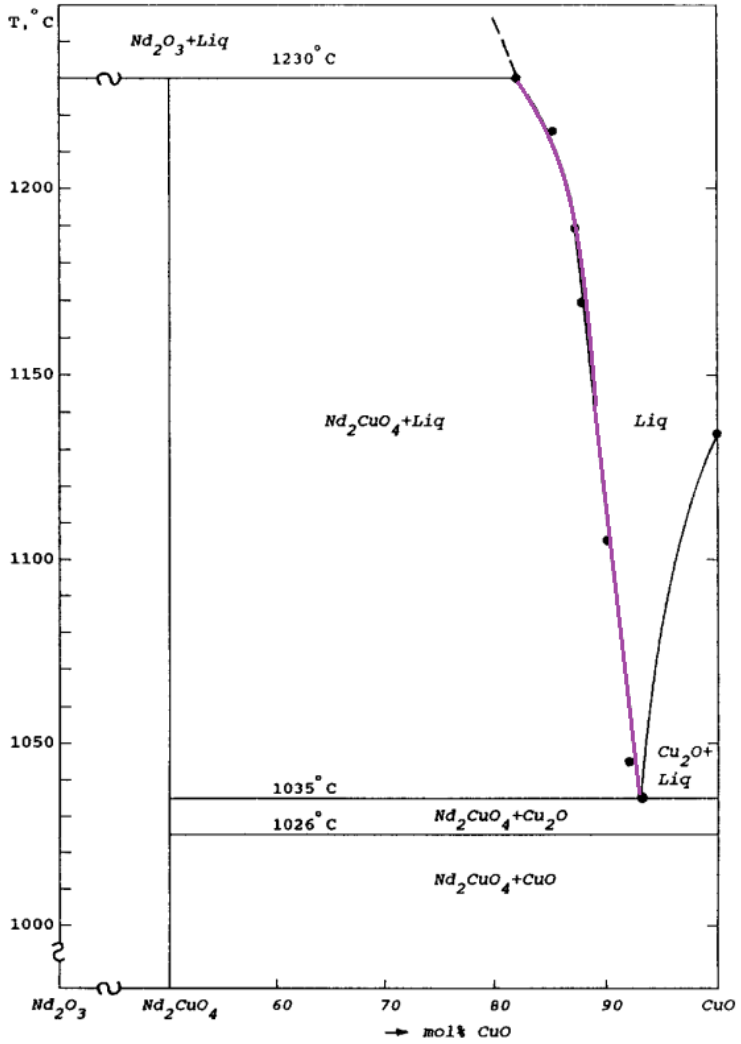

Figure 4.3: binary phase diagram for Nd_2O_3 and CuO. The desired point for a mirror growth is marked with purple, indicating that the melt zone should be kept between 1035 and 1230°C, and contain 80-90% CuO. Original from [27]

parts of the feed rod are melted, supplying the molten zone with material which is later crystallizing into the single phase crystal, thus the name feed rod.

Once the entire feed rod is used up, or the crystal growth is simply of desirable size, usually after a few days, the mirror growth is finished and the crystal can be extracted. At this point it might be a good idea to give the crystal a secondary heat treatment to fully harden it and smooth out potential impurities or excess oxygen that could be present. This is usually done by annealing the crystal under a constant oxygen flow for 50 hours at 900°C, then slowly cool it to 500°C, heating it for another 50 hours after which the growth should be fully done.

Chapter 5

Characterization methods

While the process of synthesizing new materials can be interesting in itself, figuring out what reactions can and cannot occur or how to tweak the synthesis process, the most interesting work lies in analyzing and characterizing the synthesized materials and their properties. To do this a large amount of different experimental techniques have been developed, each giving unique ways to study material properties. In this chapter we will cover the experimental procedures for the characterizations tools used throughout the thesis, as well as the theoretical background for some of the instruments.

5.1 X-ray scattering

The usage of X-rays to probe material structures has quickly proven to be one of the most versatile and practical tools available to scientists. It has many advantages, in particular it is non destructive allowing for multiple measurements on the same sample, it gives accurate information on the atomic structure of the material and compared to many other experimental probes it is inexpensive and fast.

5.1.1 Theoretical background

In X-ray scattering we use electromagnetic waves of similar wavelengths to the spacing between atoms in crystals, allowing the atoms to absorb the x-ray and re-emit them as spherical waves which is the foundation for diffraction. We can approximate the collision between the x-ray and the material as a plane wave colliding with a periodic grid. From conventional physics we know that waves scattering in a two-dimensional grid only has positive interference when obeying the Bragg condition, namely

$$2d\sin(\theta) = n\lambda, \quad n = (1, 2, 3...) \tag{5.1}$$

Where d is the distance between each layer of the grid, λ is the wavelength and θ is the incident angle of our wave with respect to the surface of our grid, which at positive interference must also be equal to the reflected angle. Real crystals however are three dimensional, and in that case we have entire planes of reflection instead of a single line grid. These planes however depend on the orientation of the

crystal, those that have had introductory condensed matter physics will recognize these planes as those labeled by the miller indexes. Each plane will have differing scattering conditions, which becomes problematic when we consider 3-dimensional scattering in more detail, following the example from Snokes chapter on X-rays in *Solid State Physics: Essential Concepts* [28].

We first construct the scattering vector which is the difference between the momentum of the scattered wave and the original incoming wave.

$$\vec{S} = \vec{k} - \vec{k_0}$$

We also know that two atoms separated by a vector $\vec{a}$ will cause a phase difference

$$\delta = \vec{S} \cdot \vec{a}$$

This means that the total amplitude of our scattered wave will be something akin to

$$A \propto \sum_{n_1,n_2,n_3} e^{i(n_1\vec{s}\cdot\vec{a_1}+n_2\vec{s}\cdot\vec{a_2}+n_3\vec{s}\cdot\vec{a_3})}$$

Where $\vec{a}_{1,2,3}$ are our unit lattice vectors. We see that if there is destructive interference in just one direction the entire amplitude vanishes, hence we only have a scattering peak when our scattering vector S overlaps more or less completely with our unit cell parameters in all three dimensions fulfilling

$$\vec{S} \cdot \vec{a_i} = 2\pi n_i$$

These three conditions, are called the Laue equations.

Experimentally we can adjust the wavelength of our x-ray, thereby adjusting the magnitude of the momentum vector $\vec{S}$, and we can adjust the lateral, or longitudinal incident angle with respect to our sample. This gives us exactly 3 degrees of freedom which allows us to fulfill all three Laue equations simultaneously, for which we can measure the diffraction. Unfortunately simultaneously finding the exact reflection angle and wavelength needed can be neigh impossible when no prior info of the material exists, requiring a scan of every reflection angle at every possible momentum. To solve this issue knowledge of either the momentum, or the scattering angle is sacrificed, in order to quickly fulfill all scattering conditions. This separates X-ray experiments into two different types, Laue diffraction, in which momentum information is lost, and powder diffraction, where the scattering angle remains unknown.

For Laue scattering we use white light on a single phase crystal, as it covers all wavelengths. That way we can quickly find the orientations of the crystal at which diffraction occurs, which lets us find all the refractive planes in the crystal and thus determine the crystal structure. The downside however is that by using white light that covers all wavelengths, the exact wavelength of the light that scattered remains unknown, which is what would otherwise grant us information on the atomic spacing distances in the crystal.

For powder diffraction we instead use monochromatic light such that we know the exact wavelength at scattering. However instead of examining a single-phase crystal we use a powder, which consists of many tiny crystals scattered completely randomly, such that they cover all possible orientations of the crystal, and thus

scatter at all possible angles. The intensity at each angle is then measured to complete the measurement. This intensity will vary with reflection angle as a result of the varying distances between reflecting planes, granting us insight into the atomic spacing, at the cost of knowing exactly what scattering plane these inter-molecular distance apply to.

The two X-ray methods are best used in conjunction. First the possible scattering planes are mapped using Laue scattering, giving full knowledge of the crystal symmetry and structure. Knowing the structure of the crystal it is possible to calculate expected powder diffraction patterns for varying possible atomic spacing. By comparing to the powder diffraction measurement an exact fit can be found, thereby giving the correct atomic spacing, with which and the entire crystal structure is known.

5.1.2 Instrument

Throughout this thesis work we have made widespread use of powder diffraction, which will be the focus of this subsection. A powder diffractometer, as mentioned before, utilizes a monochromatic x-ray beam. This beam is usually obtained by exciting a metal with electrons causing it to emit x-rays of a characteristic wavelength, after which one might use a monochromator to further ensure only the desired wavelength passes through, although this can come at the cost of intensity.

An advantage of this method is that by using the same metal type different instruments can produce exactly the same x-rays wavelengths, standardizing the measurement and allowing for easier comparisons of data. One of the most common wavelengths utilized in powder diffraction experiments is the copper K_α wavelength 1.5418Å [29]. We used an X-ray of the model Bruker D8 DISCOVER, which also utilizes this Cu source. It is important to note that this model does not utilize a monochromator, which has the consequence that the emitted X-ray is twofold with nearly identical K_α wavelengths, $K_{\alpha,1}$ and $K_{\alpha,2}$, causing the measured peaks to have a smaller "shoulder peak".

Once the beam is in place, it is aimed towards a powder sample on a flat disk that does not interact with the x-rays, giving the desired scattering at all angles. Here arises a problem which makes measurement more tricky than simply sweeping a detector through the relevant angles. As the sample has a finite width on the disk the incident and reflected angles change slightly depending on the position on the disk, causing an unfocused beam which hampers the quality of the measurements thanks to a significant uncertainty on the actual measured angle. To prevent this most diffractometers use an approximate Bragg Brenato parafocusing geometry, an example of which can be seen in Figure5.1 [30]. To achieve this geometry, which re-focuses the beams at one point, the angle between the source and sample must be equal to that between the sample and detector. This is commonly achieved simply by moving the X-ray source and detector simultaneously while performing the measurement, and schematic of this typical powder x-ray setup is shown in Figure 5.2.

Another problem many samples can encounter lies in the quality of the samples. Powder samples usually have two types of errors that can drastically lower the

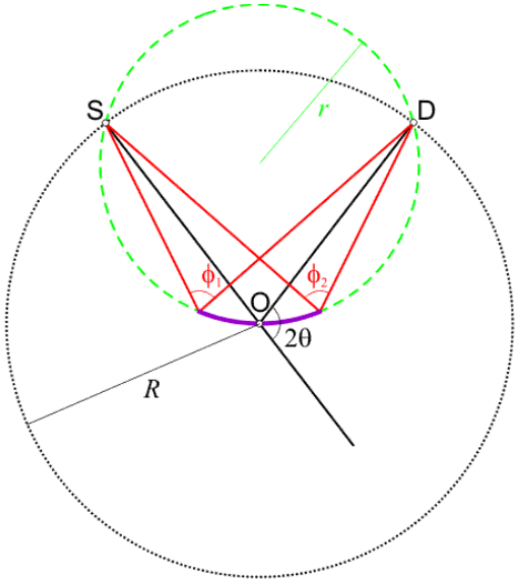

Figure 5.1: Schematic of the Bragg Brenato parafocusing geometry. When both the x-ray source and detector are angled at 2θ, and the distance large enough such that the circle section is approximately flat, the effects of the disk width are almost nullified. Adapted from [30]

quality of a measurement. The first possible problem occurs if the grains are too large. This reduces the amount of crystals on the disk, ruining the assumption that there are enough grains to cover all possible scattering orientations equally, thereby causing the relative intensities between peaks to be wrong. The second possible error is an underlying systematic orientation of the sample grains, resulting in some reflecting planes not being explored properly, if at all. This can for instance occur when dissolving a powder sample in a liquid when smearing it out on the sample disk. To help mitigate the large grain error, many instruments rotate the sample disk at a constant rate ω to broaden the orientations of the powder crystals, ensuring that a larger, and thus more statistically significant, part of reflection space is explored, although only in the two spinning dimensions. If the sample is not completely illuminated by the incident beam rotating the sample also allows for a larger amount of the sample to be examined. The only downside to this is the possibility of powder moving or falling off the sample if spun too quickly, requiring a slower rotation speed which slightly prolongs the measuring process. The second crucial error of inherent alignment is harder to mitigate instrumentally, fortunately this error often becomes clear when analyzing the actual data, as certain expected peaks will likely be almost completely absent.

5.1.3 Experimental procedure and analysis

The actual usage of a powder diffractometer is rather simple and will be covered in this subsection. First the powdered sample is put on a disk. It is important to ensure that the grain size of the sample is small so it can be advisable to ensure that it has been ground up properly, and if possible the sample can be sieved. To put

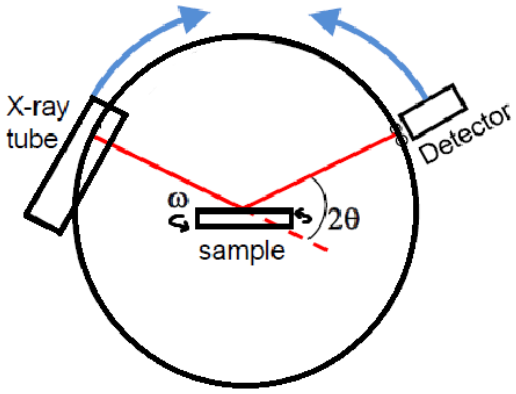

Figure 5.2: A schematic rendition of an X-ray powder diffraction instrument from [29]. The X-ray source and detector are moved in synchronization to retain a Bragg Brenato geometry, minimizing focal inaccuracy.

the sample on a disk it is often easiest to mix the sample with ethanol, provided the sample does not dissolve completely, giving better adhesion to the disk, and making it easier to smear out. Unfortunately this comes at a risk of grain alignment once the liquid evaporates, although such an error has yet to occur in our samples. The disk is placed in the instrument after which a measuring program with the desired runtime and angle spectrum is chosen. Longer runtimes or a narrower scan can give higher quality measurements, so picking the right program is often a balancing act between time and data quality. Our measurements usually took around 30 minutes and scanned up to $2\theta = 70$.

Once the scan is done the data comes in the form of a (2θ,intensity) data file, best used to create plot like the one seen in Figure 5.3. The resulting pattern is quickly compared with measurements of the same, or a similar, compounds found in one of the many powder x-ray databases, like ICSD [31]. Discerning whether all the peaks match, and if the relative intensities are as expected quickly allows us gauge the quality of our measurement and sample. If extra peaks at unexpected positions are found, these can be used to identify the impurities of the sample, as seen where Figure 5.3 where two unexpected peaks were found to belong to CuO, indicating that the reaction was not complete.

However, to fully analyze the sample a quick comparison of peak positions is not enough. Here a full analysis on both peak positions, shapes, atomic parameters and possible secondary phases are to be conducted. This is usually done with the highly flexible Rietveld refinement technique described in the next section.

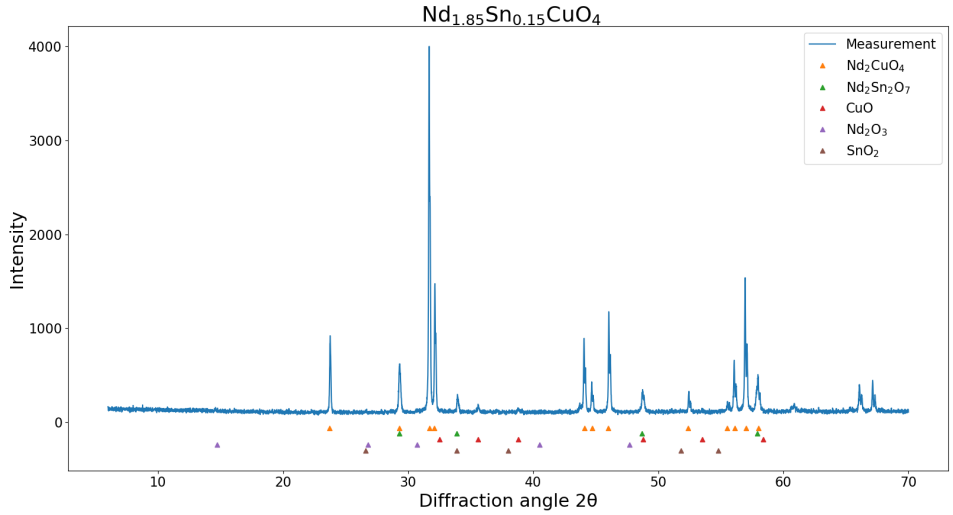

Figure 5.3: Example of an X-ray powder diffraction measurement, alongside signature peak positions of possible impurities below the measurement. The compound synthesized was intended to form $Nd_{1.85}Sn_{0.15}CuO_4$ but as seen unexpected peaks matching the signature of starting compounds SnO_2 and CuO shows that the intended material did not form.

5.2 Rietveld refinement

While it was theoretically known that diffraction patterns contained information about the crystalline structure, actually extracting that information from the diffraction patterns proved increasingly challenging for the early crystallographers, especially when it came to powder diffraction. Many of the atomic peaks would have significant overlap which caused problems as the conventional method of analysis used integrated peak strength, and overlapping peaks as such had a hard time accurately accounting for relative intensities. The solution to this problem came with the rise of computers in the 60's allowing for numeric fitting of a Gaussian model to the peak data, allowing an estimate of relative peak strength. The most famous way to tackle this problem was published by Hugo Rietveld in 1969 being the procedure which has henceforth come to be known as Rietveld refinement [32].

In Rietveld refinement you fit a model corresponding to the theoretically expected structure directly to your measurements using a least squares fit. The structure fit is calculated from a large amount of parameters which are continuously refined, such as peak positions calculated from unit cell geometry and distances and peak shape corresponding to powder grain structure. Furthermore instrument specific factors are taken into account, such as a possible general offset in the measured angles, allowing comparison of data and refinements between various different instruments. A proper refinement thus grants a solid insight into the microscopical structure of a sample, which can be a great tool in subsequent analysis. For instance when doping a material with a slightly smaller compound it can be effective to look at the modelled unit cell parameters to see if the compound has shrunk as a result

of a successful doping procedure.

However, as with all fits using a plethora of parameters, it is easy to run into false minima ruining the refinement, and just as easy to make a good fit while losing all connection to the physical reality. Thus this section will cover the basic steps of a proper Rietveld refinement along with some theoretical motivation for each step.

5.2.1 Initial procedures

To begin a Rietveld refinement it is important to have the right software specialized for refinements. We used the program Jana2020[33] which is free and contain most of the essential features needed for a Rietveld refinement, although it is prone to crashing and requires a bit of patience. Once a program is acquired the experimental data and intended structures should be imported. The data is best formatted as a simple x,y row containing angle and intensity, however the format for the crystal structure is a bit special and is called a Crystallographic Information File also known as a CIF. This file contain the crystal structure and symmetries, as well as the elements contained in the compound and expected position of the signature peaks. When importing the data you also tell the program what kind of radiation was used, x-ray,neutrons etc, and what wavelength. Finally before beginning the refinement you can add additional phases by importing additional CIF's, this could be useful if you suspect that a particular impurity might be present in your sample, and want to include it in your refinement fit.

5.2.2 Le Bail refinement

The first step in the refinement is to abandon the contents of the material completely and use the free fit method called Le-Bail, which considers only the basic structure and symmetry of the unit cell [34]. This is done because we usually don't have the correct structure available when beginning refinement, resulting in erroneous intensity estimates. Errors in intensities further propagate to misjudging other important parameters such as the full-width-half-maximum or the degree of peak asymmetry from the instrument. Le-Bail refinement simply fits the intensities freely to match the data, and is thus used to determine the correct peak shapes and positions before beginning the full Rietveld refinement, wherein the intensities are instead calculated based on unit cell content. When Le-Bail refining, the parameters refined are usually done one or two at a time in the following order

Background: Sometimes background is present in the measurement, especially at lower angles. To avoid confusing this with broad peaks the background is identified and removed. Most refinement programs do this automatically using a polynomial fit of the baseline, however it is advised to double check that the fit is correct before beginning the bulk of the Le Bail refinement.

Shift: The fist thing to identify is the inherent offset in 2θ caused by our instrument and powder alignment, ensuring that our measured peak positions align with what our model predicts.

Cell parameters: In this step we refine the unit cell dimensions, as the unit cell parameters are quintessential to the peak positions. What we don't refine here,

and first do in the full Rietveld step is the internal coordinates of the atoms with respect to the unit cell, modelling atomic displacements from the unit cell structure.

Peak asymmetry: Another refinement of instrument induced errors is the asymmetry. The peak asymmetry models the tilt of the peaks which, if noteworthy, can throw off the shape fits that usually assume a symmetric centralized distribution. While various methods exist to model this asymmetry exists we have deployed the Howard method, also called Boole's rule which refines just a single parameter. It is recommended to continue refining this parameter alongside the next step of peak shape, as they are inherently intertwined.

Peak shape: When modelling the peak shape the two most common fits are Gaussian or Lorentzian. The best distribution depends on the experimental specifics, however usually we choose to combine the two in what is called Pseudo-Voigt peak shape function which is just a linear combination of the two in the ratio $\frac{x}{1-x}$ for a mixing parameter x [35].

The pseudo-Voigt peak shape has 6 parameters that can be refined, GU, GV, GW, GP which is tied to the shape of the Gaussian, alongside LX and LY which defines the Lorenzian part of the fit. GU,GW and LX are the variables which cause the most significant change in the fit, and should thus not be refined simultaneously, however refining one of the major parameters simultaneously with a minor one will in most cases not cause problems. Our most employed order of refinement was GU+GV $\longrightarrow$ GW+GP $\longrightarrow$ LX+LY

Tweaks: With all the parameters characterizing the peak shape refined, it can be a good idea to refine some, or even all, of them again as they by and large depend on each other. A better pseudo-voigt model might mean that the unit cell parameters need some additional tuning, after which the model might need further tuning etc. When the fit is satisfactory the main refinement can begin.

5.2.3 Structural refinement

Having finished the Le-bail refinement for all phases and thus acquiring proper peak shapes the next step is completing the structural refinement. Here it is important to turn off refinement for all parameters related to the peak shape and instrument that were used in the Le-bail refinement, to avoid refining everything simultaneously. When this is done switch the refinement mode from Lebail to Rietveld, but without running the refinement yet.

Constrains: In this step we incorporate the constrains of the crystal structure that the CIF does not otherwise contain. This step is only really relevant for doped compounds like NCCO where we explicitly tell the program that our Neodymium and Cerium atoms should be interchangeable in the structure and thus have identical coordinates, and/or atomic displacement parameters(ADP). If the program can tweak occupancy use "keep overall sum". Wait with running a refinement till next step.

Fixed parameters: In this step we fix certain parameters in order to avoid immediately refining for everything simultaneously. Here we can fix either the coordinates, or ADP of each atom. It is recommended to run a refinement with both fixed first, and then a refinement keeping only the ADP locked, such that we refine

for the atom coordinates. Refining for the ADP is not always possible, so attempting this should only be attempted after the remaining steps, if the refinement otherwise seems to go well.

Absorption correction: Some elements in our materials have a tendency to absorb some of the x-rays thereby reducing the measured intensity. If this is the case it will often result in an asymmetric fit where the model undershoots for low angles and overshoots for higher angles, or vice versa. To correct for this error we run a few refinements while steadily reducing the symmetrical reflection value until the opposite type of asymmetry in our fit occurs. The exact nature of this parameter seems to be a bit of a mystery however, as changing the reflection from 1, to 0.1 and back to 1 sometimes drastically improve the fit.

Phase volume fractions: If your fit refines with respect to multiple phases it is first now, after having refined all the other parameters that refining the volume fraction should be done. When finding this ratio it is important to keep in mind exactly what kind of fraction your refinement program gives you. Jana2020 will for instance show a mass fraction of the different phases, requiring you to use the individual molar masses of each phase to convert into the more interesting molar fraction.

With this the refinement should be complete, giving a complete structure of all the possible phases in the compound, to be used in further analysis of the compound. However even after following these procedures the fit is not guaranteed to be perfect. Low sample quality or insufficient diffraction data can cause a skew in the data that is difficult to model, and with how many parameters are refined getting a perfect fit can be quite challenging. If the fit is not satisfactory most programs plot a line showcasing the difference between plot and data which is great for identifying areas of error, with which the official Rietveld guideline paper can be consulted for possible solutions [36].

5.3 Neutron Scattering

Neutron scattering is an alternative scattering technique that in many ways can complement the x-ray technique. It is a rich technique with many possible use cases, for instance we intended to use it in one of our experiments to examine the magnetic response of NCCO before and after annealing. Unfortunately this experiment was never conducted, due to a lack of crystal and beamtime, and as such we will omit explaining the instrumental and experimental procedures in this section. Instead we focus on the theoretical capabilities of neutrons as a tool, and compare them with the X-ray, investigating when to utilize which technique.

Neutron scattering has its root in the particle-wave duality of all matter. A neutron with momentum $\vec{p}$ will have a wavelength λ associated with it, which follows from de Broglies formula.

$$\lambda = \frac{h}{p} \tag{5.2}$$

Where h is Planck's constant. Knowing this we can tune the wavelength of the neutron to be similar to the inter atomic spacing of our material, and from there apply most of the same scattering theory covered in the X-ray section to the neutron,

as both act as a plane wave to the lattice which must scatter according to Bragg's law for constructive interference.

One key difference between the two however, is that the neutron reacts with our sample using the nuclear interaction, and not the electromagnetic interaction which the X-ray uses. This has the consequence that whereas the X-ray interacts with the electron clouds via a strong electromagnetic force, the neutron only interacts with the nucleus of the atoms, and only very weakly. Interacting with the electron cloud can result in significant uncertainty in the atomic position, making neutron scattering the preferred tool for exact positional measurements, however most importantly is the difference in interaction strength. Due to the strong interaction X-rays cannot really penetrate materials, only really probing the surface of a sample. The neutrons however have a weak interaction with matter, meaning that most of the scattering happens in the bulk of the material, allowing effective probing of the entire material, and even allowing probing of a material inside other equipment such as a pressure cell or cryostat. The cost of this feature however is that neutron scattering events are much rarer, requiring a significantly higher amount of neutrons to have significant measurement data throughout the entire material. This makes neutron scattering measurements unfeasible on a local lab scale and everyday use, unlike X-rays. Neutron experiments are instead restricted to massive neutron facilities with measuring periods often spanning multiple days, and require a long application process in order to acquire beamtime, resulting in X-rays being the preferred tool for diagnostic measurements on most samples.

Another useful feature of the neutron is that the energy required for our desired wavelengths are also similar to the elemental excitation energy in most solids, allowing also the momentum transfer of the neutrons to be measured. Combining the ability to probe only the nucleus, with the energy dispersion measurements, allow for additional information about the dynamics of the material, through inelastic coherent scattering, and can among other things be used to directly measure the characteristics of phonons present in the sample [37].

Finally one of the most important features of the neutron is its magnetic moment. This allows the neutron to interact with the spins of the atoms it probes, allowing the neutron scattering to extract information about the inner magnetic dynamics of a material. It is this feature which makes it a popular tool of choice for probing especially cuprate superconductors, as the local magnetic interactions within the superconductor seems to be a crucial for the onset of superconductivity in cuprates [38].

5.4 Superconducting Quantum Interference Device

As mentioned before the onset of superconductivity theoretically results in perfect diamagnetism. A SQUID is a magnetometer combined with a cryostat that allows for accurate magnetic measurements at low temperatures and thus is an excellent way of measuring superconductivity.

5.4.1 Theoretical background

A SQUID makes use of something called Josephson Junctions to measure fluctuations in the magnetic flux. If we return to Landau theory for a moment we recall that the onset of superconductivity meant that the order parameter, the wavefunction ψ, would lock into a single phase. The Josephson Junction considers what happens if two superconductors with different phases are separated by a very thin insulator, such that we have $\psi_L = |\psi_0|e^{i\phi_L}$ and $\psi_R = |\psi_0|e^{i\phi_R}$. If we let the total wave equation in the insulating material be a linear combination of these two, and plug it into the second Ginzburg Landau equation we retrieve the following expression for the current [4].

$$j_s = \frac{2e\hbar|\psi_0|^2}{m^* d}\sin(\phi_R - \phi_L) \tag{5.3}$$

As we can see a steady current flows through the junction without any voltage difference, this is called the Josephson effect. The application to the SQUID comes when we consider a magnetic field parallel to the surface of our junction, such that $B = B_z$ and $A = A_y(x)$. This field leads to a phase difference between the top and the bottom part of the superconductor, $\Delta\phi_R$ and $\Delta\phi_L$. Reminding ourselves that $\nabla\phi = \frac{-e^*}{m^*}A$ we can write

$$\Delta\phi_L - \Delta\phi_R = \oint \nabla\phi = \frac{e^*}{m^*}\oint A\,dl = 2\pi\frac{\Phi}{\Phi_0} \tag{5.4}$$

From this we see that the phase difference between the two sides of the junction depends on the magnetic field applied, which in turn means that the current going through the junction also must vary as a function of the magnetic field strength.

This is the phenomena utilized in the SQUID to measure the magnetic field, by taking advantage of the induced change in current. In practice the SQUID uses a slightly different setup which we will discuss in the next section, but the essential mechanism allowing for the measurements is still the Josephson effect.

5.4.2 Instrument

While many different types of SQUIDs exist we will discuss the inner workings of the traditional and simple DC SQUID, based on R. Simons user guide [39]. The DC SQUID is chosen as its use is still widespread, and the working principles are still fundamental for many of the modern variations.

In essence a SQUID is a superconducting ring with two opposed Josephson junctions and a voltmeter applied across the ring, a schematic of which can be seen in

Figure 5.4. An essential concept for the SQUID is the critical current, the maximal current a superconductor can sustain before losing superconductivity. The SQUID is designed such that the critical current of the Josephson junctions are significantly lower than the rest of the ring, making them gate the allowed levels of supercurrents. If we label the critical current of the entire system I_c we can see that each of the two Josephson junctions are only able to sustain a critical current of up to $I_c/2$ before losing superconductivity, at which point they turn resistive, resulting in a measurable voltage across the ring.

As discussed earlier a superconducting ring can only contain an integer amount of flux quanta Φ_0, if the field is increased slightly from that flux quanta a screening current will appear in the loop to exactly cancel out the excess flux. Interestingly once the excess magnetic field surpasses $\Phi_0/2$ the shielding current changes direction as it is now more favourable to increase the field to the next flux quanta. Thus the surface current continuously oscillates, changing size and direction as the magnetic field is increased, reaching max surface current $I_{S,Max}$ at $\Phi_0/2$ and vanishing at every flux quantum integer. This shielding current can be seen as the more intuitive explanation for the Josephson effect mentioned above.

Important to note is that the screening current superimposes itself on top of any other current applied to the system, and as the screening current circulates it effectively reduces the critical current threshold for one of the junctions, while increasing it for the other. Interestingly, if the critical current of one junction is reached, the sudden resistance will cause all the electricity to change path to the other junctions thereby also destroying superconductivity there, resulting in a measurable voltage across the ring. As such any excess flux causing a shielding current, will also lower the critical current level of the entire system.

It is by combining these two attributes, the critical current and the superconducting response current, that the SQUID can attain its high accuracy. To do so a bias current is sent through the ring, such that the bias current at each junction is exactly equal to $\frac{I_C}{2} - I_{S,Max}$. Whenever the field increases by a flux quanta, the superconducting response current will cause the system to reach a critical current, creating a voltage which is then easily measured. By simply tallying up the number of voltage signals measured, the SQUID can give the magnetic change of a sample with an accuracy of half a flux quanta. If even more accuracy is needed the bias current can be further adjusted at the final measurement, until a voltage appears, at which the exact residual flux is measured, with the only source of error being internal magnetic field fluctuations caused by the apparatus.

With the immense accuracy gained this way, the SQUID is one of the best tools available to measure magnetic response, however it does have some problems. For starters the SQUID can in principle only measure changes in the magnetic field, and thus unless calibrated with an already known magnetic field, can't give insight into the complete magnetic response of a material. Another downside is that measuring with the SQUID is a slow process, and as such if the high accuracy is not needed it might be better to use another instrument such as a vibrating-sample-magnetometer to measure the magnetic response.

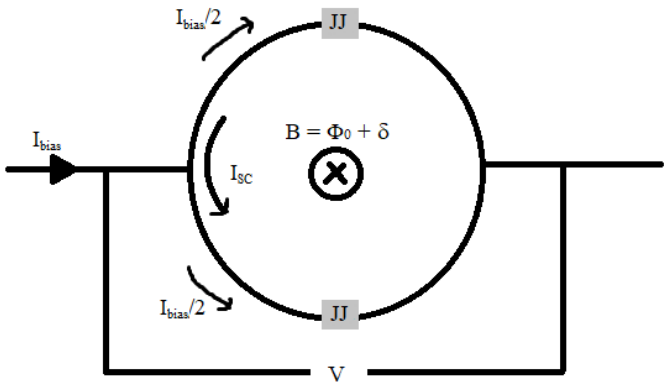

Figure 5.4: Schematic illustration of a DC-SQUID consisting of a superconducting ring, with two Josephson junctions (JJ). Surplus external magnetic field δ causes a superconducting response current in the ring, superimposing on a bias current I_{bias} causing the total current through one of the Josephson Junctions to exceed the critical current, breaking superconductivity and thereby causing a measureable voltage across the system.

5.4.3 Experimental procedures

This section will explain the experimental procedures of a SQUID experiment using our SQUID measurements as a basis. We conducted a routine scan wherein we cooled a superconducting powder to single digit temperatures, applied a small magnetic field of 10 Oe and slowly increased the temperature to measure the magnetic response as a function of temperature.

To prepare the sample a small amount of powder, usually under 100mg, is properly weighed off and put into the lid of a small cellulose capsule, after which the lid is sealed tight with another capsule. To lower the sample into the SQUID a plastic straw is used, in which the capsule is placed. Small holes are poked in the straw and capsule which increases friction keeping the magnetic sample in place. The straw is lowered into the instrument and an experimental routine is created, deciding the amount of cooling and magnetic field applied, as well as the frequency of measurements.

When picking program there are two different standard measurements. The most common is called a temperature sweep where the field is kept constant and the response is measured at various different temperatures. These are usually conducted by cooling the sample to the lowest desired temperature, with or without field, then slowly increasing the temperature while applying a slight magnetic field. This sort of measurement is great at investigating the critical temperature T_c of a system, as this point is marked by a sudden onset of magnetic signal.

The other type of measurement done is called a field sweep. The field sweep keeps the temperature constant, usually below the critical temperature, and instead measures the response at various different field strengths. A field sweep starts at no field, ramps up to H_{max} and back to zero, repeating the measurement with a flipped field direction. This is done to properly measure the flux pinning of a system, which

causes the magnetic response to be significantly higher when increasing the field strength, than when decreasing it.

It should be noted that there is a significant difference between cooling with and without applied field, called field cooling(FC) and zero-field cooling(ZFC). ZFC measurements are most commonly used, and are simply done by cooling the sample without any magnetic fields, only turning external fields on once the sample is cold. However it can be quite beneficial to also do a field-cooled (FC) measurement if time allows, where the sample is cooled in the presence of an external magnetic field. The difference between the two measurements lies in the ease at which spins can reorient themselves. FC will preemptively align the spins of the sample with the field used for cooling, resulting in maximal response. If the ZFC magnetization measurements are significantly lower it implies that the magnetic structure of the sample is inflexible at lower temperatures, preventing some spins from aligning with the field. This causes the sample to respond poorly to changes in the magnetic field and should be kept in mind.

Once the measurement is done you retrieve a detailed file containing, sample temperature, applied field, field response and errors on the measurements alongside a slew of lesser relevant data. The two graphs we are often most interested in are as mentioned the (temperature, magnetization) plot, and (applied field, magnetization) plot, which are used to showcase a phase transition. Unfortunately the instrument often gives the field response in the elusive "electromagnetic unit" called emu, while giving the applied field in Oersted, preventing an immediate conversion to the magnetic susceptibility χ.

To convert from emu to Oe we need to know the volume of the sample, which for a powder sample is impossible to measure directly. Instead we divide the mass of the sample with the density. This can however pose a problem as most of the samples we measure are new materials for which the actual density often is unknown. To find this we use the Rietveld refinement of the X-ray data as mentioned before, and extract the parameters of the unit cell, with which we can calculate the volume of a unit cell. Calculating also the mass of the unit cell from the atoms contained within it finally allows you to find the density of our material. In finding the mass of a unit cell it is important to keep in mind that the unit cell does NOT necessarily contain the same amount of atoms as the chemical formula, for instance the unit cell of Nd_2CuO_4 actually contains 4 Nd atoms, 2 Cu atoms and 8 O atoms. Once the material density is found, and the sample volume calculated, following formula can be used for conversion from emu to magnetic susceptibility χ in standard units.

$$\chi = \frac{\text{Response[emu]} \cdot 4\pi}{\text{Volume}_{\text{Sample}}[cm^3] \cdot \text{Field}[Oe] \cdot} \tag{5.5}$$

In literature magnetic measurements are often given in the cgs unit system, where the factor of 4π is inherent. Is this the case their magnetic susceptibility volume measures are usually labeled $4\pi\chi$ which corresponds to our SI-unit χ. It is also common to present the susceptibility as emu/mol, often labeled χ_M, where the susceptibility we find, uses the volume of the sample and is called χ_V. It should also be noted that while the theoretical susceptibility value for superconductors is -1, this will rarely be the case in our actual measurements. Often we have significantly

lower response due to inhomogenities in our sample, which is especially the case for our electron doped samples where it is not certain that every part of the material is properly annealed and thus superconducting.

Chapter 6

NCCO synthesis and superconductivity measurements

An integral part of this thesis has been the focus on using solid state synthesis as a basis for new experiments to improve our knowledge on superconductors. We have however conducted many different types of synthesis with differing experimental purpose, and as such we have sorted our work in three different categories, the replicating, exploratory and tweaking experiments, which will be defined shortly. To better order the experiments conducted, this and the following two chapters will cover experiments of each their category.

What we label a *replicating experiments*, are the experiments in which we synthesize an already established material using known techniques, with the intention of investigating it further. These types of experiments will be the focus of this chapter, wherein we replicate the classic n-type superconductor NCCO with the intention of using it for crystal growth and neutron scattering experiments. From a chemical standpoint replicating a compound does not offer much information of value, however repeating a synthesis and creating new samples for various experiments is quintessential for the ongoing experimental investigation of interesting materials, and as such should not be disregarded. Furthermore these kind of experiments are great to establish that the method of synthesis is functional, enabling further experimentation using the same methodology. Finally it should be noted that just because a particular synthesis is confirmed to work, it does not mean that it is easy to replicate, evident by the lack of interest in n-type superconductors partially due to the annealing process.

On the different end of the spectrum is the *exploratory experiments* which will be covered in the next chapter. Experiments of this type attempt to synthesize brand new compounds, either by using new elemental combinations or new preparation techniques, and then characterize them should the synthesis work. Naturally, the synthesis involved in these experiments are highly likely to fail, either because the procedure is not quite correct, or because the desired compound is simply does not exist. However when exploratory synthesises do succeed they are usually the ones of most interest, both chemically and physically, as they have the potential to bring with them brand new attributes and avenues of investigation. Thus, despite their low success rate, these types of experiments are still of utmost importance to

conduct, as it is almost exclusively through this sort of exploratory work that new breakthrough materials, like the first cuprates, can be found.

Finally comes the third type of experiments covered in chapter 8, the *tweaking experiments*. These experiments bridge the space between the two other categories, and contain experiments wherein existing compounds are tweaked slightly and then investigated, usually to change or investigate a specific attributes of the compound. While the synthesises involved in these experiments technically are treading uncharted territory, they still lean themselves heavily on established theory, and are as such much more likely to succeed. An example of these types of experiments, could be exploring a newly found cuprate superconductor at various other doping levels not yet tested, to explore the phase space. While technically not done before, the likelihood of doping level x=0.19 working when x=0.16 is established is quite high.

However as mentioned this chapter covers our experimental work done on the classical electron doped superconductor $Nd_{1.85}Ce_{0.15}CuO_4$, as it will lay the foundation for many of the other experiments.

6.1 Superconductivity test

The very first experiment done in this thesis work was the attempted synthesis, annealing and following magnetic measurements of $Nd_{1.85}Ce_{0.15}CuO_4$, to ensure that we were indeed able to create a high quality electron doped superconductor using the experimental equipment available to us.

Sample quality

Following the synthesis method outlined in chapter 4, we successfully synthesized powdered NCCO. We scanned the sample using XRD both before and after annealing the sample to discover any potential changes that annealing might have caused, but found no difference between the two measurements. All diffraction peaks measured aligned with literature, and no signs of unexpected impurities were found. A following Rietveld refinement on the XRD data can be seen in Figure 6.1, and resulted in an almost perfect fit, both with respect to peak shape and intensities. With this we could confidently conclude that the sample was pure NCCO, and continue with the magnetic response measurements, to see if the annealing process had worked as intended.

Magnetic measurements

The magnetic measurements were done using a regular DC SQUID, and were taken both with field, and zero field cooling, for both an annealed, and unannealed sample, albeit with a few months delay between the two measurements. The results for the zero-field cooled measurements can be seen in Figure 6.2 and show a clear transition to superconductivity for the annealed sample, whereas the unannealed sample remain in the normal state even at low temperatures. The diamagnetic onset indicating superconductivity begins at T = 25K, which also aligns well with the commonly cited $T_{c,opt}$ value of 24K for the compound [13]. The field cooled

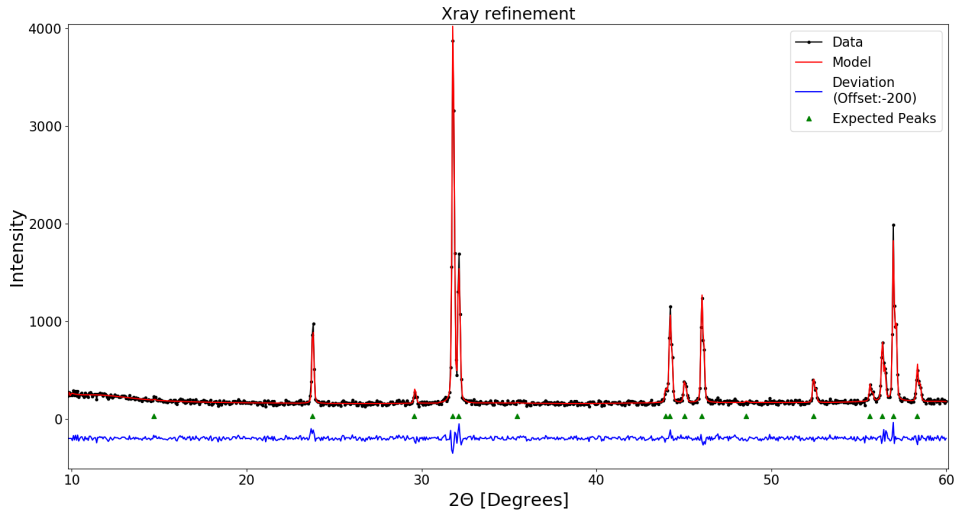

Figure 6.1: Results of a Rietveld refinement on the first NCCO sample. As seen all peaks occur at the expected peak positions.

measurements had an identical onset, however the maximal response was about twice as strong, indicating some stiffness in our material, but nothing of concern to the experiment. With these results we were confident in our synthesis and annealing process, allowing us to continue with alternative experiments.

6.2 Effects of reductive annealing on spin gap

Confident in our synthesis we looked into the literature to find ways in which NCCO had already been thoroughly studied and what parts of the NCCO understanding were still lacking. A surprising finding was that the effects of the annealing process have not been studied in depth, and that many scientists seem to simply assume that results of experiments comparing NCCO above and below T_c to apply for NCCO before and after annealing, given that in both cases the compound go from superconducting to non-superconducting. Seeing as the annealing process in our view is one of the most interesting parts about the electron doped superconductors, acting as a point of pseudo phase transition, we decided to focus on investigating this discrepancy.

In doing so we found two articles which were particularly interesting. The first article is from Yamada et al. [40] in which the magnetic fluctuations of two superconducting NCCO crystals were measured above and below their critical temperatures. The experiment showed a 3meV gap in the spin fluctuation for both samples when below T_c, and that this gap disappeared once going above T_c. In this way it was concluded that such a spin gap is strongly tied the onset of superconductivity in NCCO, however the experiment did not perform these measurements on an unannealed sample. It is possible that a similar spin gap is found in the unannealed non-superconductive sample at low temperatures, in which case the spin gap would have no dirrect correlation with onset of superconductivity, but merely have

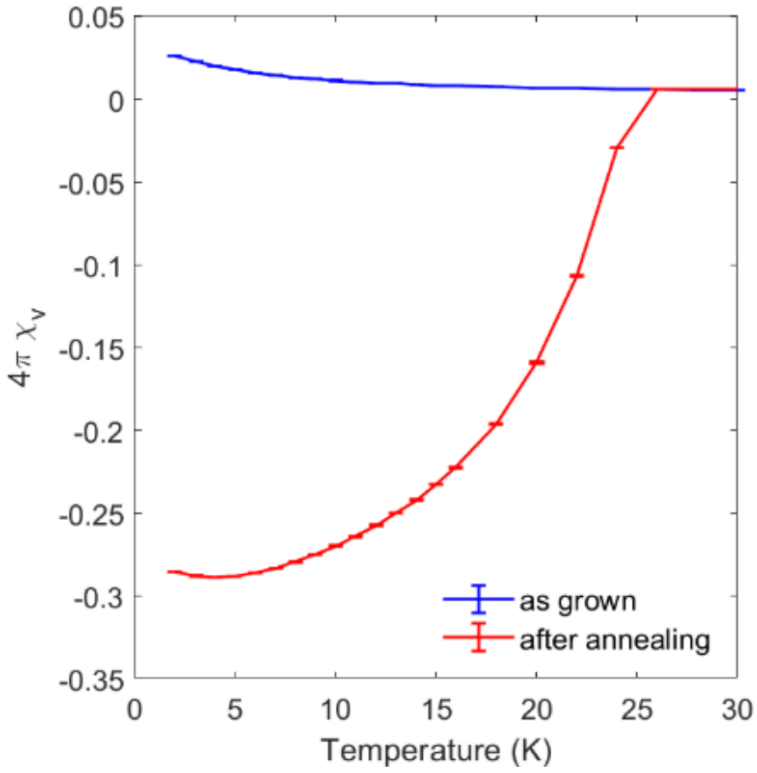

Figure 6.2: SQUID measurement of zero-field cooled $Nd_{1.85}Ce_{0.15}CuO_4$ before(as-grown) and after annealing. A clear onset of superconductivity is seen for the annealed sample at around T = 25K, whereas the unannealed sample remains non-superconducting all the way to 2K. The low temperature upswing is likely caused by paramagnetic sample impurities.

a quintessential overlap in onset temperature.

This experimental flaw is made more interesting when looking at the second article of interest by Dai, Wilson and Li [41]. They performed a similar measurement on the sister compound PLCCO, but they also measured the spin susceptibility of a non-superconducting sample at various temperatures. Most surprisingly they found an almost diametrically opposite result, namely that the non-superconductive sample indeed showed a spin gap below temperatures of 40K, but that the superconducting samples unlike the NCCO measurements had no spin gap. A comparison of the results of both Yamada and Dai can be seen in Figure 6.3.

Failing to find any resolution of this inconsistency in the literature we decided to explore it ourselves. To do this another neutron scattering experiment would be needed, and as such we send a proposal to use the EIGER beamline at the Paul Scherrer Institute (PSI) for our experiment. The planned experiment consisted of us synthesize a large homogeneous crystal using the TFSZ method as described in chapter 4, split it in and anneal only one of the two halves. That way any difference in measurements would purely be due to the annealing process, as all other growth procedures would be identical. At the EIGER beamline we would then proceed to measure the magnetic inelastic scattering at various different energy levels, for both samples at temperatures beyond and below T_c, hopefully clearing up the confusions and inconsistencies surrounding the NCCO spin gap.

Unfortunately there has been a general shortage of available neutron facilities in Europe, partially due to the planned closure of the ILL facility in Grenoble, which has caused an overload in applications at the PSI, leading to our proposal being rejected. A similar proposal has been made to the TAIPAN instrumentin Australia, however no response has been given at this time. Fortunately the efforts put into this proposal has not been completely wasted. We have gained important first hand experience in synthesizing larger single phase crystals, although the growth was never finalized. During the synthesis of the powder samples needed for the TFSZ growth, we also discovered a persistent impurity not present in our first sample, which would also show in many of our other experiments. Subsequent analysis of this impurity, which is the subject of the next section, allowed us to resolve the issue, improving the quality of our many other experiments.

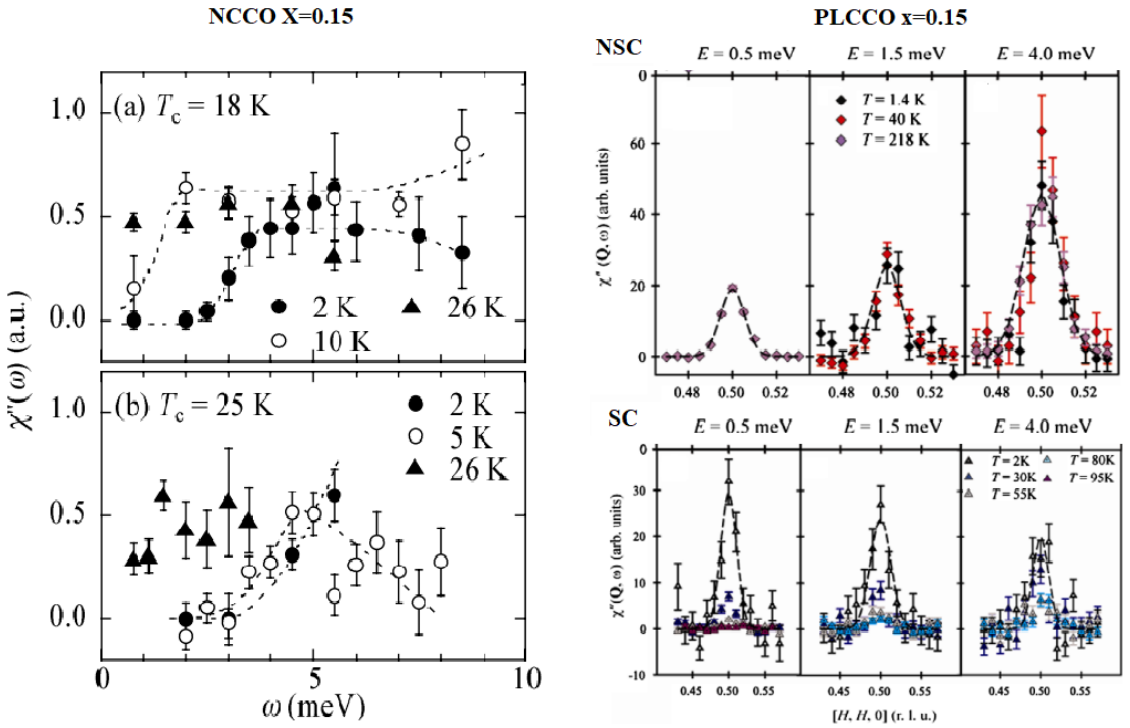

Figure 6.3: **Left:** Experimental NCCO data from Yamada et al [40]. A low energy gap is visible between sub and super critical temperature. **Right:** Experimental PLCCO data from Dai et al [41]. The SC low temperature measurement exhibits a clear magnetic response at low energy, contrary to the NCCO what was measured for NCCO. The same behavior is not present in the unannealed non-superconducting (NSC, top) sample.

6.3 Impurity analysis

In our progress to grow a large crystal for the neutron experiment we made ten 5g samples of NCCO which were to be used in the crystal growth. To our surprise however there was an additional impurity peak in the XRD scans of almost all of the samples, at $2\theta = 28.3$. This was somewhat surprising as our first NCCO sample was almost perfect and as we had used exactly the same synthesis procedure. Fortunately for 7 of our 10 of the samples the impurity signal was insignificant, however for the last three samples the impurity was very clear, as is seen in Figure 6.4a, and could have significant consequences for a crystal growth process.

Impurity identification

First we assumed that the impurity peak might have been caused by a systematic error tied to the XRD measurement, with the variation in severity being caused by the different measurement disks the sample was placed on. However when repeating the measurements on different disks, the results came back almost identical, making us conclude it was indeed an impurity in the samples.

Given that the impurity was present to some degree in almost all the samples, despite each sample being made independently of each other, we suspected the error to be a systematic result of the equipment we used, such as the mortar and pestle, or an impurity caused by the crucibles used. This assumption proved to be wrong though, as no $2\theta = 28.3$ peak is found in the XRD patterns of Si or Al, which are the materials the mortar and the crucible are made of. Looking into more advanced combinations, suspecting a mixture of Si and Nd or similar to be the cause of the error, we again found no peaks matching our impurity. With this we could rule out most possible external systematic errors, which left the most likely explanation for the impurity to be an incomplete or faulty synthesis process, despite the general synthesis procedure being identical for all samples. Looking at the XRD patterns for sample with the largest impurity we could also identify a minor second peak at $2\theta = 46.8$. Looking for these two peaks in all possible secondary phases containing a mixture of either Nd,Ce,Cu or O, we found the two impurity peaks to almost exactly match the signature peaks for the compound $Ce_{1-x}Nd_xO_2$ which is a plausible secondary phase in our reaction. In particular the ratio $Nd_{0.5}Ce_{0.5}O_2$ fit well, so we have assumed this to be the impurity, although some variation is possible.

This was unfortunate news for our experiments, as this type of impurity could have large implications on our experiments. The impurity $Nd_{0.5}Ce_{0.5}O_2$ is likely formed by a form of Nd doping of our CeO_2 that we otherwise intended to act as electron doping for the main material. This means that a large impurity will result in a low-Ce primary compound, and we can treat the impurity as siphoning surplus electrons out of our intended NCCO structure. As the superconducting dome for NCCO is narrow, even a small impurity of this type has the potential to reduce the carrier concentration to a point where a sample is rendered non-superconducting.

Impurity cause

Knowing that the impurity is the result of an incomplete synthesis, and likely detrimental to many of our experiments, figuring out the root cause of it, and how to prevent the impurity from showing up in the future, became an important task.

When trying to identify the cause of the impurity, we recalled the many reports from literature that NCCO was not superconducting without an excess amount of copper in the sample, of around 1-5% [12]. This could mean that we added too little Cu in our synthesis, which would result in surplus Nd,Ce and O, which is exactly what is in the impurity. Doing a rough two-phase Rietveld refinement on the sample with greatest impurity indicated that the impurity made up 4.8 mol% of the sample, which is aligned surprisingly well with our expectation given a 3-5% Cu deficiency. There were however, some questions to be asked about the validity of our theory. After all none of the relevant articles indicated that impurities would spawn if no excess copper was added, and if the impurity spawned from leftover material, shouldn't it contain a large amount of Nd and not so much Ce? Furthermore this explanation contained no explanation as to why the size of the impurities would vary so heavily from sample to sample. There were however possible explanations to these questions, for instance the $Nd_{0.5}Ce_{0.5}O_2$ impurity could be the most stable secondary phase, exchanging excess Nd with Ce from the main compound to form. The variations could be due to the uncertainty tied to weighing off Ce and Cu. Thus we decided to test out the theory by synthesizing two new NCCO x=0.15 samples with 3% and 5% more copper, seeing if the same impurity would appear.

When analyzing the two samples we saw that there were no impurities present in the 5% sample, however the 3% sample had larger $Nd_{0.5}Ce_{0.5}O_2$ impurities than any of the other samples. These results were interesting for two reasons. The first reason is that they directly contradicts our working theory, namely that Cu deficiency caused the impurity. While the 5% sample lacking impurities could be taken as supporting evidence for our Cu deficiency theory, we have already concluded that the error is mostly random and as such could simply not be present in that sample. However the presence of an error larger than seen before, in a sample where we supposedly should have minimized its source by adding extra copper, clearly showcases that the underlying assumption was wrong. It should be noted that this experiment does not disprove the prior claims that surplus Cu is essential for superconductivity, it merely shows that our impurity was not caused by a lack of Cu in the sample. The second, perhaps minor, point of interest, was that we found no traces of CuO in the 5% sample. This suggests that the NCCO structure can somehow sustain 5% or more additional copper, while also being perfectly stable with no extra copper. How exactly this compound adapts to surplus copper is a bit of a mystery, and could be interesting to look further into in another project, given that the Cu plays such an integral part in superconductivity.

Having now exhausted most reasonable causes for our impurity we finally wondered if it could simply be a sign that the synthesis was not finished yet. In hindsight this should perhaps have been our first consideration, however the lack of Cu impurities, and the fact that heating duration followed were consistent among literature, made us forego such a possibility. The last experiment however showed us that the NCCO structure can support larger amounts of Cu without resulting in CuO impu-

rities, explaining why only the $Nd_{0.5}Ce_{0.5}O_2$impurity would be present. Furthermore an incomplete synthesis could also explain the variation in impurity sizes, as synthesis progress would likely dependent on how well the material was grind together in the mortar, a part of the procedure exceptionally prone to human error. Testing this hypothesis we re-heated NCCO samples with a high impurity for 16 hours at 1100°C, XRD scanning both before and after the additional heat treatment. The reheated XRD measurement can be seen in Figure 6.4b, where it is evident that the impurity at $2\theta = 28.2$ almost completely has vanished as a result of the additional heating. Redoing the experiment and observing similar results, we have with high confidence concluded that the $Nd_{0.5}Ce_{0.5}O_2$ impurity was simply a product of an incomplete synthesis. This is fortunate as fixing the error seems to be an easy process, that to some degree should happen automatically once the compound is reductively annealed at 1100°C for a prolonged duration in order to obtain superconductivity.

Going forward a few questions still remain to be answered regarding this impurity. Does re-heating the sample remove the impurity in other variations of the NCCO compound, like the Ga doped NCCO tested later, or only the base compound? Is the problem solvable by simply heating for a longer time, eg. 40 hours, or does the sample need to be taken out of the oven, reground and then reheated? Also how much of a role in the impurity formation does improper powder grinding play? Finally it is still unclear as to why this problem does not seem to occur for any of the other experiments in literature. Fortunately these questions are minor issues, and straightforward to investigate if need be, so for now we decided to be satisfied with finding a method to remove the impurity and call the impurity investigation a success.

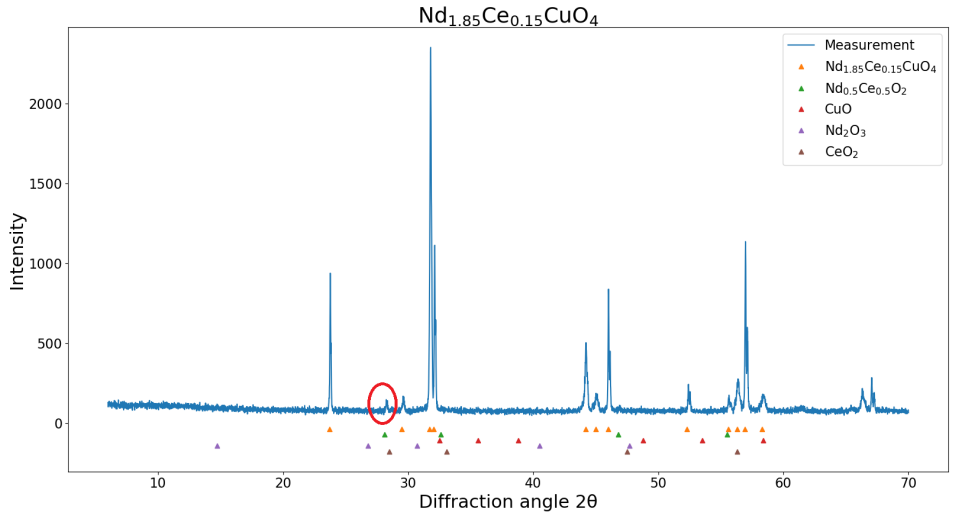

a) Impure sample of NCCO

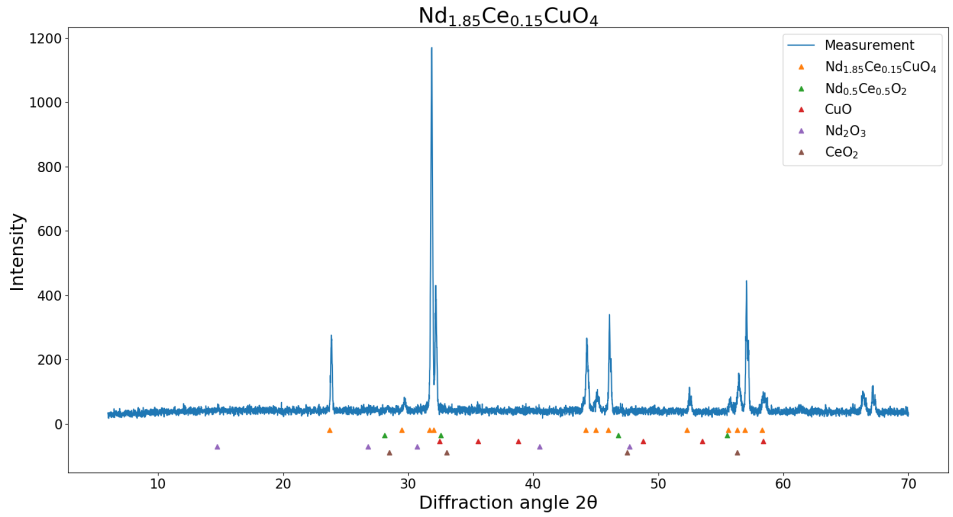

b) Same sample after second heat treatment

Figure 6.4: **Top:** Powder X-ray diffraction on faulty NCCO sample. A clear impurity peak is seen at $2\theta = 28.3$, marked by the red circle, most likely belonging to the impurity $Nd_{0.5}Ce_{0.5}O_2$. **Bottom:**Same sample after being heated for 16 hours at 1100°C. The impurity is no longer present suggesting the cause was an unfinished synthesis.

Chapter 7

Exploratory synthesis of new superconductors

This chapter is as said before dedicated to the exploratory experiments, and will cover our many attempts at creating brand new variations of the NCCO superconductor. This includes explaining the underlying motivation that lead to each of the attempted synthesises, the synthesis result and any subsequent work done on the samples.

7.1 New electron doped superconductors

The first set of exploratory experiments we conducted had the simple goal of creating a new compound, that would also be an electron doped superconductor. The motivation for such experiments stem from the fact that variations of the same superconductors often have historically had significantly different attributes, such as a much higher critical temperature or lower critical magnetic field. Finding such a compound would make further studies of the n-type cuprates easier and more rewarding, not to mention the ever looming hope of accidentally finding a room temperature superconductor. Unfortunately there is no solid recipe for finding new superconductors so these experiments consisted largely of trying new doping materials for NCO and see if the synthesis "sticks", forming the desired compound. Still, there are some rules of thumb that we have utilized when trying to make new variations of known structures.

When doping a material, a few key factors are essential to consider when picking the possible dopants. The most important thing to consider the size of the atom we are replacing. Looking at the compound NCCO we notice that Cerium which is the dopant, has roughly the same atom size as the Neodymium that it replaces. A larger difference in size usually corresponds to a larger distortion of the lattice, making it more unstable and thereby reducing the likelihood of succeed. Next it is important to consider the electron structure, and in particular the redox number of the compounds. As we have attempt to create and electron doped superconductors, it is of essence that our doping material contains more free electrons than what we replace. We see that Cerium has a redox number of 4+ in the original compound CeO_2 used for the synthesis, whereas Neodymium only has redox number 3+ given

the base compound Nd_2O_3, meaning that replacing Nd with Ce adds an electron to the sample as intended.

Finally a factor to consider is whether or not the dopant is even likely to fit into the crystal structure. For instance if our doping material is never found in compounds with a tetrahedral coordination, it is unlikely that it would create a stable T-structure cuprate. A way to check this is by looking it up in the brilliant paper by Waroquiers et al. [42]. Through statistical analysis of more than 8000 different oxides, the paper breaks down the most common coordinations for almost every element relevant for doping.

7.1.1 $Nd_{2-x}Sn_xCuO_4$ and $Nd_{2-x}Zr_xCuO_4$

After thorough consideration we found that Tin and Zirconium were good candidates for new dopants in the NCO structure, as both materials have the +4 oxide structure SnO_2 ZrO_2 required for electron doping, and as their had seemingly not been attempted before. Their biggest problem was in the difference in atomic size, since they with an atomic mass of 118u for Sn, and 91u for Zr were a fair bit smaller than Nd which have a mass of 144u. Both of the materials however do have a natural T structure coordination, which made them some of the best candidates for dopants outside of the lanthanides despite their smaller atom size. We decided to use the doping level x=0.15, being the optimal doping level for NCCO.

Unfortunately both materials showed clear signs of impurities after a classical solid state synthesis. The XRD pattern from the Sn sample was showed in the example of Figure5.3 showed clear CuO in the sample, indicating that our dopant did not form the structure intended. It occurred to us however that starting the experiment at 15% doping could be problematic, as there was a chance the NCO structures saturation point for the new doping materials was somewhat lower, like 10%, meaning that the leftover materials found in the x-ray could simply be due to the phase being over saturated, and not due to the reaction not happening at all. As such we remade both samples using the much lower dopant value x=0.05These samples unfortunately showed the same impurities, making it clear that no compound of the desired structure had formed. Instead the sample most likely consisted of regular NCO alongside spare CuO and some Sn/Zr based impurity.

Of interest was that the tin and zirconium did most likely react in some way, but instead of forming T' structures they instead seemed to have formed pyrochlores of the structure $(Sn, Zr)_2Nd_2O_7$. While pyrochlores are not superconducting their structure is quite complex and they are interesting in their own right, being prime examples of materials containing frustrated magnetism. The Sn version only had a few reports in the XRD database [31], and most interestingly was that when we tried to synthesize it directly using proper stoichiometry and no Cu, the compound did not form. While much interesting work could be done figuring out exactly why this was the case, given it had nothing to do with superconductivity we did not pursue these pyrochlore synthesis any further, leaving their mysteries to be solved in future projects.

Thus our attempts at finding a new electron doped superconductor ultimately proved to be fruitless. Going forward however there are still plenty of suitable

doping candidates for new electron doped superconductors. The first place to look are among materials of the structure XO_2, where particular suitable candidates would be HaO_2 or WO_2 as these materials also have a similar atomic size to Ce. Unfortunately we did not have access to these materials, so our exploration ended at Sn and Zr.

7.2 Hole doping electron doped superconductors

For these experiments we were inspired by the findings that both electron and hole carriers existed simultaneously in the electron doped superconductors, as well as Hirsch's controversial theory that holes actually drive n-type superconductivity [23].

With the observations and Hirsch's radical theory in mind, it seemed interesting to examine what would happen if we doped NCO with holes instead of electrons, making a similair compound to LSCO but with the T' structure and NCO as a mother compound. Would it be superconducting at all, and if it was would it still behave like an electron doped superconductor, or would it be just another regular hole doped SC. Even if it was a hole doped superconductor having the same mother compound as NCCO would allow for easy direct comparisons between the electron and hole doped superconductors. As such, even disregarding Hirsch's controversial theory, exploring hole doped NCCO seemed to have a lot of potential for further work, if the synthesis could be made to work.

Barium was found to be an immediate candidate for this experiment as the size is almost identical to cerium and neodymium, being the element closest to the lanthanites. We also decided to attempt strontium doped NCO, as we found a previous study claiming to have made $NdSrCuO_4$ indicating it was possible to form the T' structure [43]. However by the time of this experiment we found no evidence that a Sr doped NCO compound had been tested superconductivity near 15% doping, which is the doping level most common for superconductivity. Thus we decided to move forward with the experiment.

We began using only 5% doping to make sure there weren't any impurities as a result of an over-saturated structure, and initial results where promising with no clear signs of the original compounds meaning everything had reacted. Unfortunately when moving on to 15% doping it became clear that the alternative structure $Nd_2SrCu_2O_6$ and Nd_2BaCuO_5 were favoured, using up all of the dopant material leaving the rest to form basic Nd_2CuO_4. This is evident from our rietveld refinement on the compounds seen in Figure 7.1. These impurities are heavily studied semiconductor compounds, with no interest to us [44]. Thus these experiments perfectly illustrate the difficulty in properly assessing doping levels, as impurities can be impossible to spot if the doping level is too low, whereas too high doping levels makes the cause of any impurities unclear, as they can both be due to a faulty synthesis, or over-saturation of the structure.

To prevent Sr and Ba from prioritizing the $Nd_2(Sr, Ba)Cu_2O_6$ structure, deeper knowledge of the actual reaction, as well as more advanced synthesis methods would be needed. Looking deeper into literature we found that Sr doped NCO with x=0.15 had already been successfully created twice, indeed using a more advanced technique called acetate pyrolysis, wherein solvent Nd,Sr and Cu acetates are made to react

using microwaves [45]. Curiously only one of the two articles, the one from Rosseinsky et al, made any mention of superconductivity [46], and even then it did not contain any direct measurements or clear indications of whether or not the sample was reductively annealed. With this little interest in the compound from literature, there is still a significant amount of potential work that can be done in investigating these compounds. Using acetate pyrolysis to attempt the Ba doped version is a solid place to start, as Ba doped NCO is found nowhere in literature, but also clearly investigating the effect of annealing on the Sr compound to make sure it really cannot be made superconducting seems essential. Should it be non-superconducting, further investigating the magnetic dynamics of the compound, putting it in relation to much of the NCCO knowledge gained after 1992, could be essential in figuring out what criteria are essential for the superconductivity.

However as we currently have neither the tools nor the knowledge to fully utilize the acetate pyrolysis method, and as it did not seem possible for us to make the synthesis work without, we decided not to pursue this line of experiments further, leaving it instead for a possible future project should the opportunity arise.

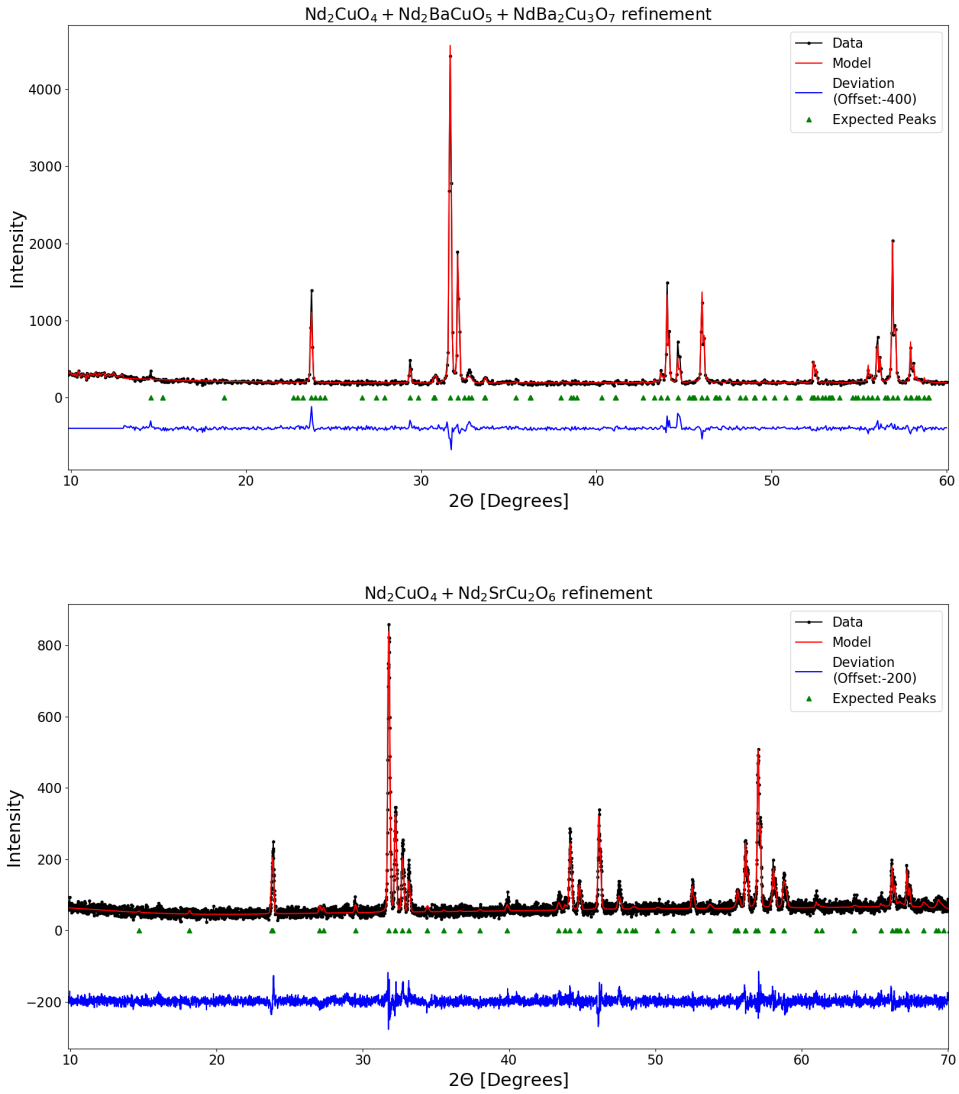

Figure 7.1: **(Top)** Rietveld refinement of NCO + Ba based impurity on the attempted $Nd_{1.95}Ba_{0.05}CuO_4$ synthesis product. **(Botton)** Rietveld refinement of NCO + Sr based impurities on the attempted $Nd_{1.85}Sr_{0.15}CuO_4$ synthesis product. Both refinements showed great agreement, indicating that the final compound was indeed a mixture of NCO and Ba/Sr impurities, and not the intended compounds.

Chapter 8

Effects of doping in the cuprate layer

The standing theory for superconductivity believes, that the additional carriers added by doping makes their way into the cuprate layer, wherein the mechanisms that cause superconductivity occur. This has caused a large interest in the exact workings of the cuprate layer, which is why we in this series of experiments decided to focus on the copper in particular. To gain information on coppers role in causing superconductivity, we would tweak the cuprate layer by replacing the Cu atoms with various other elements, and observing the resulting differences in superconductive behavior.

8.1 Cuprate layer spin dependency in LSCO

For this experiment we decided to investigate one of the cornerstone p-type cuprate superconductors, namely $La_{1.85}Sr_{0.15}CuO_4$ also known as LSCO. One of the key findings in the field of p-type cuprates, and the motivation for this experiment, has been that very slight magnetic changes in the Cu layer has significant consequences for the superconductive qualities of the sample. Even replacing as little as 2% of the Cu in LSCO with a similar metal like Zn, or Ni, almost completely kills off all superconductivity, however the reason why is still not immediately clear.

This experiment investigates whether or not the spin of the doping material plays a significant role in causing this deterioration of superconductivity. After all the spin of Cu is $\frac{1}{2}$, whereas the spin of its neighbours Zn and Ni is 0 and 1 respectively, so it is plausible that the spin-$\frac{1}{2}$ difference could be a significant reason as to why superconductivity vanishes.

To investigate the importance of this spin-$\frac{1}{2}$ difference, we synthesized the compound $La_{1.85}Sr_{0.15}Cu_{0.98}Ni_{0.01}Zn_{0.01}O_4$. This compound has an even mixture of spin-0 and spin-1 doping, such that the average spin of the cuprate layer will remain the same as in the undoped case. In this way we can examine whether the deterioration of superconductivity is due to a long range spin change, or whether it is more local in nature. Furthermore we can investigate how the deteriorating qualities of Ni and Zn interplay, whether their effects are additive or cancel out, and whether one impurity will be a dominating in dictating the superconductive response quality. We

also synthesized $La_{1.85}Sr_{0.15}Cu_{0.98}Ni_{0.02}O_4$ and $La_{1.85}Sr_{0.15}Cu_{0.98}Zn_{0.02}O_4$ such that we could properly compare the effects of the mixed doping with the effects of each element separately. Finally we also had a regular $La_{1.85}Sr_{0.15}CuO_4$ sample, however due to time constraints we could not perform measurements on this sample, and instead compare our results with the LSCO results in literature.

8.1.1 Sample quality

The synthesis of all three compounds went mostly well, especially the mixed sample, which is the basis of this experiment, contained almost no sign of impurities. However in XRD pattern of the non-mixed samples two peaks around $2\theta = 32.9, 37.9$ appear with completely unknown origins. This can be seen in our Rietveld refinements of the compounds in Figure 8.1

To resolve this issue we first needed to identify the impurity, by comparing with possible second phases that could occur in the synthesis. As the impurity shows up in both the Zn and Ni sample it was unlikely that these elements directly caused the impurity, and if they did it would be because they are structurally interchangeable, allowing us to ignore impurities containing Ni, as they should have identical counterparts containing Zn instead.

To identify the impurities we looked at the XRD patterns for every combination of La, Sr, O, Cu and Zn, while also considering aluminum oxide which the crucibles are made of, silicon-oxide which the mortar is made of, and the possibilities of Nd traces in the sample from prior NCCO experiments. The signature peak of the possible compounds can be found in table 8.1, however no proper match was found for the impurity, so we gave up on properly identifying it. Despite failing to identify the impurity we can still say a few things about it, based on the XRD peak structure. It is most likely a simple and highly symmetric impurity consisting of only one or two elements given the limited amount of peaks. Furthermore the unit cell is likely quite small as the impurity peaks begin at relatively high angles. This fortunately makes it unlikely to be a magnetically advanced impurity that could interfere with our superconducting measurements. It is also likely the impurity is caused by an external factor, as none of the compounds involving the reactants fit, making it probable that the synthesis was complete, and that the intended stoichometry was conserved. Thus the impurity seemed to do little harm to the experiment and as the synthesis was seemingly successful, we decided to continue with the SQUID measurements to investigate the superconducting qualities of all three samples.

8.1.2 Magnetic response measurements

To measure the magnetic response, and thereby the superconductive properties, of our three LSCO samples we used a regular DC SQUID. For all three samples we conducted the same routine doing a temperature sweep both with and without field cooling, in a 10 Oe magnetc field, for temperatures between 2 and 45 degree Kelvin. The results of the measurements can be seen in Figure 8.3. For the mixed compound also a field sweep was done which can be seen in 8.2

One of the first things we notice is that the magnetic response overall is extremely

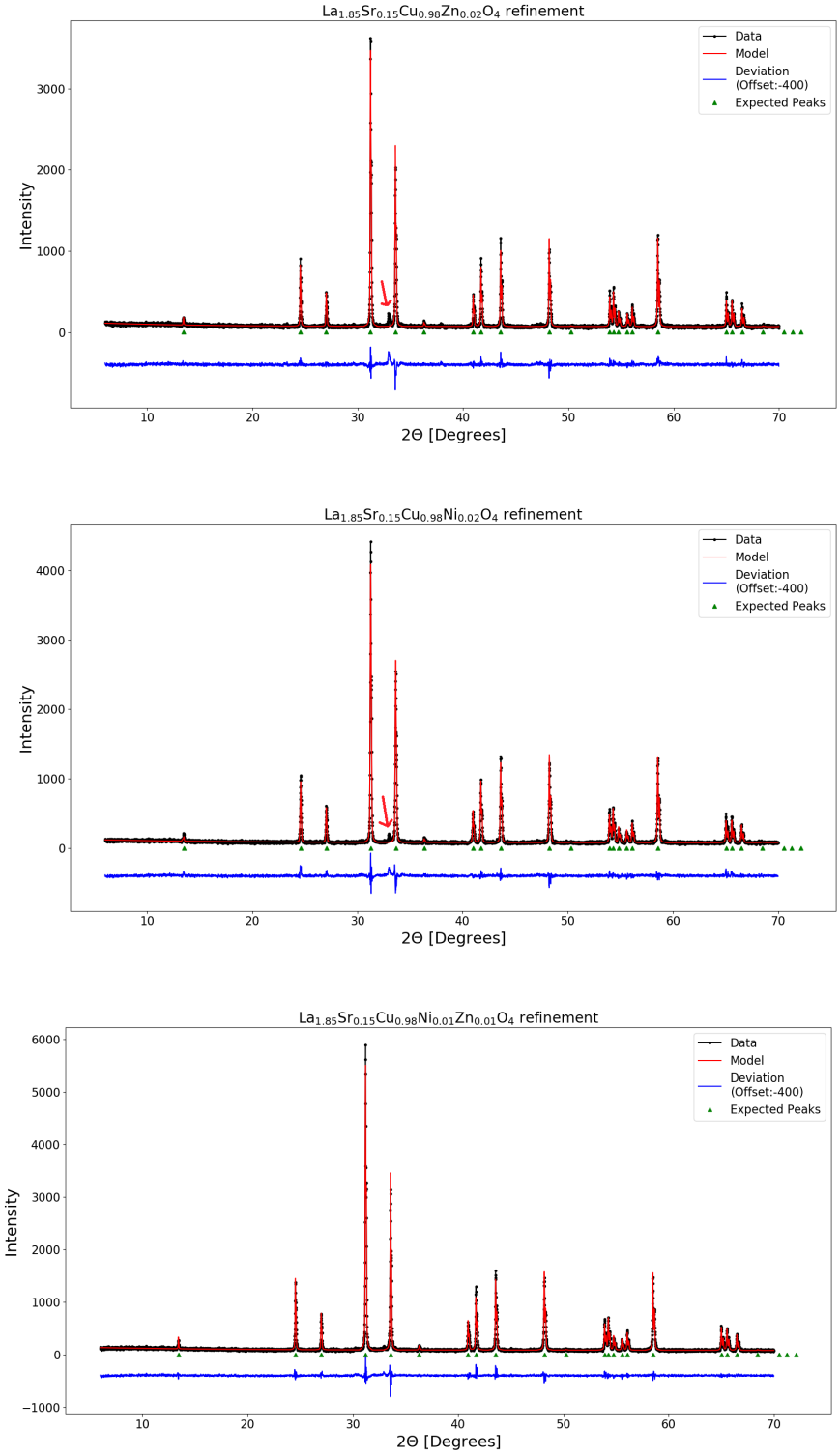

Figure 8.1: Rietveld refinement of LSCO x=0.15 doped with 2% Zn *(top)*, 2% Ni *(middle)*, and 1% Zn + 1% Ni *(bottom)*. A clear impurity is found at $2\theta = 32.9$, visualized by an arrow.

Compound	Main peak	Second peak
Impurity	32.9	37.9
Single Element		
La	29.2	33.9
Sr	25.4	29.4
Cu	43.6	50.8
O	14.7	29.6
Zn	43.5	36.9
Two Elements		
La_2O_3	29.6	45.6
SrO/SrO_2	34.8 / 35.6	30.0 / 28.5
CuO	38.8	35.6
ZnO	36.3	31.8
La+Sr	N/A	N/A
LaCu / $LaCu_5$	39.0 / 41.2	30.6 / 29.4
LaZn / $LaZn_5$	33.8 / 39.2	60.4 / 28.2
SrCu / $SrCu_5$	29.5 / 40.9	11.5 / 39.5
$SrZn_5$	38.7	37.5
CuZn	43.3	79.3

Compound	Main peak	Second peak
Impurity	32.9	37.9
Three elements		
$La_4Sr_3O_9$	29.5	36.8
LaCuO3	33.0	47.0
La+Zn+O	N/A	N/A
$Sr_4Cu_6O_{10}$	34.8	32.4
$SrZnO_2$	39.00	31.8
Zn+Cu+O	N/A	N/A
La+Sr+Cu	N/A	N/A
La+Sr+Zn	N/A	N/A
Sr+Zn+Cu	N/A	N/A
LSCO x=0.15	32.4	33.6
Alternative errors		
SiO (Mortar)	20.6	23.3
Al2O3 (crucible)	43.3	57.5
NCCO (prior sample)	31.7	56.9
$Nd_4Sr_3O_9$	30.0	37.4
NdSiAl	32.6	28.2

Table 8.1: Primary and secondary peaks (2θ) for all likely impurity phases containing a combination of La, Sr, Cu, O or Zn [31]. None of the possibilities align with the signature peaks of the impurity leaving its elemental composition a mystery

low. As mentioned this is quite common for type-2 superconductors such as our LSCO, and as such no cause for concern. If we look at the difference between FC, and ZFC measurements all three samples show minimal hysteresis, which shows us that our samples are magnetically homogeneous and free as intended.

Looking at the field sweep measurement of the mixed sample we also see that it qualitatively behaves as expected, with a clear hysteresis between the measurements with increasing and decreasing magnetic field. Since the hysteresis never vanishes we can also conclude that the critical field of our mixed compound must lie above 5T, which was our measurement limit.

When looking at the temperature sweep measurements we see that a large problem is the wide nature of the superconducting transitions, spanning up to 36K, as they never really seem to be reaching full diamagnetic response. When looking at other similar samples in literature, such as those from Kofu et al. [47], all samples have reached maximal magnetic response at 10K, and the temperature difference between onset of superconductivity and maximal response is only between 5 and 10K. Furthermore Kofu's x=0.018 Ni sample had a diamagnetic onset at 25K, much lower than that of our sample for which a response begins already at 37K. This leads us to conclude that our samples are likely highly in-homogeneous, which would explain the large transition area. In particular we suspect that our Ni sample might contain areas of LSCO with no, or at least very light, Ni doping, as that would result in part of the sample giving superconducting response already at 37K, the onset temperature for regular LSCO. Fortunately our samples are consistently inconsistent, still allowing direct comparison, and our results look less dire once we begin analyzing them.

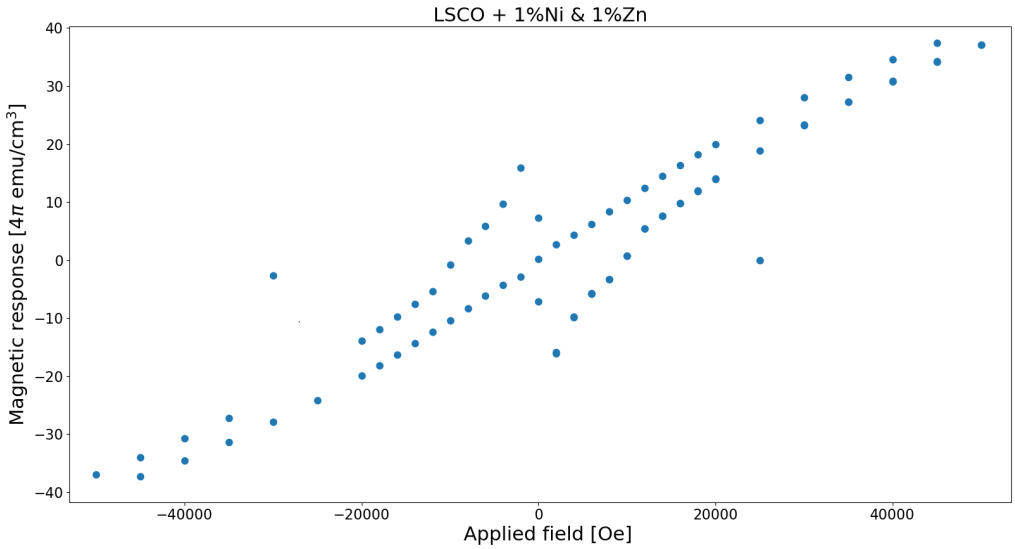

Figure 8.2: Field sweep measurement of LSCO x=0.15 doped with 1% Ni and 1% Zn. A clear hysteresis is observed up to 5T indicating that the critical magnetic field strength was not reached.

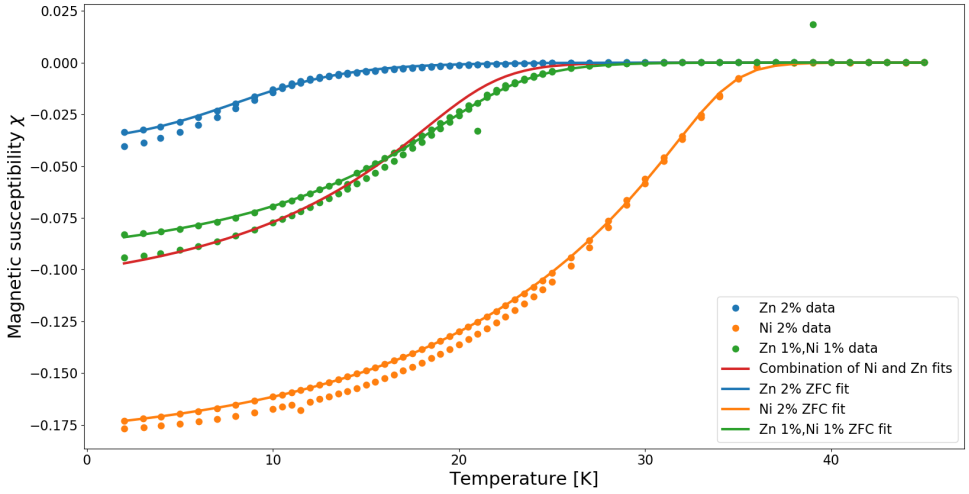

Figure 8.3: **Dots:** Measured magnetic response of LSCO x=0.15 doped with 2% Ni, 2% Zn or 1%Ni and 1%Zn. Both FC and ZFC measurements were done, resulting in two curves for each measurement, with the upper being ZFC and lower being FC. **Lines:** Modified logistic fit on the corresponding data. The red line represents a model generated by averaging the fit parameters of the 2% Ni and 2% Zn fits, acting as a rough expectation value for the mixed compound.

8.1.3 Analysis

One of the key issues with our measurements, is that the shape of each function vary significantly, making it hard to find a proper point of comparison. For instance it is unclear how we should find the critical transition temperature, as some of our transitions stretch out over tens of kelvin, and trying to comparing the transition lengths, or midpoint temperatures is also prevented by irregular size.

To mitigate this effect we decided to fit a model onto each data set. That way we can identify key values of the model and quantitatively compare them, drawing conclusions based on their correspondence to physical properties. As there is no solid theory behind the nature of the superconducting transition, the model we pick is somewhat arbitrary. However a good model should be able to accurately fit the data, and have a clear comparison between parameters, and physical properties of our measurement.

For that purpose we initially decided to model the data using a modified logistic fit,

$$M = \frac{L}{(1 + e^{-k(X-X_0)})^{1/\nu}} - L$$

This was done as the logistic graph has many similar attributes to our response graph, it starts out flat, then declines in some form before it flattens out at a lower value. Such a fit allows us to model a value for the maximal magnetic response as L, a midpoint temperature as X_0 and the sharpness of superconducting transition as k. The modification from a regular logistic function comes in the form of the factor ν which dictates where maximal growth occurs, thereby modelling the curve asymmetry, which evidently is quite significant in most of our measurements. A visual illustration of how ν and k impact the fit can be found in Figure8.4.

Something to keep in mind when working with the modified logistic fit is to consider the effect the ν factor has on the physical understanding of x_0. By varying the variable ν from 1, x_0 stops representing the actual midpoint of the graph, but instead works in conjunction with the μ and k value to determine the position of the point, at which the rate of change is steepest, which will be at $x_0 - \frac{ln(\nu)}{k}$. Thus a direct comparison of x_0 might not physically make much sense. Instead we draw conclusions by comparing the new critical point, at which rate of change is highest, and label it as

$$\mathrm{T_{c,fit}} = x_0 - \frac{\ln(\nu)}{k}$$

Some would suggest that we instead compare the conventional $\mathrm{T_c}$, defined as the immediate point at which the magnetization changes from 0, however given the large inhomogeneity in our sample, this would only measure the $\mathrm{T_c}$ of the underdoped parts of the compound, as they would magnetize first. Thus we do not believe using it for our measurements to be appropriate, and will stick to comparing the point of steepest descent, $\mathrm{T_{c,fit}}$.

Another thing to consider is the nature of the factor ν. As is visible in Figure 8.4 a value of ν below 1 results in the transition at low temperature, near full magnetization, to be sharper than when going from normal conductor to superconductor. This seems unphysical, and does not agree with the general structure of a magnetization plot. For the most part this shouldn't matter as a good fit would simply

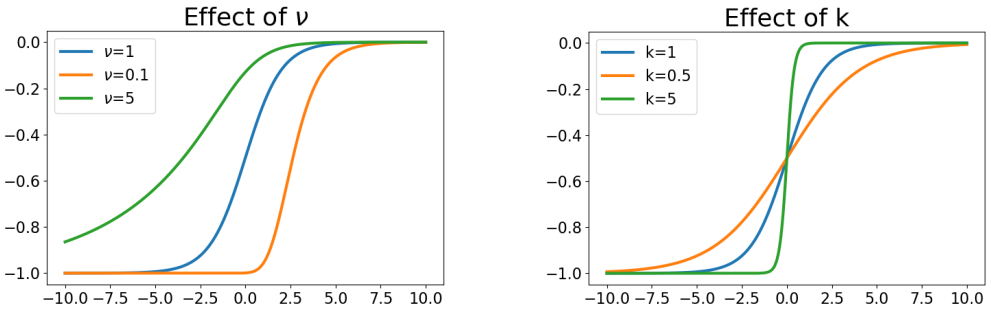

Figure 8.4: Visualization of the effects of the K and ν parameter in the modified logistic model $M = \frac{L}{(1+e^{-k(X-X_0)})^{1/\nu}} - L$. Standard parameters were L=1, k=1, $X_0 = 0$, $\nu = 1$ unless otherwise specified. As can be seen k changes the steepness of the curve, whereas ν changes the position of maximal growth.

have a positive ν value, however for our Zn data the T_c is quite low, resulting in a lack of data points in the transition region. This allows for some quite exotic fits to function quite well, where the ν value is immensely low and X_0 is close to 0K. To prevent this we have imposed the restriction that $\nu \geq 1$ ensuring that the sharpest transition occur somewhere at temperatures above the midpoint.

Utilizing the modified logistic model we found close to perfect fits for all three samples, and we were able to accurately establish the critical transition point for each sample, which we treat as an equivalent to T_c. The results of the fits can be found in 8.2, where the critical points of our Zn,Ni and Mixed sample were 7.91K, 37.0K and 25.5K respectively.

Having a nice model for our data we can begin to draw conclusions from our experiment. Immediately when we examine our data we see that the mixed graph lies in between the other two. For that reason we can quickly conclude that our initial working theory, namely that having an average of spin 1/2 would cancel the negative effects of each individual doping, was untrue, and that doping with a mixture of Zinc and Nickel still hampers the superconductive properties of the sample. Despite this, our results are still quite interesting.

Another possible outcome of the experiment, and perhaps the one we initially thought most likely, was that our sample would simply be consisting partially of LSCO+Ni and LSCO+Zn, as if we had mixed such two powders together. This would result in a split graph with two different transitions, at two different temperatures, matching LSCO+2%Ni and LSCO+2%Zn. Fortunately this is not the case, and our data instead forms a nice single phase response, which is a clear sign that the zinc and nickel have at the very least mixed somewhat homogeneously throughout the sample, creating a co-doping.

Returning to the fact that the mixed response graph qualitatively lies pretty much in the middle of the two other response graphs, both in terms of magnetization, critical temperatures and slope, we wondered if it could really be the case that mixing 1% Zn and 1% Ni would simply create a sample with features equal to the average of the two 2% samples. This would imply that the superconducting response to both Ni and Zn doping in the Cu layer is linear with the doping amount and independent

	L	k	x_0	\nu	T_{c,fit}
Data fit	0,10	0,5	22,35	4,84	25,49
Prediction	0,11	0,61	21,16	5,93	24,05
Deviation	17%	22%	-5%	22%	-6%

Table 8.2: Comparison of different parameters between logistic fit on LSCO+Ni+Zn measurements, and a model prediction from LSCO+Ni and LSCO+Zn fits. All parameters are within 25% of the predicted value.

of the other impurities, at least for small doping levels.

To test this hypothesis out we needed a way of finding the average of two magnetic response graphs. Simply taking the average value of the two magnetization graphs would not work, as we instead of having an onset at a midpoint $T_{c,mix}$ we instead would have an onset at $T_{c,Ni}$ with half the steepness, until reaching $T_{c,Zn}$ at which a second onset begins. While such a technique would result in the 0 point magnetization being equal to the average of the two graphs, many other important features would be missing. Instead we returned to our modified logistic fits. These fits almost perfectly replicated the shape of a response graph, and combining two different fits is a lot easier, as we simply take the mean of the parameters that go into the fit such as the steepness k, asymmetry ν and midpoint X_0, and generate a new logistic graph using these values. When constructing this expected response graph and comparing with the fit of the actual magnetic response of our mixed sample, we saw that the fit was surprisingly close. The constructed expectation graph can be seen in 8.3, and a parameter comparison between our mixed graph and the averaged fit can be found in 8.2. We see that the deviation for all parameters is below 25% which is quite close, when considering all the other possible sources of error in such an experiment. The exact doping level can vary a fair bit after all, there is a significant impurity present in the samples, and for unknown reasons the sharpness of the response in all samples are significantly less than similar samples found in literature.

All in all this experiment supports the interesting possibility that the superconducting response to doping in the cuprate layer is directly proportional to the amount of doping, however to be sure the experiment would have to be repeated with more samples, and an explanation to the discrepancy between literature samples and the ones produced by our self seem in some way necessary, before any conclusions can be drawn about the effects of cuprate layer doping. So far the only thing we can say more or less for certain is that the mean spin of the sample is not the key factor that kills the superconductivity, which is what we set out to investigate in the first place.

8.2 Carrier doping in the NCCO cuprate layer

For these experiments we considered if it was possible to add the surplus of carriers directly to the cuprate layer, which as mentioned is believed to be the source of the superconductivity. As seen in our LSCO experiments, doping directly into the Cu layer kills superconductivity for hole doped superconductors, however the phenomenon has not been explored as much in the n-type counterpart, despite there being many compelling arguments to do so. First of all N-types have the structural difference of having purely 2D cuprate layers, which could change the dynamics of the layer significantly, and thereby our expectations. Another problem for p-type superconductors is that it is difficult to find Cu-like materials with a lower oxidation number than Cu, that can act as hole doping candidates. However for electron doping both Gallium and Iron are prime candidates for Cu substitution, with Ga(3+) in particular being almost identical to Cu(2+) in size.

Finally we found a paper by Felner et al. claiming to have reached superconductivity in NCCO x=0.12, a dopant level where NCCO traditionally is not considered superconducting, by doping the Cu layer with 3% Ga [48]. This would indicate that whether the doping electrons come from a charge reservoir or the Cu layer itself is at least somewhat interchangeable, something that could have large theoretical implications. For some reason however the paper does not attempt lower dopings than x=0.12, and seemingly no follow-up has been done on this experiment since then, despite more than 30 years passing since it was published. We believe many other reasons could be the underlying explanation for the found results, such as an extraordinarily successful annealing of their samples, or small sample flaws in the synthesis resulting in higher doping levels. Hence we decided to re-enact the experiment by synthesizing variants of $Nd_{2-x}Ce_xCu_{1-y}Ga_yO_4$ and subsequently perform magnetic measurements on them. We also expand the Ga doping range all the way to 10% to find the Ga saturation point of the structure, and to better distinguish if successful doping through the Cu layer is a general trait of the NCCO compound.

8.2.1 Sample quality

For this experiment we synthesized $Nd_{2-x}Ce_xCu_{1-y}Ga_yO_4$ using the ratios x=[12, 10, 7.5, 5]% and y=[3, 5, 7.5, 10]% thus keeping the total amount of added carrier pr mol x+y=0.15. We also made a regular NCCO x=0.12 sample in order to confirm that NCCO below this doping threshold is not superconducting. The synthesis showed no signs of Ga impurities, indicating successful Cu doping, except for the 10% Ga sample where a large impurity peak appeared, indicating that the compound was over-saturated with Ga, as is evident from our Rietveld refinements seen in Figure 8.5.

One major problem, however, was that the impurity peak at $2\theta = 28.3$, discussed at length in section 6.3 was also present in all of the Ga samples. As mentioned the impurity consists of a mixture of Nd and Ce in some form $Ce_{1-x}Nd_xO_2$, and while the impurity itself is not superconducting and would in no way directly interfere with any magnetic measurements we might wish to conduct, the problem lied in what it could mean for the primary sample. A Ce heavy second phase, would inherently

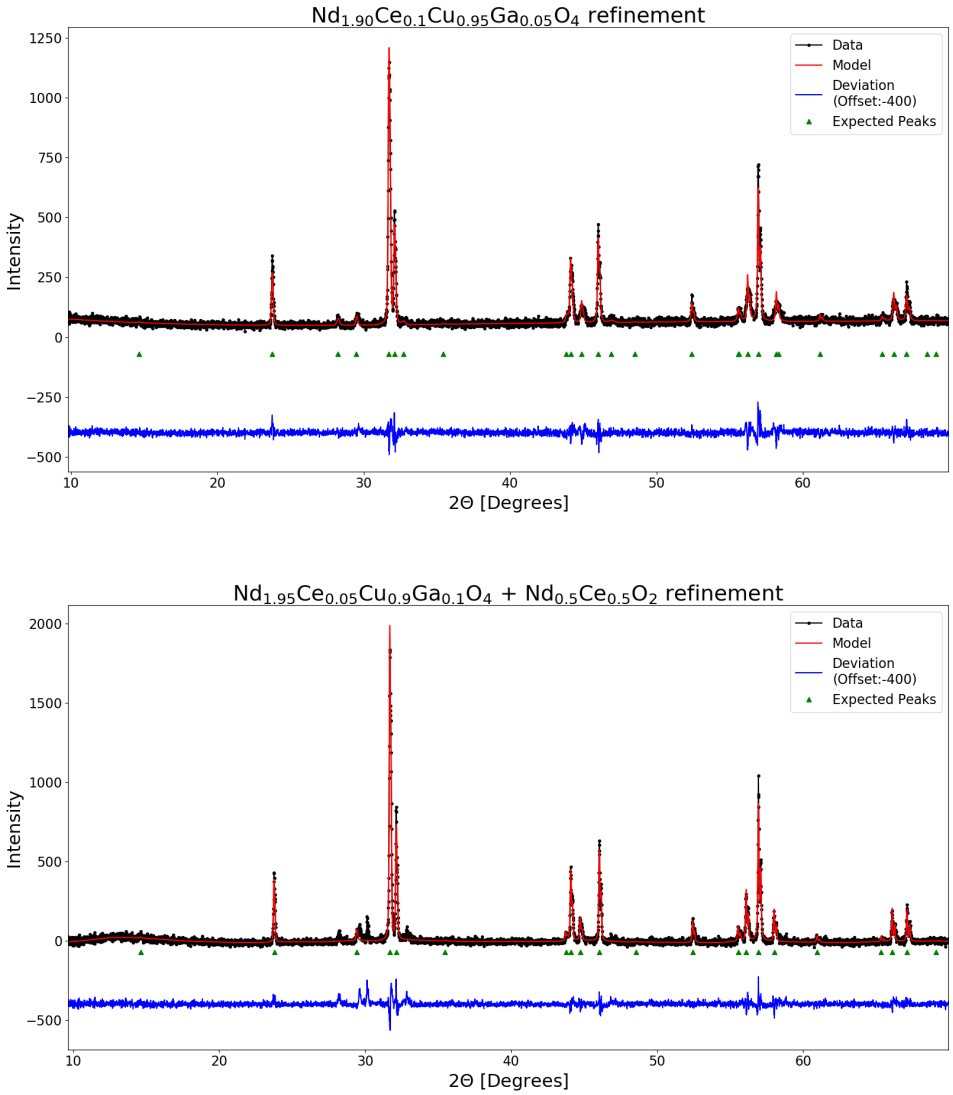

Figure 8.5: Rietveld refinement of $Nd_{2-x}Ce_xCu_{1-y}Ga_yO_4$ at x=0.1, y=0.05 *(top)* and x=0.05 y=0.1 *(bottom)*. A clear impurity that isn't the already investigated $Nd_{0.5}Ce_{0.5}O_2$ is present in the 10% Ga sample, marked by a red arrow, most likely due to Ga over saturation.

mean that some Ce was missing in the primary compound, such that the effective doping level is lower anticipated. For an experiment, for which the entire point is to keep the total carrier concentration constant, this kind of impurity has the potential to be a severely detrimental flaw, potentially turning would-be superconducting samples non-superconducting, thereby ruining any conclusions we could draw from the experiment.

As this experiment was conducted before we managed to figure out how to remove the impurity, we had to gauge the significance of this impurity, and the potential impact it would have on our experiment. To do that we conducted a multiple phase Rietveld refinement on every sample, assuming the impurity to be $Nd_{0.5}Ce_{0.5}O_2$. From a two phase refinement of the x=0.1,y=0.05 sample the fit estimated that impurity made up 5 mol% of the sample, giving similar estimates for the other samples. With the amount Ce used for the synthesis, having 5mol% $Nd_{0.5}Ce_{0.5}O_2$ meant that the main compound intended to be $Nd_{1.9}Ce_{0.1}Cu_{0.95}Ga_{0.05}O_4$ would instead have the structure $Nd_{1.92}Ce_{0.08}Cu_{0.95}Ga_{0.05}O_4$, giving a carrier concentration of x+y=0.13, which is just barely enough for superconductivity in NCCO. This technique however only gives a very rough estimate on the impurity size, and in general has quite a significant uncertainty tied to it. So considering how close to nonsuperconducting the estimate given was, we decided to also use a secondary method in gauging the size of the impurity, for better comparison.

The other way of gauging the size of the impurity is by looking at primary compounds unit cell parameters, which are also found in by Rietveld refinement. As mentioned before, in NCCO the c-axis length in particular changes a lot with doping level, and as such can be used as an indicator of the actual doping level. While the standard size of NCCO varies a fair bit in literature, the CIF archive is fairly consistent, having c=12.08Å for NCCO with x=0.15 and c=12.17Å for the undoped compound. Assuming that it falls linearly with doping we can roughly tell how much cerium has fused with our compound. For our x=0.1 y=0.05 sample Rietveld analysis found c=12.12Å, corresponding to a Ce doping of x=0.083, which is well in line with the value found by two phase analysis. This method is not entirely accurate either, as the CIF that we use for reference are from base NCCO, and as such does not account for the distortions that Ga would bring to the sample. Fortunately Ga is larger than Cu, and should in theory increase the c-length of our compound, which in turn would mean that we use an inflated c-value, thereby underestimating the Ce content, meaning we could be even closer the the x=0.1 cerium doping than anticipated.

With the two methods giving similar estimates of the impurity level, and both predicting that the samples should be superconducting, although just barely, we decided to continue with the magnetic measurements on the samples.

Magnetic Response

The initial plan for the experiment was to measure the sample properties using a different type of magnetometer called a Vibrating-Sample-Magnetometer (VSM), while also doing some measurements comparing our NCCO 12% and 15% samples. This was planned as the VSM had access to a strong 16T magnet, allowing us to compare not only temperature transitions, but also response to high magnetic fields

and critical field transitions. Unfortunately the VSM was taken down for long term maintenance shortly before we intended to use it, and we instead had to make do with conventional SQUID measurements, measuring these samples alongside our LSCO samples.

To achieve superconductivity the samples would still need reductive annealing. We annealed the x=0.12, 0.1 and 0.075 samples for 12 hours at 1100°C. Unfortunately an error occurred for the x=0.12 sample, causing the furnace to not cool down after the intended 12 hours, causing the sample to be annealed for 48 hours instead. This is quite unfortunate, given that overannealing as stated before has the potential to kill superconductivity in a sample. Furthermore our reference material on the damage of overannealing from Serquis et al. [17] skips directly from 24 hours, where the sample was very superconducting, to 200 hours wherein superconductivity stopped, meaning we are unsure just how detrimental to superconductivity 48 hours of annealing is.

None the less we continued with the SQUID measurements, checking samples of progressively higher Ga doping. The measurements found that regular NCCO with x=0.12 was not superconducting, neither was the Ga doped x=0.12 sample, nor the x=0.1 sample. With those results we decided against measurements on the rest of the samples, as the high Ga samples were even less likely to be superconducting, instead spending our SQUID time on improving the quality of our LSCO measurements.

Unfortunately we are unable to conclude whether the x=0.12 sample was non-superconducting due to the overannealing, or if the compound actually does not turn superconducting, which would dispute the claims from the Felner paper. Luckily the x=0.1 experiment is more conclusive, seeing as the predicted carrier concentration would still be high enough for superconductivity, and as we with our subsequent impurity analysis found that the impurity most likely disappeared under the annealing. The fact that this sample was also not superconducting shows strong evidence that one cannot generally substitute regular doping with Ga in the Cu layer, contrary to what one could expect from Felners experiments [48]. We do have to note though that it is still possible that the Ga substitution might work to some degree, given Felners original claims, and the uncertainty regarding our reproduction of the experiment. One reason it might break down at larger doping levels could be a general instability of the Cu layer when increasing the doping, similar to the breakdown witnessed in p-type superconductors. It could also be because the the electrons from Ga doping and regular doping are not generally interchangeable on a larger scale.

Either way we find the phenomenon explained in Felners paper significantly less interesting if it cannot be extrapolated to greater Ga doping levels. Thus, while we could acquire greater certainty about their results by making another sample and redo the experiment, we were contempt with having disproved the general viability of Ga doping, and decided to regard the experiment as finished.

Chapter 9

Summary and final remarks

We can see that our thesis work was quite successful in attaining many of the goals set out at the beginning, that is to explore the n-type superconductors and variations thereof using solid state synthesis.

For instance we have attempted to create many brand new variations of the classic n-type superconductor NCCO. This includes swapping the doping from Ce to the other similar candidates Sn and Zr, as well as exploring the possibility of making a p-type version of the same compound by doping with Sr or Ba. And while all of the synthesises ultimately failed that should not be mistaken for a failed experiment. The point of these exploratory synthesises are after all to investigate which compounds are possible to create, and which are not, something our experiments were successful in. While a successful synthesis would undoubtedly be of more interest, the majority of the process is unfortunately trying and failing to make many other compounds.

We also successfully managed to synthesize Ga doped NCCO to test the claim that it is possible to make the compound superconducting by doping electrons directly into the cuprate layer as opposed to the charge reservoirs normally used. Ultimately there were no indications that this was the case in our experiments, and our experiments even showed different results from those previously claimed, although that could be due to a faulty annealing process.

Finally there is also what is likely our most interesting experiment, the combination of Ni and Zn doping in LSCO. While this experiment was not directly conductive towards the main goal of the thesis, exploring n-type cuprates, it still gave a lot of insight into the workings of superconductors in general. This experiment showed that using multiple doping compounds in the Cu layer created a magnetic response measurement that could be modelled as an average of each individual doping response. This in some way suggested that the doping effects on the primary compounds are independent and linear.

That said we unfortunately also failed to carry out many of the intended core experiments tied to the classical NCCO compound. In particular the growth of an NCCO crystal using the TSFZ method, subsequent neutron diffraction measurements on it to research the effects of annealing, as well as magnetic response measurements on NCCO in a 16T field were all abandoned, although it was mostly due to factors outside our control.

Going forward there are many ways to continue this line of experimentation and many improvements which can be applied to the process. Throughout this thesis we have come to realize how important it is for the synthesis quality that the samples are given ample time in the furnace, and it could very well prove beneficial to redo the Cu layer doping experiments using higher quality samples to ensure the conclusions drawn are correct. The hole doped NCO compounds could also with high likelihood be made to work using more advanced techniques given the existence of samples with even higher doping levels in literature. Furthermore there is still ample room for investigation of alternatives to the Ce doping, with many different dioxides like WO_2 or HfO_2 making for good doping candidates. Finally many of the experiments we failed to carry out are still prime candidates for future experiments should the chance present itself.

In conclusion we have in this thesis explored many potential avenues for finding new types of superconductors, and investigating existing ones. While no new superconductors were found, we have had great success in investigating the behavior of the superconducting cuprate layer, and with the methods used and refined in the process, we have laid a solid foundation for more efficient investigation and exploration of the n-type superconductors in the future.

Bibliography

[1] Onnes, H.K. (1991). Further experiments with Liquid Helium. G. On the Electrical Resistance of Pure Metals, etc. VI. On the Sudden Change in the Rate at which the Resistance of Mercury Disappears.. In: Gavroglu, K., Goudaroulis, Y. (eds) Through Measurement to Knowledge. Boston Studies in the Philosophy of Science, vol 124. Springer, Dordrecht. https://doi.org/10.1007/978-94-009-2079-8_17

[2] Bednorz, J. G., and K. A. Müller. "Possible High T C Superconductivity in the Ba — La — Cu — O System." Ten Years of Superconductivity: 1980–1990, 1986, pp. 267–271., https://doi.org/10.1007/978-94-011-1622-0_32.

[3] Takagi, H., et al. "Superconductivity Produced by Electron Doping in CuO2-Layered Compounds." Physical Review Letters, vol. 62, no. 10, 1989, pp. 1197–1200., https://doi.org/10.1103/physrevlett.62.1197.

[4] Andersen, Brian. "Condensed Matter Physics 2". Teaching notes. Niels Bohr Institute, University of Copenhagen. 2017.

[5] Tinkham, Michael. Introduction to Superconductivity. Dover Publications, 1996.

[6] Meissner, W., and R. Ochsenfeld. "Ein Neuer Effekt Bei Eintritt Der Supraleitfähigkeit." Die Naturwissenschaften, vol. 21, no. 44, 3 Nov. 1933, pp. 787–788., https://doi.org/10.1007/bf01504252.

[7] London, F. "A New Conception of Superconductivity." Nature, 6 Nov. 1937, pp. 793–796.

[8] "Le Diagramme De Phase." La Supraconductivité Dans Tous Ses États, https://www.supraconductivite.fr/fr/index.phpsupra-levitation-phase.

[9] Bardeen, J., et al. "Theory of Superconductivity." Physical Review, vol. 108, no. 5, 1 Dec. 1957, pp. 1175–1204., https://doi.org/10.1103/physrev.108.1175.

[10] Grimes, C. C., and Sidney Shapiro. "Millimeter-Wave Mixing with Josephson Junctions." Physical Review, vol. 169, no. 2, 10 May 1968, pp. 397–406., https://doi.org/10.1103/physrev.169.397.

[11] He, Ke, et al. "Quantum Anomalous Hall Effect." National Science Review, vol. 1, no. 1, 31 Dec. 2013, pp. 38–48., https://doi.org/10.1093/nsr/nwt029.

[12] Prado, F. et al. "Copper Content And Superconductivity Of $Nd_{1.85}Ce_{0.15}Cu_{1\pm\Delta}O_y$ And $Sm_{1.85}Ce_{0.15}Cu_{1\pm\Delta}O_y$". Physica C: Superconductivity, 235-240, 1994, pp. 785-786. Elsevier BV, doi:10.1016/0921-4534(94)91617-9.

[13] Armitage, N. P. et al. "Progress And Perspectives On Electron-Doped Cuprates". Reviews Of Modern Physics, vol 82, no. 3, 2010, pp. 2421-2487. American Physical Society (APS), doi:10.1103/revmodphys.82.2421.

[14] Brinkmann, Matthias, et al. "Extended Superconducting Concentration Range Observed in $Pr_{2-x}Ce_xCuO4$." Physical Review Letters, vol. 74, no. 24, 12 June 1995, pp. 4927–4930., https://doi.org/10.1103/physrevlett.74.4927.

[15] Kang, H. J. et al. "Antiferromagnetic Order As The Competing Ground State In Electron-Doped Nd1.85Ce0.15Cuo4.". Cheminform, vol 34, no. 32, 2003. Wiley, doi:10.1002/chin.200332011.

[16] Mang, P. K. et al. "Phase Decomposition And Chemical Inhomogeneity In $Nd_{2-x}Ce_xCuO_{4\pm\Delta}$". Physical Review B, vol 70, no. 9, 2004. American Physical Society (APS), doi:10.1103/physrevb.70.094507.

[17] Serquis, A. et al. "Copper Nonstoichiometry At High Temperatures In $Nd_{1.85}Ce_{0.15}Cu_{1\pm\Delta}O_y$". Physica C: Superconductivity, vol 273, no. 1-2, 1996, pp. 163-176. Elsevier BV, doi:10.1016/s0921-4534(96)00635-1.

[18] Takayama-Muromachi, E., et al. "Oxygen Deficiency in the Electron-Doped Superconductor ND2XCEXCUO4Y." Physica C: Superconductivity, vol. 159, no. 5, 1989, pp. 634–638., https://doi.org/10.1016/0921-4534(89)91296-3.

[19] Radaelli, P. G., et al. "Evidence of Apical Oxygen inNd_2CuO_y Determined by Single-Crystal Neutron Diffraction." Physical Review B, vol. 49, no. 21, 1 June 1994, pp. 15322–15326., https://doi.org/10.1103/physrevb.49.15322.

[20] Richard, P., et al. "Role of Oxygen Nonstoichiometry and the Reduction Process on the Local Structure of $Nd_{2-x}Ce_xCuO_4$

[21] Dagan, Y. et al. "Origin Of The Anomalous Low Temperature Upturn In The Resistivity Of The Electron-Doped Cuprate Superconductors". Physical Review Letters, vol 94, no. 5, 2005. American Physical Society (APS), doi:10.1103/physrevlett.94.057005.

[22] Helm, T. et al. "Evolution Of The Fermi Surface Of The Electron-Doped High-Temperature Superconductor $Nd_{2-x}Ce_xCuO_4$ revealed By Shubnikov–De Haas Oscillations". Physical Review Letters, vol 103, no. 15, 2009. American Physical Society (APS), doi:10.1103/physrevlett.103.157002.

[23] Hirsch, J.E., and F. Marsiglio. "Understanding Electron-Doped Cuprate Superconductors As Hole Superconductors". Physica C: Superconductivity And Its Applications, vol 564, 2019, pp. 29-37. Elsevier BV, doi:10.1016/j.physc.2019.04.013.

[24] Tanaka, Isao et al. "Growth And Superconductivity Of $Nd_{2-x}Ce_xCuO_4$ Single Crystals". Physica C: Superconductivity, 185-189, 1991, pp. 437-438. Elsevier BV, doi:10.1016/0921-4534(91)92021-3.

[25] Eliasen, Kira. "Growing of La2xSrxCuO4 single crystals and study of magnetic order of superconductivity in La2xSrxCuO4 near the insulating-superconducting phase boundary", Thesis, 2018.

[26] Loïc Le Dréau. Phase transitions and oxygen ordering in La2CoO4+ and (T, T')-La2CuO4 : single crystal growth and structural studies using synchrotron and neutron diffraction methods. Chemical Sciences. Université Rennes 1, 2011. English. ffNNT : 2011REN1S072ff. fftel-00634848

[27] Maljuk, A.N., et al. "Investigation of Phase Equilibria near the Eutectic in the Nd2O3-(CeO2)-CuO System." Journal of Alloys and Compounds, vol. 234, no. 1, 1996, pp. 52–55., https://doi.org/10.1016/0925-8388(95)02005-5.

[28] Snoke, David W. Solid State Physics: Essential Concepts. Cambridge University Press, 2008.

[29] Banerjee, D. "X-Ray Diffraction (XRD) - IIT Kanpur." X-Ray Diffraction (XRD), 2020, https://iitk.ac.in/che/pdf/resources/XRD-reading-material.pdf.

[30] Cockcroft, J., et al. "Instrumentation I: Laboratory Methods." Instrumentation I: Laboratory Methods, 2006, http://pd.chem.ucl.ac.uk/pdnn/inst1/labindex.htm.

[31] "ICSD ." ICSD Version 4.8, FIZ Karlsruhe GmbH, 2022, https://icsd.fiz-karlsruhe.de/.

[32] Rietveld, H. M. "A Profile Refinement Method for Nuclear and Magnetic Structures." Journal of Applied Crystallography, vol. 2, no. 2, 1969, pp. 65–71., https://doi.org/10.1107/s0021889869006558.

[33] "Crystallographic Computing System." Jana, 2020, http://jana.fzu.cz/.

[34] Le Bail, Armel. "Whole Powder Pattern Decomposition Methods and Applications: A Retrospection." Powder Diffraction, vol. 20, no. 4, 2005, pp. 316–326., https://doi.org/10.1154/1.2135315.

[35] "Rietveld Method - Pennsylvania State University." Refinement Parameters, https://personal.ems.psu.edu/ ryba/coursework/Rietveld/Rietveld-1.pdf.

[36] McCusker, L. B., et al. "Rietveld Refinement Guidelines." Journal of Applied Crystallography, vol. 32, no. 1, 1999, pp. 36–50., https://doi.org/10.1107/s0021889898009856.

[37] Lefmann, Kim, et al. "Neutron Scattering: Theory, Instrumentation, and Simulation". Teaching notes. Niels Bohr Institute, University of Copenhagen. 2022.

[38] Tranquada, John M. "Topological Doping and Superconductivity in Cuprates: An Experimental Perspective." Symmetry, vol. 13, no. 12, 2021, p. 2365., https://doi.org/10.3390/sym13122365.

[39] Simon, R. "Mr. Squid User's Guide." Mr. SQUID® User's Guide, STAR Cryoelectronics, LLC, 2004, https://www.uni-frankfurt.de/50341695/Josephson_Effect_MrSQUID.pdf.

[40] Yamada, K., et al. "Commensurate Spin Dynamics in the Superconducting State of an Electron-Doped Cuprate Superconductor." Physical Review Letters, vol. 90, no. 13, 2003, https://doi.org/10.1103/physrevlett.90.137004.

[41] Dai, Pengcheng, et al. "Evolution of Spin Excitations in Electron-Doped PR0.88LaCe0.12CUO4." Physica C: Superconductivity and Its Applications, vol. 460-462, 2007, pp. 52–55., https://doi.org/10.1016/j.physc.2007.03.090.

[42] Waroquiers, David, et al. "Statistical Analysis of Coordination Environments in Oxides." Chemistry of Materials, vol. 29, no. 19, 2017, pp. 8346–8360., https://doi.org/10.1021/acs.chemmater.7b02766.

[43] Labbe, Ph., et al. "Structural Peculiarities of Two Layered Cuprates, NDSR-CUO3.5 and nd1.8sr1.2cu2o6." Journal of Solid State Chemistry, vol. 91, no. 2, 1991, pp. 362–369., https://doi.org/10.1016/0022-4596(91)90091-u.

[44] Chen, Xiaolong, et al. "The ND2O3-SRO-Cuo System: Compounds and Phase Relations." Journal of Alloys and Compounds, vol. 205, no. 1-2, 1994, pp. 101–106., https://doi.org/10.1016/0925-8388(94)90773-0.

[45] Khandale, A.P., and S.S. Bhoga. "Effect of SR Doping on Structural, Electrical and Electrochemical Properties of ND2CUO4 for It-SOFC Application." Solid State Ionics, vol. 262, 2014, pp. 416–420., https://doi.org/10.1016/j.ssi.2014.01.048.

[46] Rosseinsky, Matthew J., et al. "Magnetic Ordering and Spin Reorientation Transitions in Hole-Doped T Phases nd2xsrxcuo4: A +Sr Study." Journal of Magnetism and Magnetic Materials, vol. 104-107, 1992, pp. 599–600., https://doi.org/10.1016/0304-8853(92)90942-h.

[47] Kofu, M., et al. "Zn and Ni Doping Effects on the Low-Energy Spin Excitations in $La_{1.85}Sr_{0.15}CuO4$." Physical Review B, vol. 72, no. 6, 2 Aug. 2005, https://doi.org/10.1103/physrevb.72.064502.

[48] Felner, I., et al. "Effect of Ga Substitution on the Superconducting Properties of the Electron-Doped System: ND-Ce-Cu-O." Physical Review B, vol. 40, no. 16, 1 Dec. 1989, pp. 11366–11369., https://doi.org/10.1103/physrevb.40.11366.

[49] da Silva Neto, E. H. et al. "Charge Ordering In The Electron-Doped Superconductor $Nd_{2-x}Ce_xCuO_4$". Science, vol 347, no. 6219, 2015, pp. 282-285. American Association For The Advancement Of Science (AAAS), doi:10.1126/science.1256441.

[50] da Silva Neto, E. H. et al. "Coupling Between Dynamic Magnetic And Charge-Order Correlations In The Cuprate Superconductor $Nd_{2-x}Ce_xCuO_4$". Physical Review B, vol 98, no. 16, 2018. American Physical Society (APS), doi:10.1103/physrevb.98.161114.

[51] Dorantes, A. et al. "Magnetotransport Evidence For Irreversible Spin Reorientation In The Collinear Antiferromagnetic State Of Underdoped $Nd_{2-x}Ce_xCuO_4$". Physical Review B, vol 97, no. 5, 2018. American Physical Society (APS), doi:10.1103/physrevb.97.054430.

[52] Hinton, J. P. et al. "Time-Resolved Optical Reflectivity Of The Electron-Doped $Nd_{2-x}Ce_xCuO_{4\pm\Delta}$ cuprate Superconductor: Evidence For An Interplay Between Competing Orders". Physical Review Letters, vol 110, no. 21, 2013. American Physical Society (APS), doi:10.1103/physrevlett.110.217002.

[53] Horio, M, and A Fujimori. "ARPES Studies On New Types Of Electron-Doped Cuprate Superconductors". Journal Of Physics: Condensed Matter, vol 30, no. 50, 2018, p. 503001. IOP Publishing, doi:10.1088/1361-648x/aab824.

[54] Kaul, Ribhu K. et al. "Destruction Of Néel Order In The Cuprates By Electron Doping". Physical Review B, vol 78, no. 4, 2008. American Physical Society (APS), doi:10.1103/physrevb.78.045110.

[55] Lee, W. S. et al. "Asymmetry Of Collective Excitations In Electron- And Hole-Doped Cuprate Superconductors". Nature Physics, vol 10, no. 11, 2014, pp. 883-889. Springer Science And Business Media LLC, doi:10.1038/nphys3117.

[56] Motoyama, E. M. et al. "Spin Correlations In The Electron-Doped High-Transition-Temperature Superconductor $Nd_{2-x}Ce_xCuO_{4\pm\Delta}$". Nature, vol 445, no. 7124, 2007, pp. 186-189. Springer Science And Business Media LLC, doi:10.1038/nature05437.

[57] Piñol, S. et al. "Crystal Growth And Phase Diagrams For The $Nd_2O_3-CeO_2-CuO$ System". Physica C: Superconductivity, vol 165, no. 3-4, 1990, pp. 265-269. Elsevier BV, doi:10.1016/0921-4534(90)90202-p.

[58] Stadlober, B. et al. "Is $Nd_{2-x}Ce_xCuO_4$ High-Temperature Superconductor?". Physical Review Letters, vol 74, no. 24, 1995, pp. 4911-4914. American Physical Society (APS), doi:10.1103/physrevlett.74.4911.

[59] Tarascon, J.-M. et al. "Growth, Structural, And Physical Properties Of Superconducting $Nd_{2-x}Ce_xCuO_4$ crystals". Physical Review B, vol 40, no. 7, 1989, pp. 4494-4502. American Physical Society (APS), doi:10.1103/physrevb.40.4494.

[60] Yang, H.S. et al. "Anomalous Thermopower Of The Electron-Doped Superconductor, $Sm_{2-x}Ce_xCuO_4$". Physica C: Superconductivity, vol 403, no. 3, 2004, pp. 203-208. Elsevier BV, doi:10.1016/j.physc.2003.12.012.

Appendix A

XRD patterns

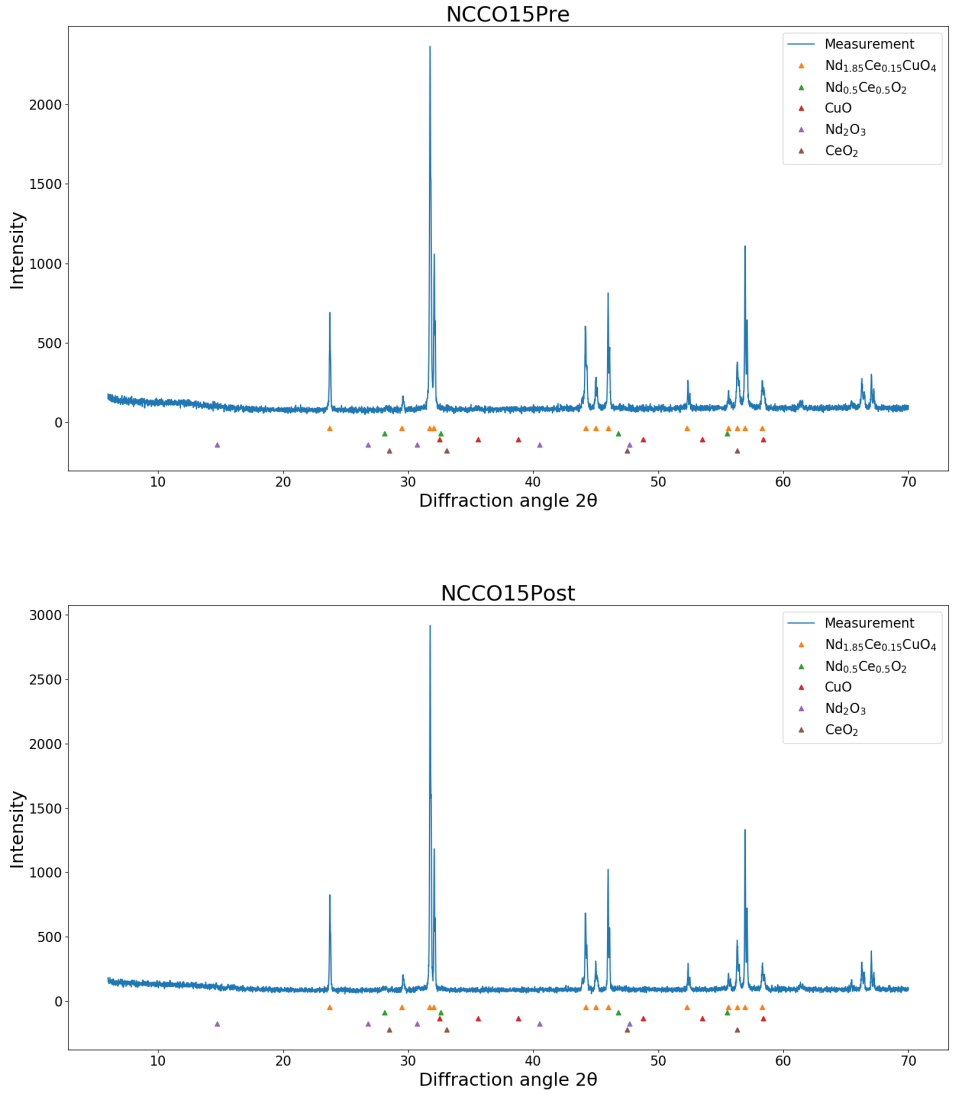

Figure A.1: First NCCO15 sample before*(top)* and after*(bottom)* annealing.

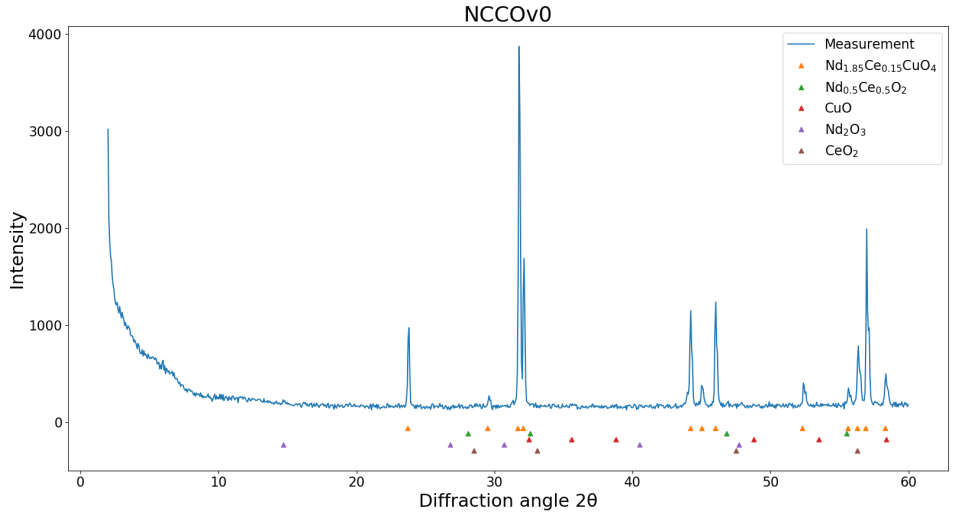
NCCOv0
Measurement
$Nd_{1.85}Ce_{0.15}CuO_4$
$Nd_{0.5}Ce_{0.5}O_2$
CuO
Nd_2O_3
CeO_2
Intensity
Diffraction angle 2θ

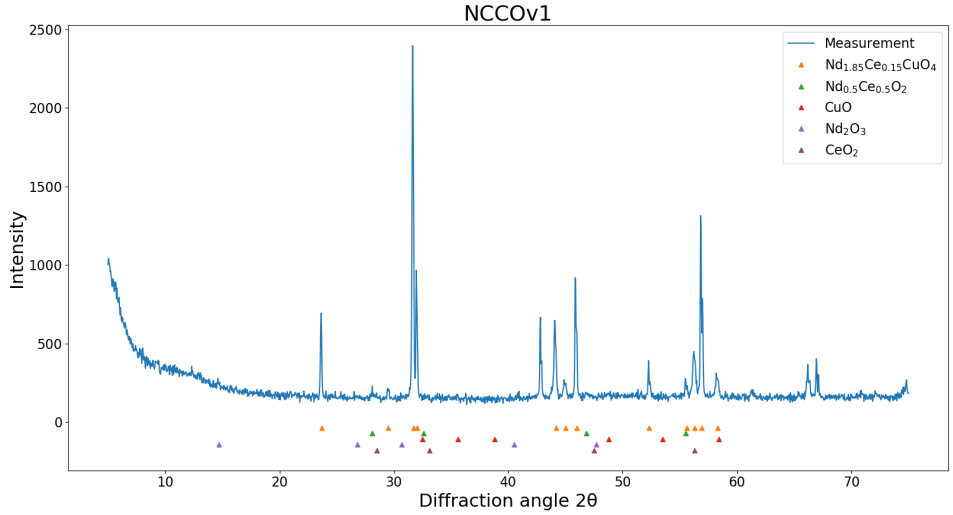
NCCOv1
Measurement
$Nd_{1.85}Ce_{0.15}CuO_4$
$Nd_{0.5}Ce_{0.5}O_2$
CuO
Nd_2O_3
CeO_2
Intensity
Diffraction angle 2θ

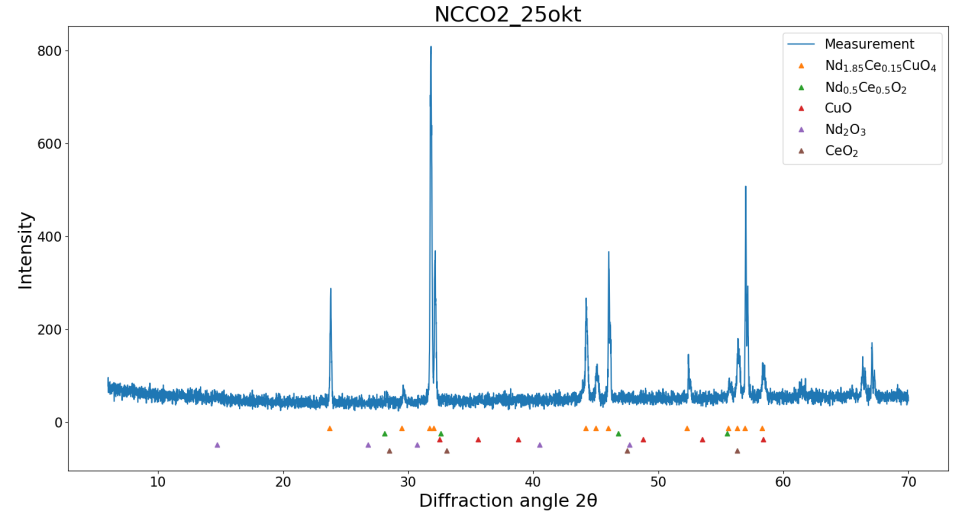
NCCO2_25okt
Measurement
$Nd_{1.85}Ce_{0.15}CuO_4$
$Nd_{0.5}Ce_{0.5}O_2$
CuO
Nd_2O_3
CeO_2
Intensity
Diffraction angle 2θ

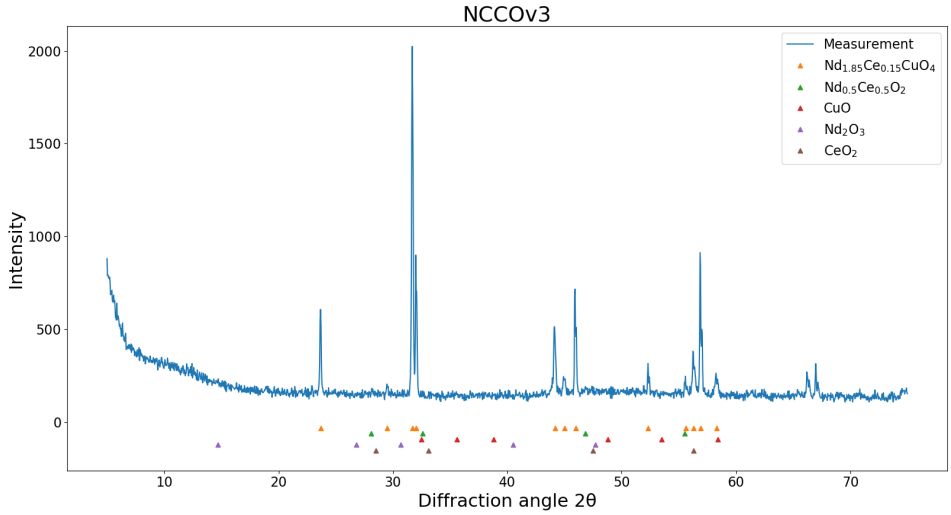
NCCOv3
Measurement
$Nd_{1.85}Ce_{0.15}CuO_4$
$Nd_{0.5}Ce_{0.5}O_2$
CuO
Nd_2O_3
CeO_2
Intensity
Diffraction angle 2θ

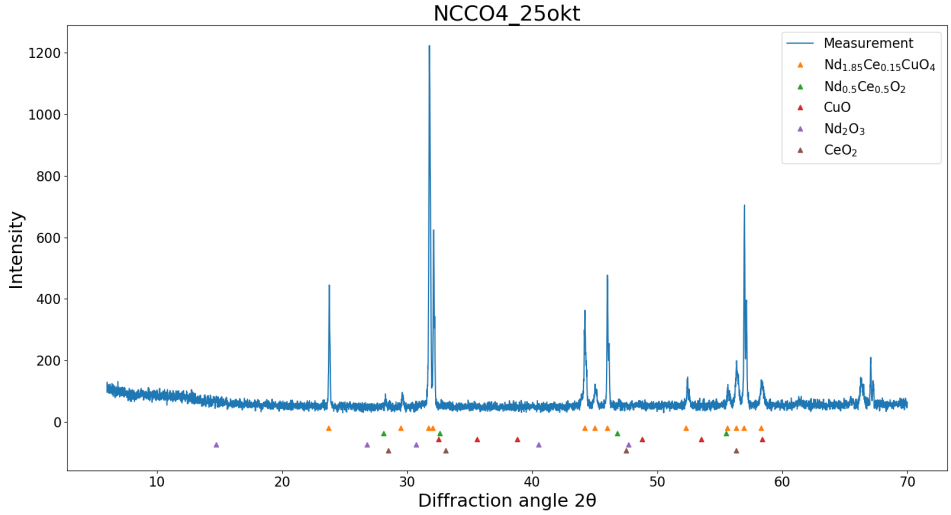
NCCO4_25okt
Measurement
$Nd_{1.85}Ce_{0.15}CuO_4$
$Nd_{0.5}Ce_{0.5}O_2$
CuO
Nd_2O_3
CeO_2
Intensity
Diffraction angle 2θ

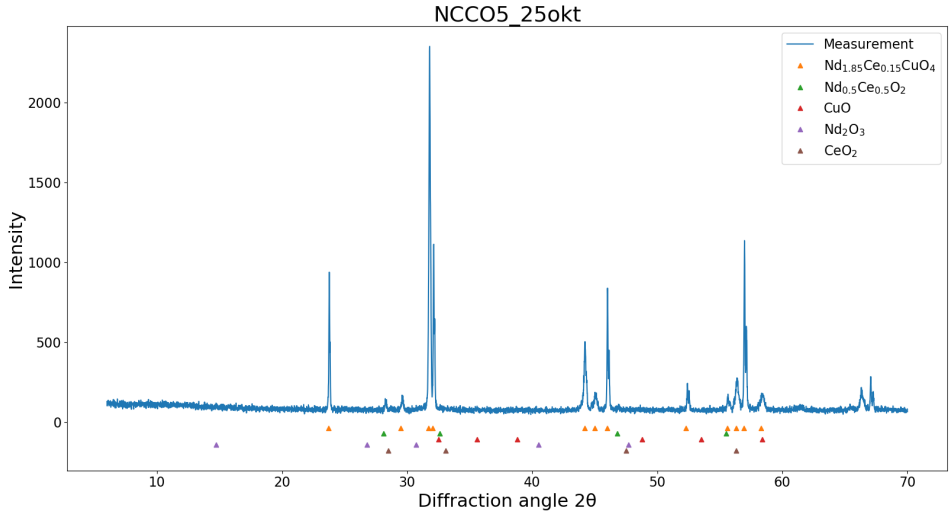
NCCO5_25okt
Measurement
$Nd_{1.85}Ce_{0.15}CuO_4$
$Nd_{0.5}Ce_{0.5}O_2$
CuO
Nd_2O_3
CeO_2
Intensity
Diffraction angle 2θ

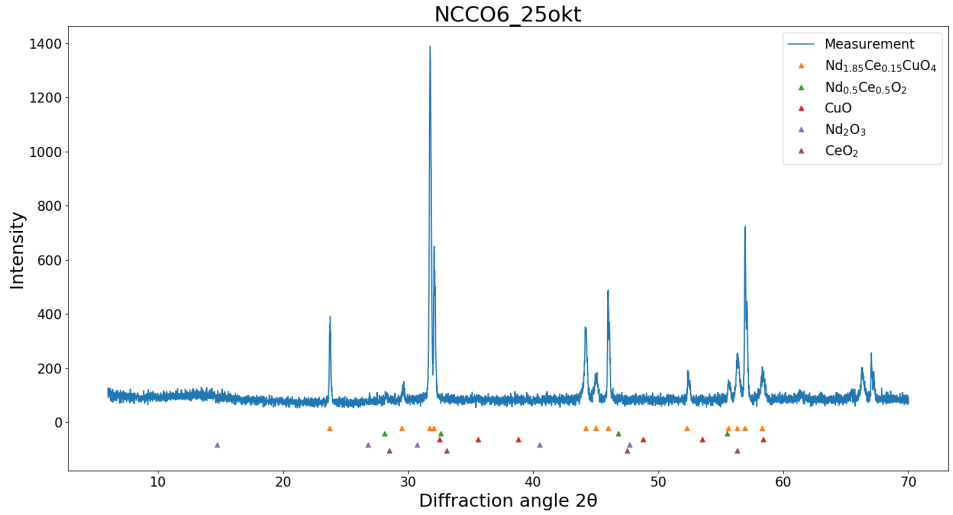
NCCO6_25okt
Measurement
$Nd_{1.85}Ce_{0.15}CuO_4$
$Nd_{0.5}Ce_{0.5}O_2$
CuO
Nd_2O_3
CeO_2
Intensity
Diffraction angle 2θ

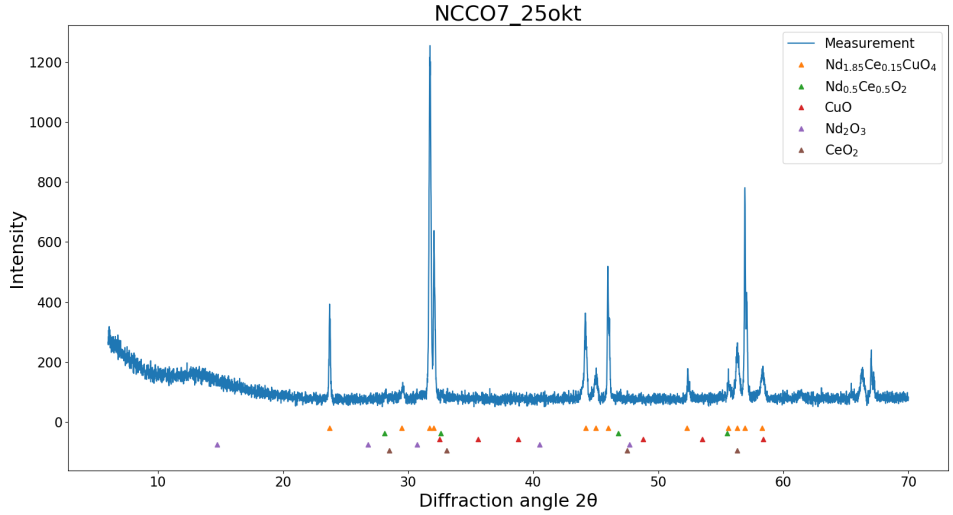
NCCO7_25okt
Measurement
$Nd_{1.85}Ce_{0.15}CuO_4$
$Nd_{0.5}Ce_{0.5}O_2$
CuO
Nd_2O_3
CeO_2
Intensity
Diffraction angle 2θ

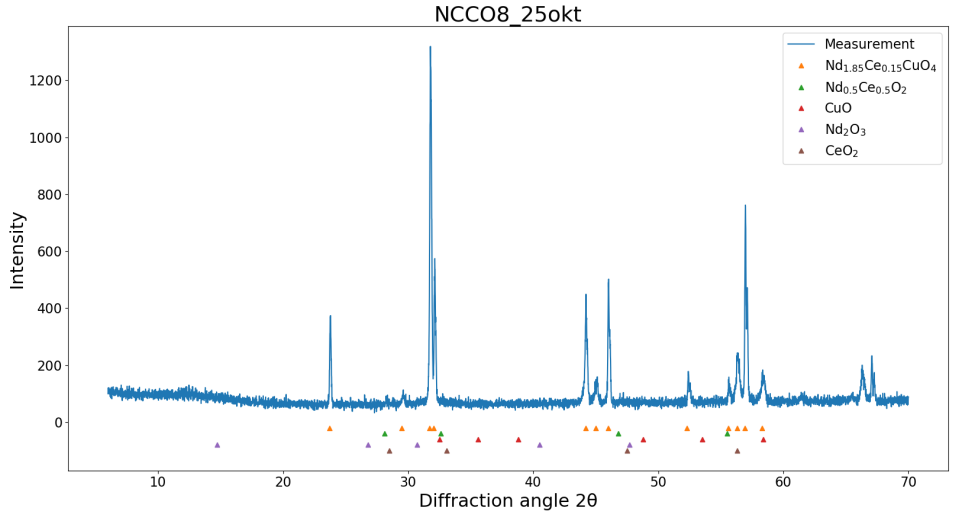
NCCO8_25okt
Measurement
$Nd_{1.85}Ce_{0.15}CuO_4$
$Nd_{0.5}Ce_{0.5}O_2$
CuO
Nd_2O_3
CeO_2
Intensity
Diffraction angle 2θ

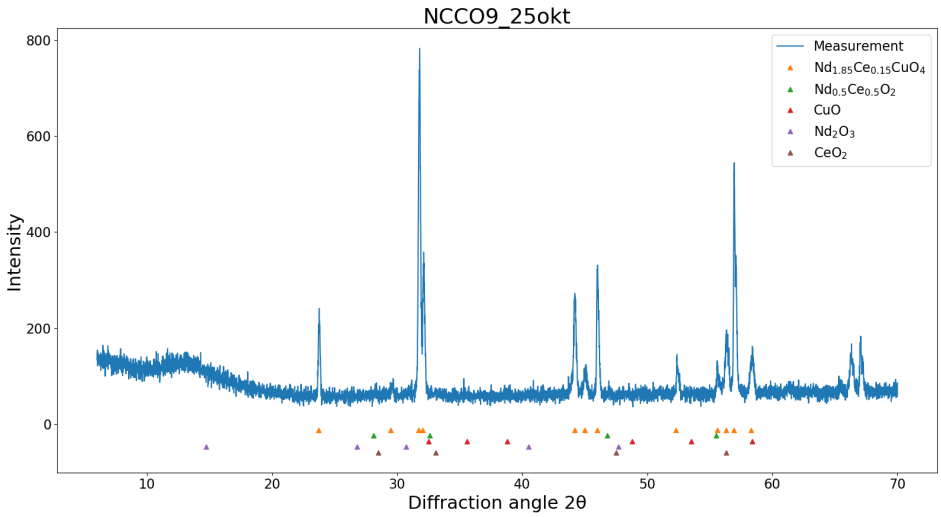

Figure A.2: All 10 NCCO x=0.15 samples intended for crystal growth. Labeled NCCOvX or simply NCCOX with X being their sample number.

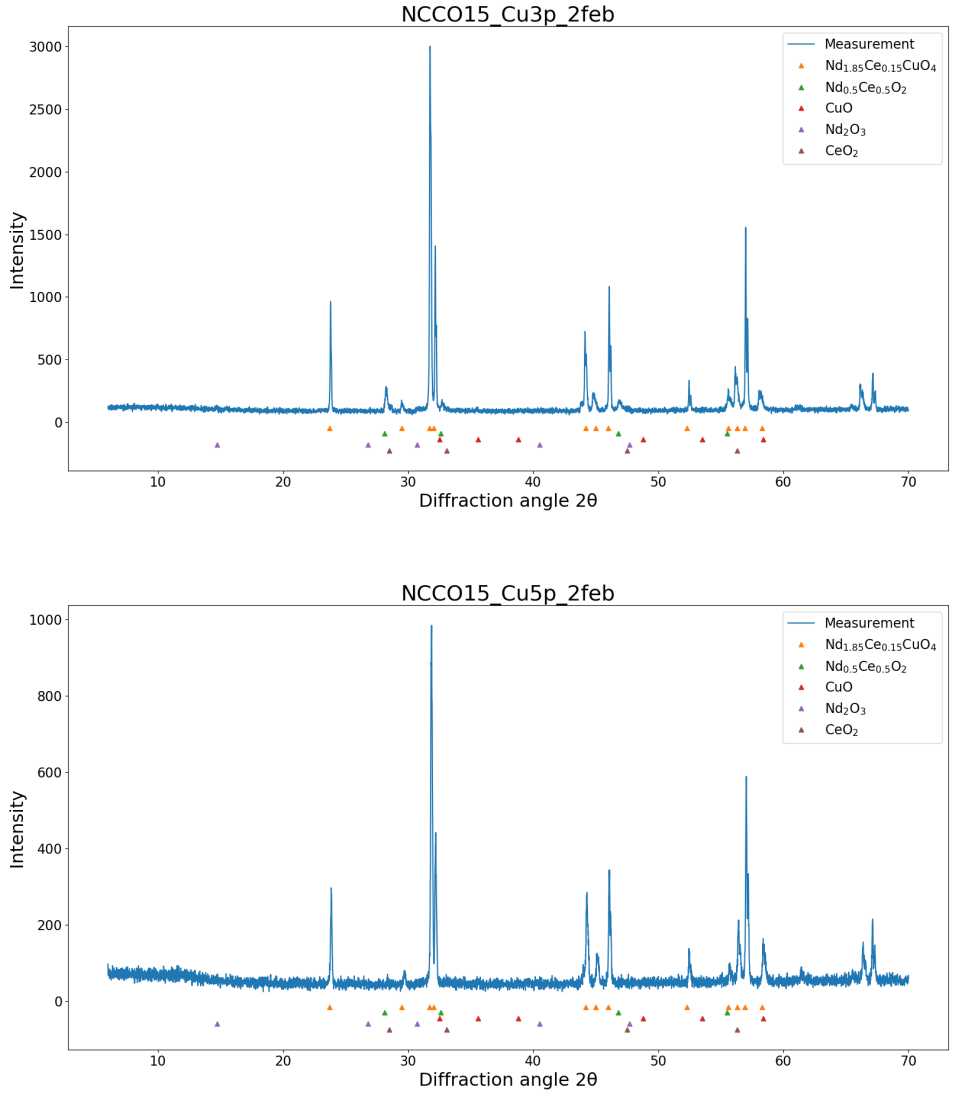

Figure A.3: NCCO x=0.15 samples with additional 3%*(top)* and 5%*(bottom)* Cu.

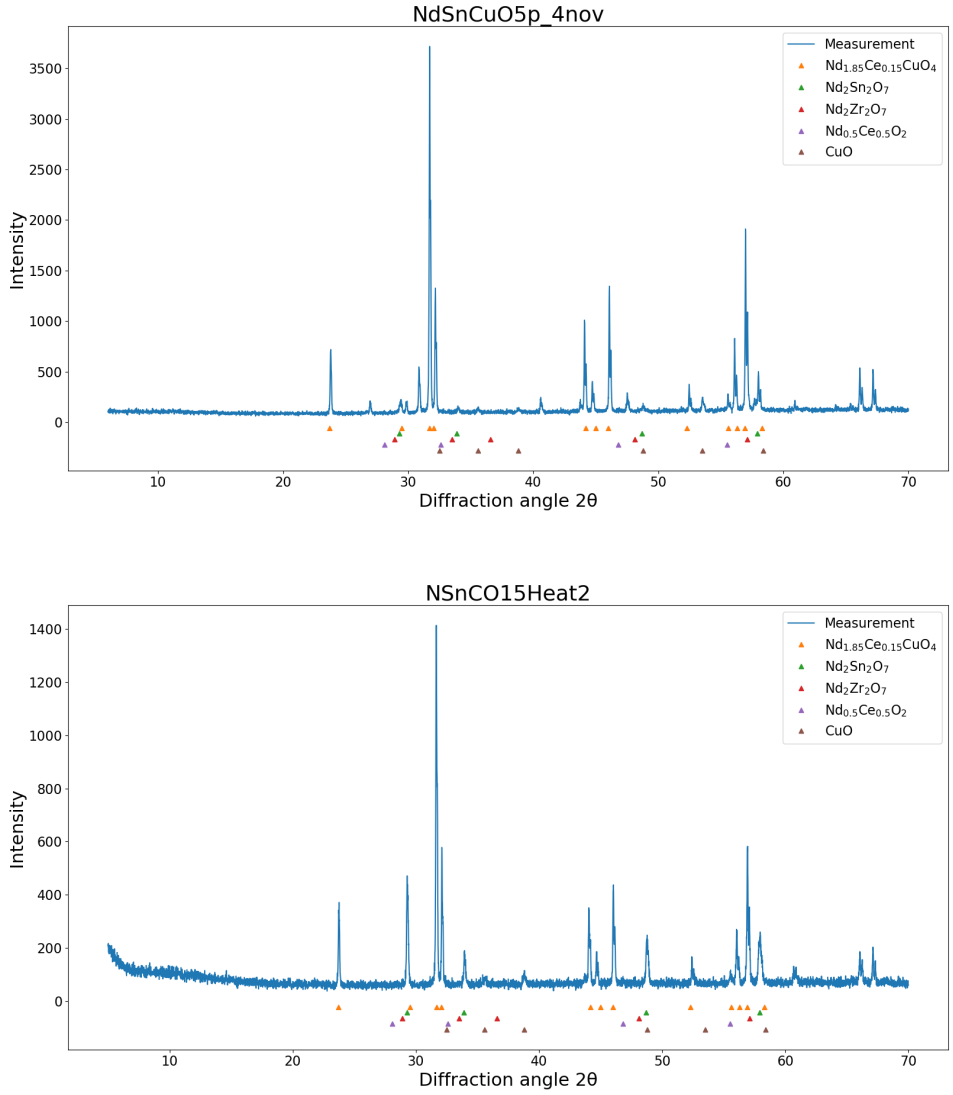

Figure A.4: $Nd_{2-x}Sn_xCuO_4$ for x=0.05*(top)* and x=0.15*(bottom)*.

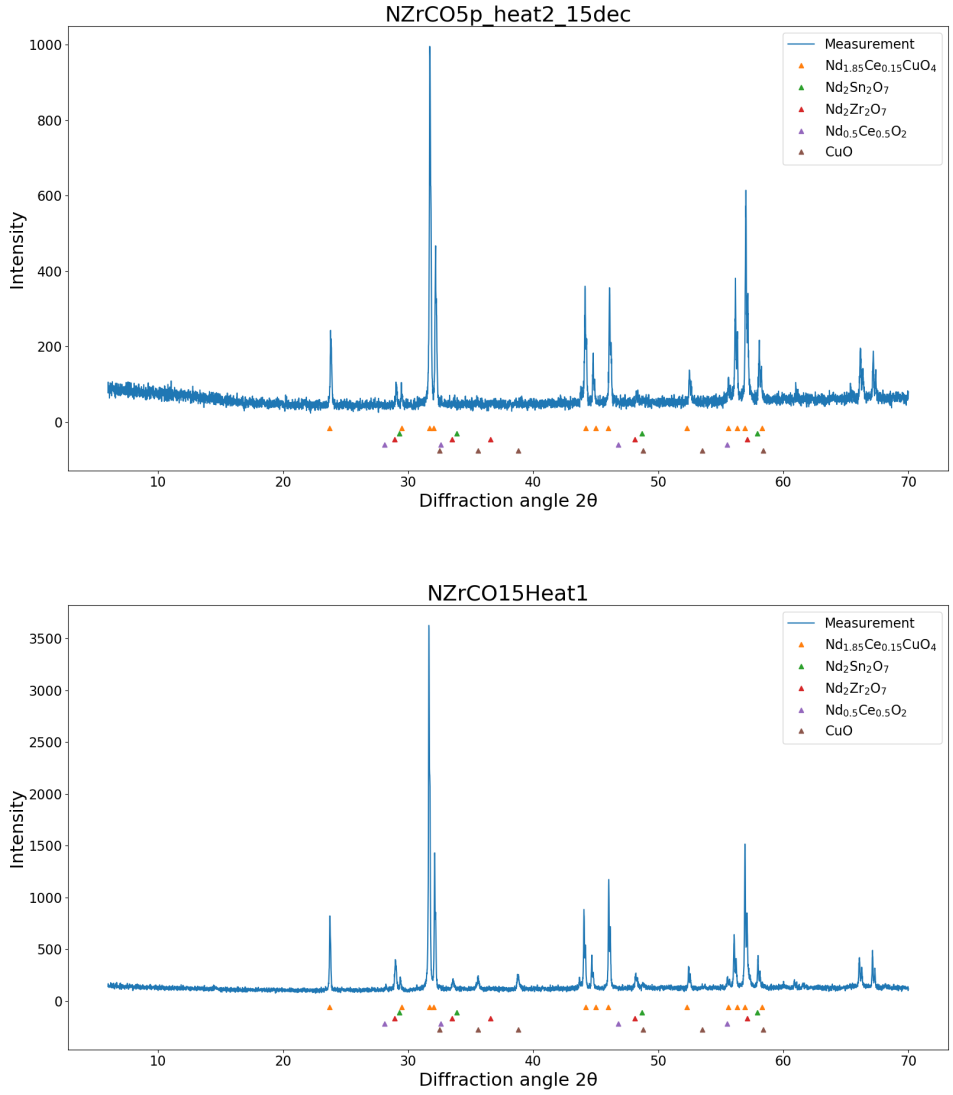

Figure A.5: $Nd_{2-x}Zr_xCuO_4$ for x=0.05*(top)* and x=0.15*(bottom)*.

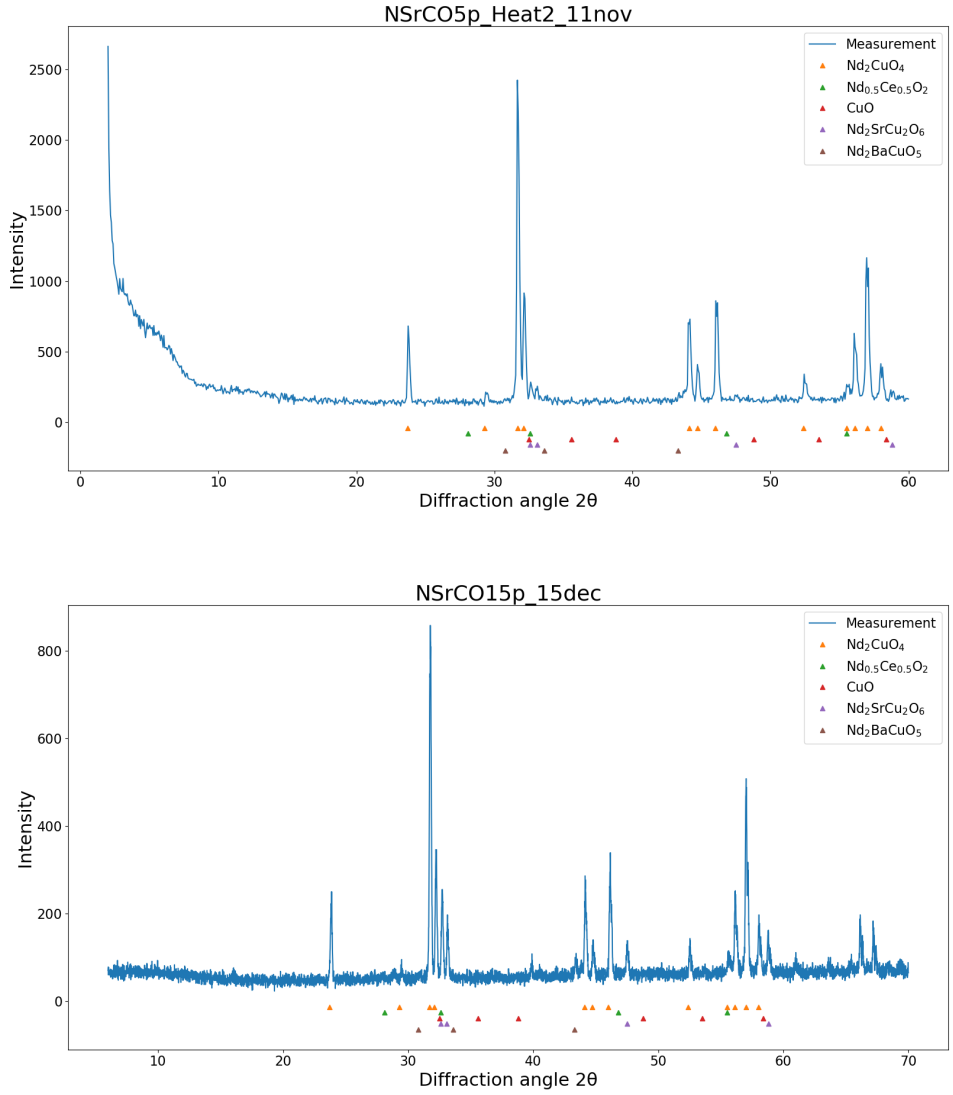

Figure A.6: $Nd_{2-x}Sr_xCuO_4$ for x=0.05*(top)* and x=0.15*(bottom)*.

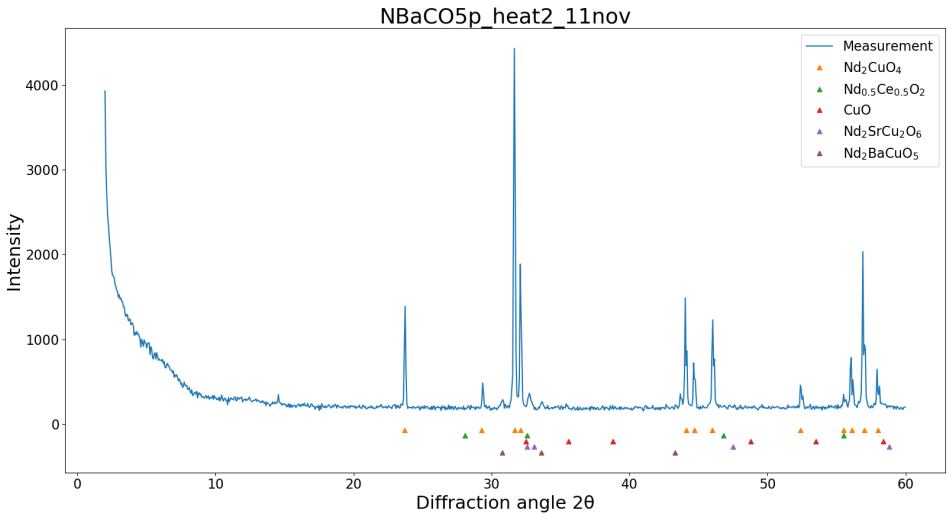

Figure A.7: $Nd_{1.95}Ba_{0.05}CuO_4$

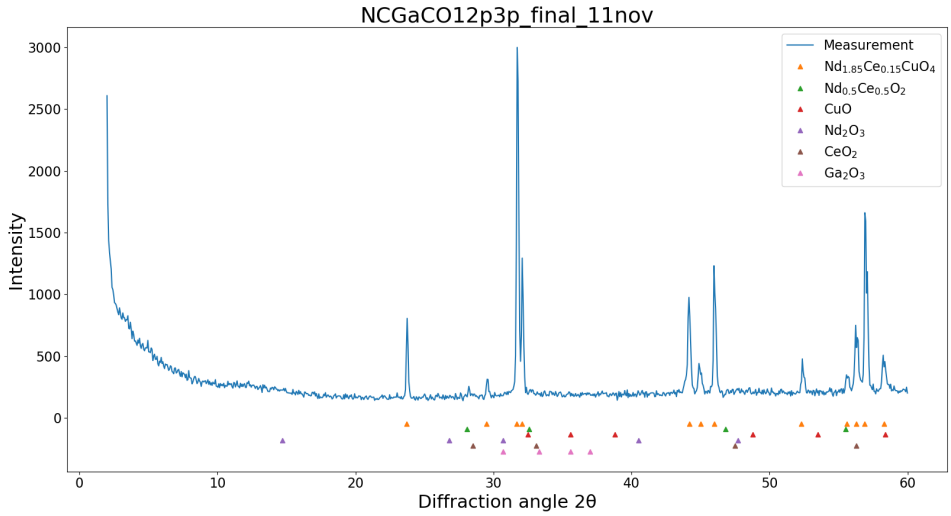
NCGaCO12p3p_final_11nov
Measurement
$Nd_{1.85}Ce_{0.15}CuO_4$
$Nd_{0.5}Ce_{0.5}O_2$
CuO
Nd_2O_3
CeO_2
Ga_2O_3
Intensity
Diffraction angle 2θ

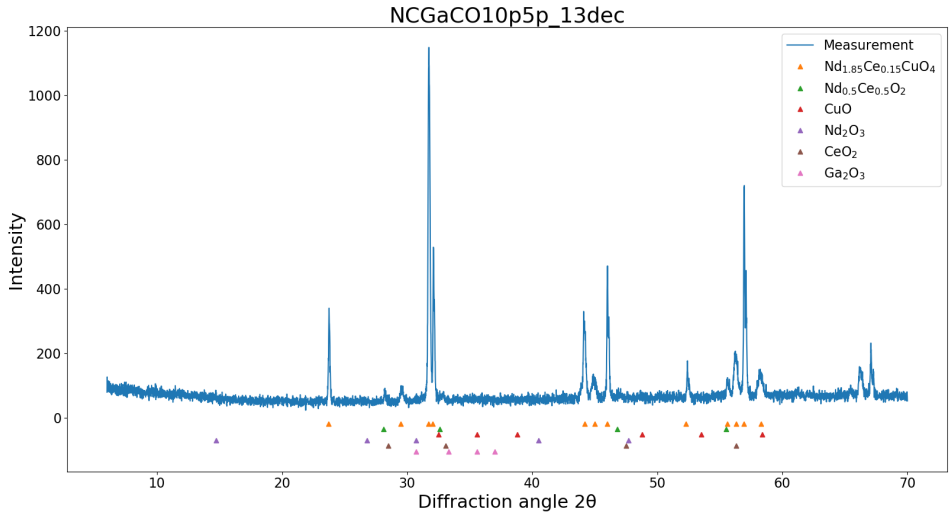
NCGaCO10p5p_13dec
Measurement
$Nd_{1.85}Ce_{0.15}CuO_4$
$Nd_{0.5}Ce_{0.5}O_2$
CuO
Nd_2O_3
CeO_2
Ga_2O_3
Intensity
Diffraction angle 2θ

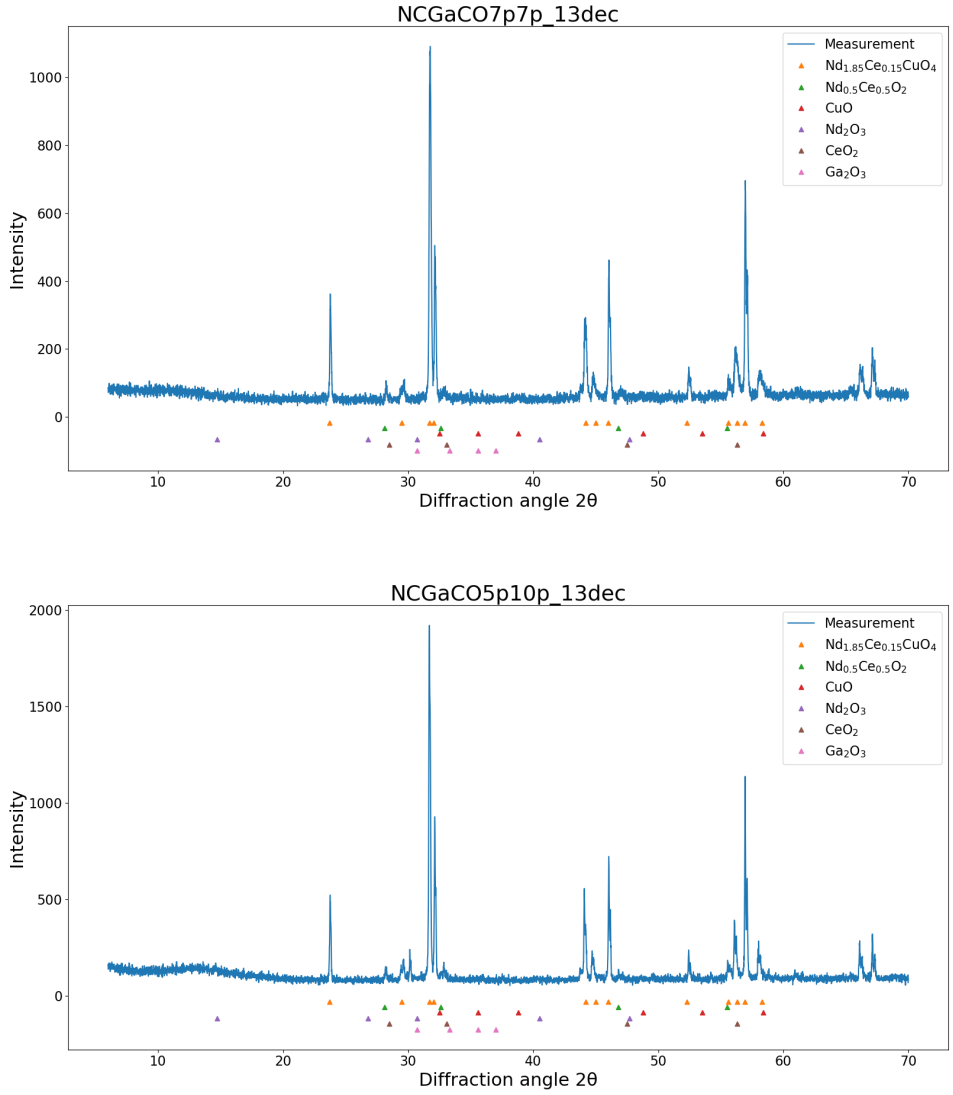

Figure A.8: $Nd_{2-x}Ce_xCu_{1-y}Ga_yO_4$ labeled NCGaCOXpYp.

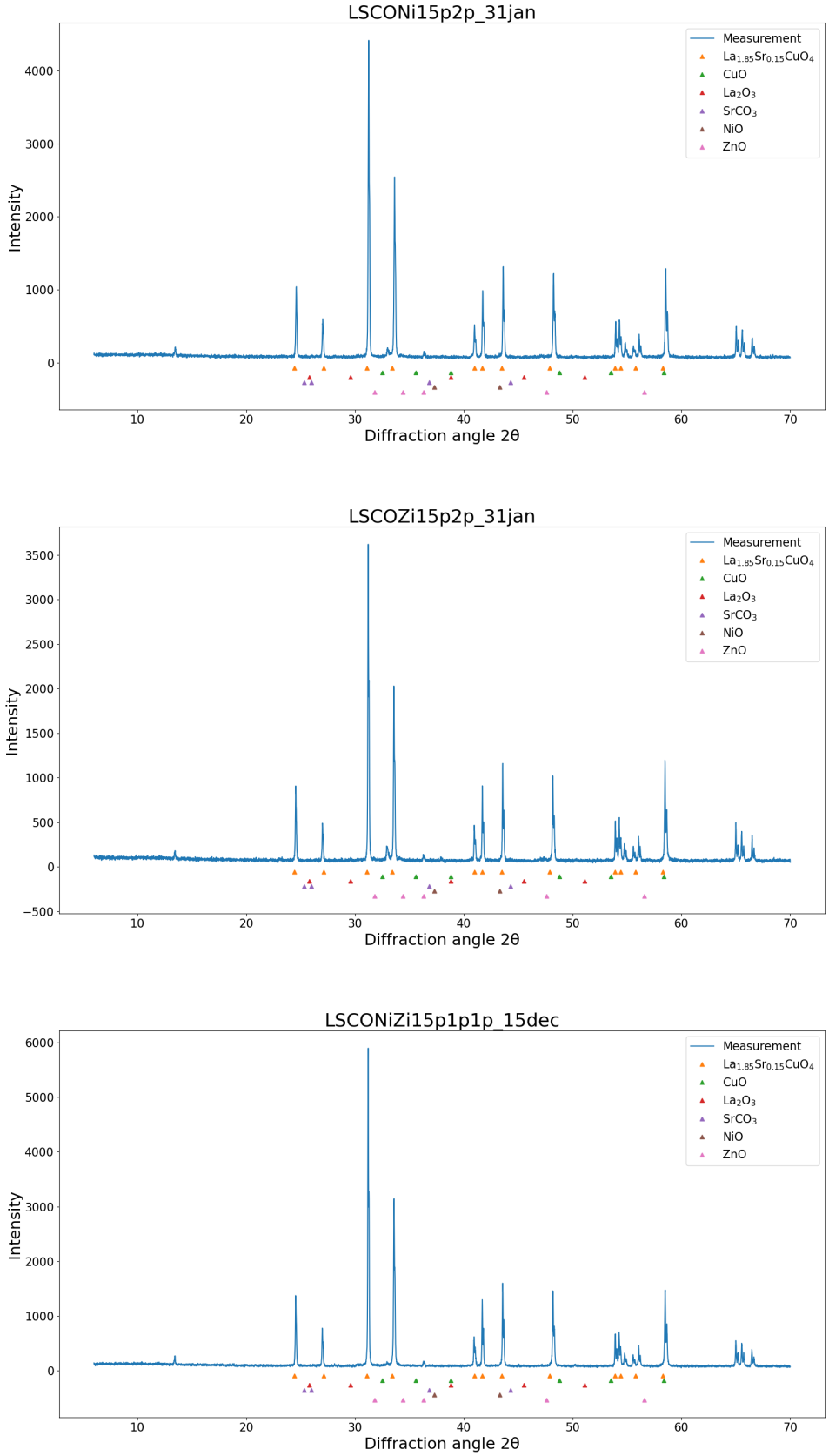

Figure A.9: $La_{1.85}Sr_{0.15}Cu_{0.98}O_4$ samples doped with 2% Ni *(top)*, 2% Zn *(middle)* and 1% Ni and 1% Zn *(bottom)*.

Appendix B

Magnetization measurements

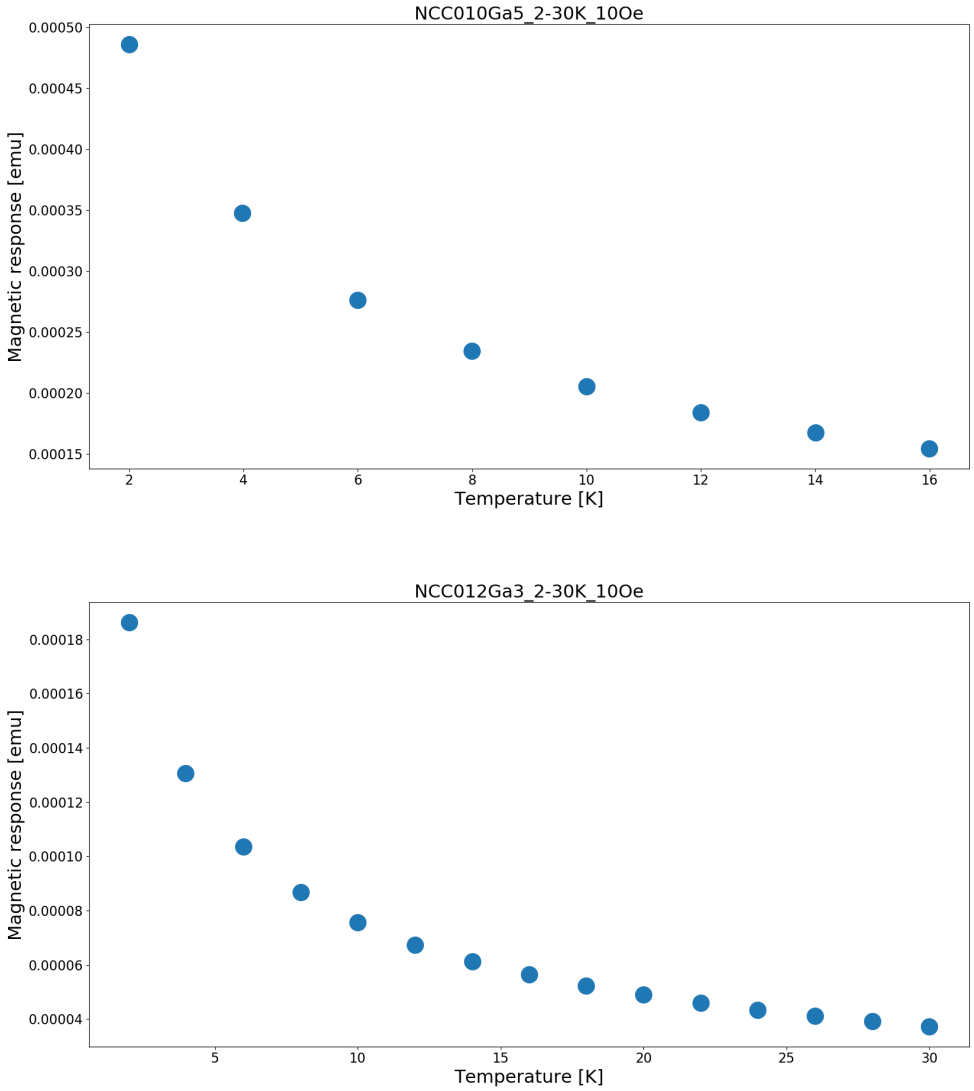

Figure B.1: SQUID measurements on $Nd_{2-x}Ce_xCu_{1-y}Ga_yO_4$ with x=0.1, y=0.05 *(top)* and x=0.12, y=0.03 *(bottom)*. There is no sign of superconductivity and low temperature upswing likely caused by paramagnetic impurities in the samples.

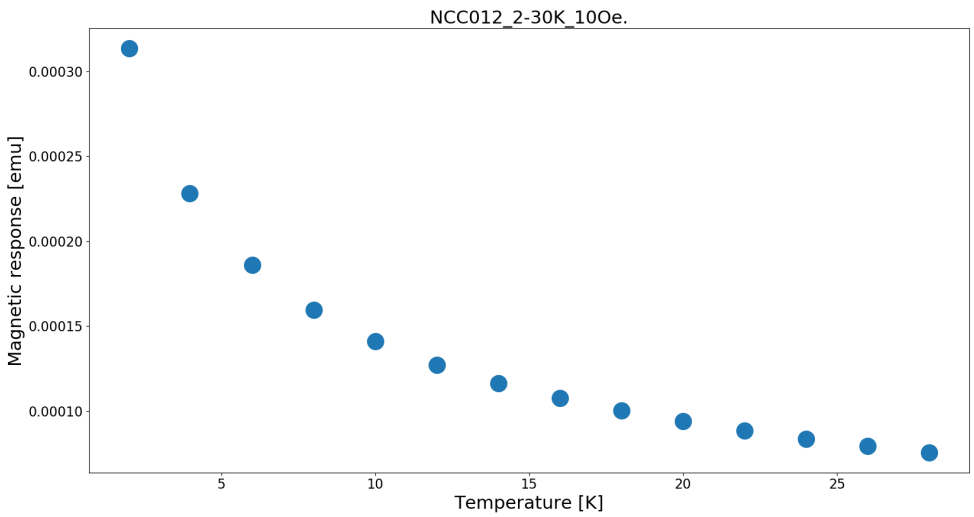

Figure B.2: Magnetic measurement of regular NCCO x=0.12 after annealing. No superconductivity is found, and the low temperature upswing is likely caused by paramagnetic impurities in the sample.